Control Strategy for Fully Flexible Valve Technology

JOAKIM KARLSSON

KTH Industrial Engineering
and Management

Master of Science Thesis
Stockholm, Sweden 2010

Reglerstrategi för fria ventiler

JOAKIM KARLSSON

KTH Industriell teknik
och management

Examensarbete
Stockholm, Sverige 2010

Reglerstrategi för fria ventiler

– Utveckling av en fyrtakts förbränningsmodell för att prediktera optimala ventilinställningar

Joakim Karlsson

Examensarbete MMK 2010:18 MFM135
KTH Industriell teknik och management
Maskinkonstruktion
SE-100 44 STOCKHOLM

Control Strategy for Fully Flexible Valve Technology

- Development of a four-stroke combustion model to predict optimal valve settings

Joakim Karlsson

Master of Science Thesis MMK 2010:18 MFM135
KTH Industrial Engineering and Management
Machine Design
SE-100 44 STOCKHOLM

KTH Industriell teknik och management

Examensarbete MMK 2010:18 MFM135

Reglerstrategi för fria ventiler

– Utveckling av en fyrtakts förbränningsmodell för att prediktera optimala ventilinställningar

Joakim Karlsson

Godkänt	Examinator	Handledare
2010-11-19	Hans-Erik Ångström	Richard Backman
	Uppdragsgivare	Kontaktperson
	AVL SPEAB	Richard Backman

Sammanfattning

I takt med att internationella emissionslagstiftningar driver motorutvecklingen framåt, måste verkningsgradsförbättringar och bränslebesparande teknologier hela tiden sättas i fokus och varje litet delsystem i ett fordon måste förses med enorma utvecklingsresurser för att förbättra prestanda och möta marknadens krav. Under det senaste årtiondet har variabla ventiltider utvecklats till en populär metod för att bredda och spetsa till motorprestanda. Dessa system är dock vanligtvis mekaniskt begränsade och en annan aktueringsprincip är önskvärd.

En möjlig lösning kan vara att driva ventilerna med tryckluft istället för en kamnock. Ett sådant system tillhandahålls av *Cargine Engineering* och det är detta system som utgör grundstommen i det här arbetet. För att styra det här ventilsystemet krävs ett reglersystem och till detta används det av AVL utvecklade *Raptor*. Användarmiljön är *Simulink*-baserad och med hjälp av återkoppling från lägesgivare monterade på varje ventil har reglering av öppning, stängning och lyfthöjd implementerats. Testcellen har dessutom utrustats med ett skript som möjliggör automatisk drift av testcellen utifrån ett fördefinierat körschema. Dessa modifieringar har tillsammans möjliggjort insamling av stora mängder mätdata på förhållandevis kort tid.

Utifrån de mätningar som gjorts har en befintlig (AVL-utvecklad) förbränningsmodell vidareutvecklats. Modellen används för att prediktera ett komplett cylindertrycksspår för en fyrtakts Ottomotor och modifieringarna har innefattat en mer detaljerad gasväxlingsmodell. För att uppnå detta har det varit nödvändigt att ta hänsyn till de variabla ventiltiderna och lyfthöjderna och resultatet är en cylindertrycksmodell som har en standardavvikelse på 4,9% i skattning av indikerat medeltryck (IMEP). Motsvarande siffra för pumpmedeltrycket (PMEP) är 8,8%.

Med denna modellnoggrannhet ansågs det vara realistiskt att svepa möjliga ventilinställningar offline för att på så sätt kunna hitta de optimala inställningarna med hänsyn till maximal verkningsgrad. Givet motorvarvtal och luft-/bränsleblandning är optimeringsrutinen kapabel att generera nivåkurvor motsvarande optimala inställningar. Rutinen fungerar bra för vissa driftpunkter och sämre för andra och slutsatsen är att mer arbete behövs, framför allt rörande modellering av själva förbränningen, i nuläget beskriven av Vibefunktionen.

KTH Industriell teknik och management

Master of Science Thesis MMK 2010:18 MFM135

Control Strategy for Fully Flexible Valve Technology

- Development of a four-stroke combustion model to predict optimal valve settings

Joakim Karlsson

Approved	Examiner	Supervisor
2010-11-19	Hans-Erik Ångström	Richard Backman
	Commissioner	Contact person
	AVL SPEAB	Richard Backman

Abstract

As emission legislations across the world continuously pushes engine development forward, engineers constantly need to come up with and implement fuel saving technologies. During the last decade, variable cam phasing has become a popular solution to increase gas exchange efficiency. This configuration is typically mechanically constrained by camshaft limitations, and a solution to circumvent this problem would be to use a different valve actuation principle.

One example of this is to use pressurized air controlled by electrical solenoids. Such a system has been developed by *Cargine Engineering* and this provides the starting point for this work. To be able to operate the valvetrain on an actual engine, a control system is needed. For this purpose, the AVL developed *Raptor* provides a suitable design environment. The *Simulink* implementation is straightforward to alter and customize and based on feedback from position sensors mounted on each valve, closed loop control on both intake and exhaust valve timings has been implemented. Together with the implementation of a script for predefining a large number of operating points that the engine test bed can then execute automatically, gathering of large quantities of data has become easy.

Based on this data set, an existing combustion model for predicting a full four-stroke cylinder pressure trace has been modified. Focus has been on taking the influence of valve timings and lift heights into account and the result is a model that, for the current data set, predicts IMEP with a standard deviation of 4.9% for the relative error. The corresponding relative error standard deviation for PMEP estimation is 8.8%.

With this model accuracy, an optimization routine for looping through possible valve settings offline has been developed. This routine is able to, based on user defined engine speed and fuel mass (and assuming stoichiometric combustion), provide a level curve corresponding to a map of optimal valve settings with respect to minimal fuel consumption. This routine works well for certain operating points, but shows low prediction accuracy for others. The conclusion is that more work needs to be done regarding modelling of the actual combustion event, currently characterized by the Vibe function.

Preface

Many hours of thinking, frustration and countless discussions have gone into this project. The author wishes to take the opportunity to give a special thanks to a few people.

First of all thanks to Richard Backman, AVL SPEAB, who has been supervising the project and been very helpful in giving valuable hints and pointers during the model development. He also provided the foundation for the combustion model, which made this work a lot easier.

Thanks also to Jonas Cornelsen, AVL SPEAB, who has provided excellent support when it comes to troubleshooting and configuration of the *dSPACE* system. Jonas has also given some valuable hints concerning *Simulink* and *Matlab* programming technique.

The third thanks goes to Henrik Dembinski, formerly AVL SPEAB, for spending almost half a day introducing the single cylinder environment. He has also had to put up with a number of phone calls during this work, and the answers he delivered somehow always seemed to solve the problem at hand.

Finally, thanks to Professor Hans-Erik Ångström, Gustav Ericsson and the other employees at the Royal Institute of Technology for providing a fascinating educational experience during the last few years. After spending 18 years in school, I don't think I have ever learned more than I did at the Department of Internal Combustion Engines.

Södertälje, October 2010
Joakim Karlsson

Contents

1. Introduction

This master thesis is commissioned by and carried out at AVL SPEAB, Södertälje. The testing environment is a test cell with a single cylinder engine, an electric brake, an electronically controlled pneumatic/hydraulic valve actuation system and a flexible control and maintenance system for cell supervision and engine control.

1.1 Background

During the last 30 years, the primary target variable for engine development engineers has been fuel consumption and resulting emissions. As the continuously updated emission legislations are becoming stricter and CO_2 emissions are becoming an increasingly important factor, more development resources have been directed towards efficiency improvements and fuel consumption reductions. To improve the overall engine efficiency is a great challenge and to complicate things additionally, this should be achieved without losing power output and performance. Consequently, this means that every small efficiency gain in the engine subsystems will be of importance, whether it is bearings with lower friction, more thermally durable materials or any other alterations. One of the most essential subsystems where improvements can be accomplished is the valvetrain system. Traditionally, the gas exchange process (i.e. induction of fresh air and evacuation of exhaust gases) in the ICE (Internal Combustion Engine) is controlled by poppet valves actuated by camshafts (or in some cases push rods), figure 1.1. This strictly mechanical solution is preferred because of its reliability, relative simplicity and its inherent synchronization with the crankshaft. However, because the average ICE operates over a wide speed and load range, compromises have to be made in order to maintain driveability and functionality across the operating range. A number of automotive companies have proposed and developed various solutions to this problem. Camshaft-based VVT (Variable Valve Timing) systems are becoming increasingly common but due to limited mechanics the adjustment range is still comparatively small and far from optimal. By using other actuating principles, for instance an electro-pneumatic or hydraulic system, these compromises can be circumvented and the gas exchange process can be made more efficient for a greater number of operating points. A fully flexible valvetrain system with the possibility to adjust lift height, opening and closing times for each valve individually, is an extremely useful tool for investigating valve timing strategies as well as different cycle strategies (4-stroke, 6-stroke, 8-stroke, Atkinson, etc.) and cylinder deactivation for multi cylinder engines.

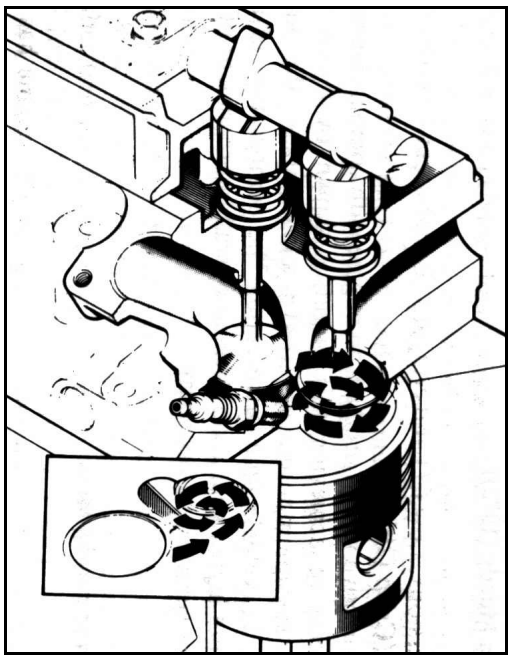

Figure 1.1. Example of a camshaft actuated valvetrain.

1.2 Objective

The primary task of this work is to modify and continue developing an existing combustion model that takes the immense freedom of the free valves into account. The model should also, based on current operating point, suggest a valve strategy that provides the lowest specific fuel consumption, i.e. gives the highest efficiency. To accomplish this, a number of things must be done prior to the model development. The existing control system must be further developed in a number of areas; requested timings must be fulfilled and a safety system to avoid collision between piston and valve needs to be designed. Figure 1.2 shows an example of the variation possibilities implicated by the flexible valvetrain.

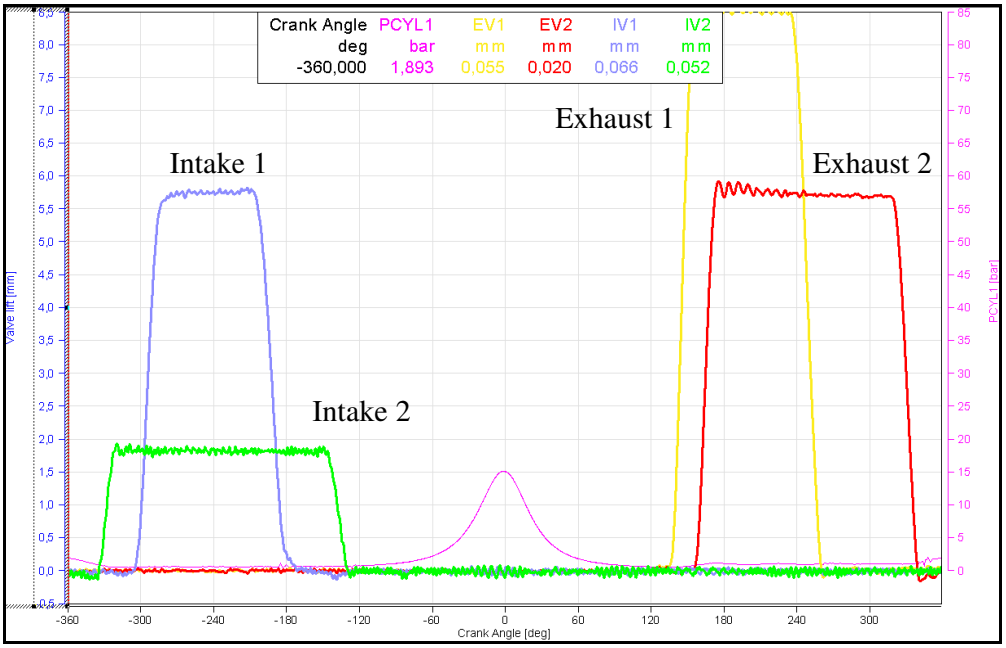

Figure 1.2. Example of possible valve settings.

Furthermore, the engine test bed should be modified to include a new measurement system which is strongly linked to the engine control system, making the entire measurement process more efficient. The combustion model has a solid foundation developed prior to this work and the main objective is to increase modeling accuracy of the gas exchange revolution, since the closed part of the cycle has already proven to give good results. The entire project specification can be read in appendix A.

1.3 Limitations

The project will only consider steady-state engine operation in a test cell environment. This means that no transient tests will be conducted and the system will only be operated around room temperature. The system is not ready for implementation in an actual car and focus will be on maximizing efficiency on the engine currently installed in the test cell. The valve lifts and timings have highest priority in the modeling part but spark timing, fuel pressure, SOI (Start Of Injection), etc. should also be taken into account.

Due to the limited time frame and the almost infinite number of combinations when more than two valves are used (e.g. different lift height on the two intake valves, timing offsets, etc.) the main part of this work will be to focus on one intake valve and one exhaust valve. Another distinction needs to be made regarding usage of the valves. With individually controlled valves, it is possible to choose whether to use e.g. intake valve 1 or intake valve 2. From now on, if nothing else is stated, exhaust valve 2 and intake valve 2 (defined in figure 1.3) have been used during the measurements. The primary reason for this is that post-processing of data becomes easier and the chosen valves also turned out to display the smallest variations on a day-to-day basis.

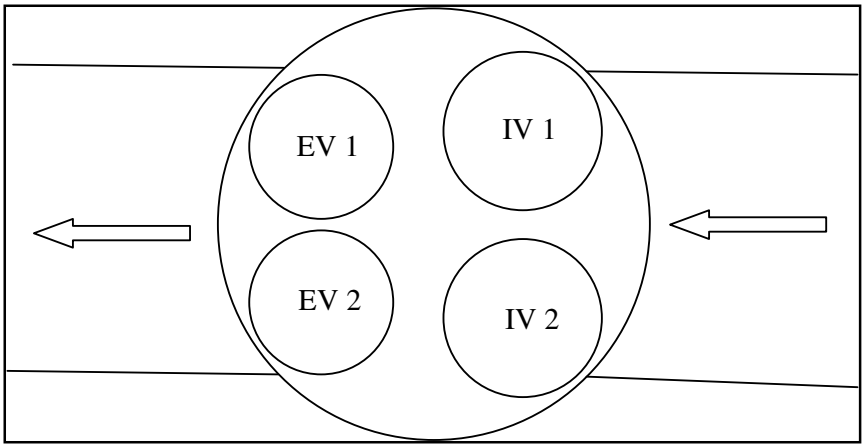

Figure 1.3. Definition of valve numbering on the single cylinder engine used in this work. The arrows mark the nominal air flow direction and the engine is seen from above.

1.4 Working methodology and definitions

All programming and model development is done in *Mathworks' MATLAB* and *Simulink*, which are extensively used for all sorts of engineering purposes. The model will be integrated into Raptor, an in-house developed engine control system used at AVL for managing both single and multi cylinder engines. Raptor is based entirely on *MATLAB* and *Simulink* code and communicates with the engine via a *RapidPro* control unit and a *MicroAutoBox* developed by *dSPACE GmbH*. The user interface is designed in the software *ControlDesk*, supplied by *dSPACE*. An overview of *Raptor* is shown in figure 1.4.

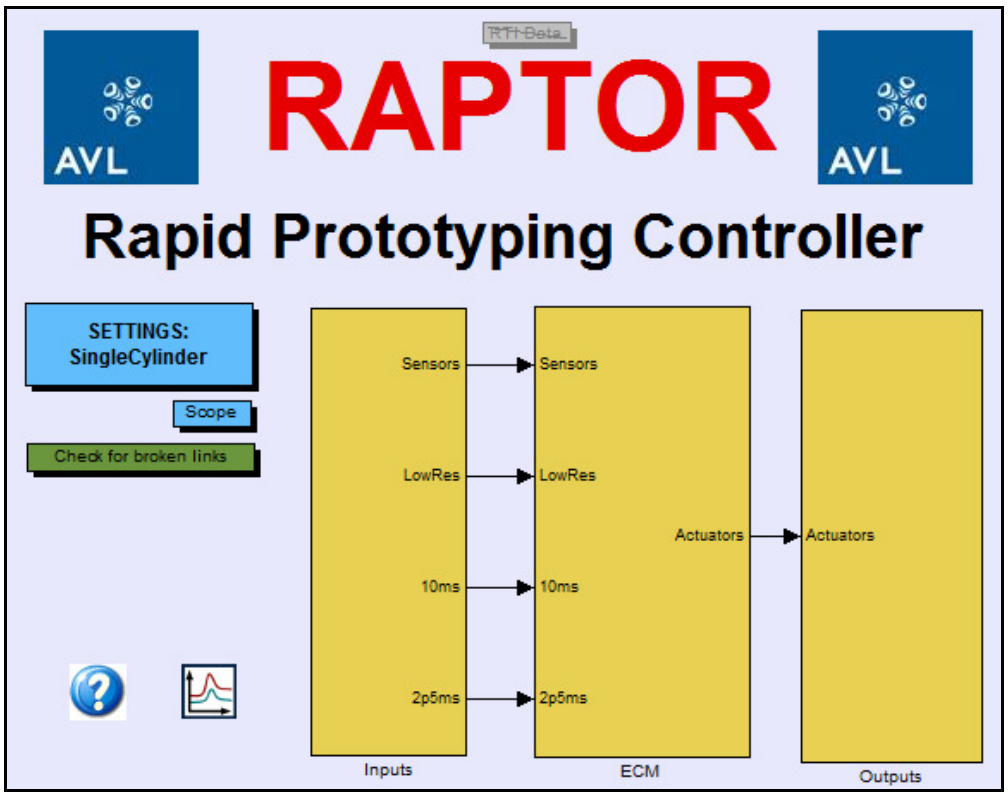

Figure 1.4. Overview of *Raptor* adjusted for use in the single cylinder environment. The 'Inputs' block reads measured signals with the appropriate resolution, the 'ECM' block is the core of the control system and the 'Outputs' block sends out actuator voltages, etc.

For simplicity, it is practical to define valve timings with aid from figure 1.5, where two generic intake and exhaust valve lifts are depicted. Since valve openings and closings typically occur in the region of one of the three piston turning points (crank angle 180, 360 and 540 in the figure), it is convenient to refer to valve timings as "early" or "late" with respect to one of these points (TDC – Top Dead Center – in this case is gas exchange TDC). Thus, if nothing else is stated, the following convention will be used from now on:

- Early EVO (negative) occurs before BDC 1 and late EVO (positive) occurs after BDC 1
- Early EVC (negative) occurs before TDC and late EVC (positive) occurs after TDC
- Early IVO (negative) occurs before TDC and late IVO (positive) occurs after TDC
- Early IVC (negative) occurs before BDC 2 and late IVC (positive) occurs after BDC 2.

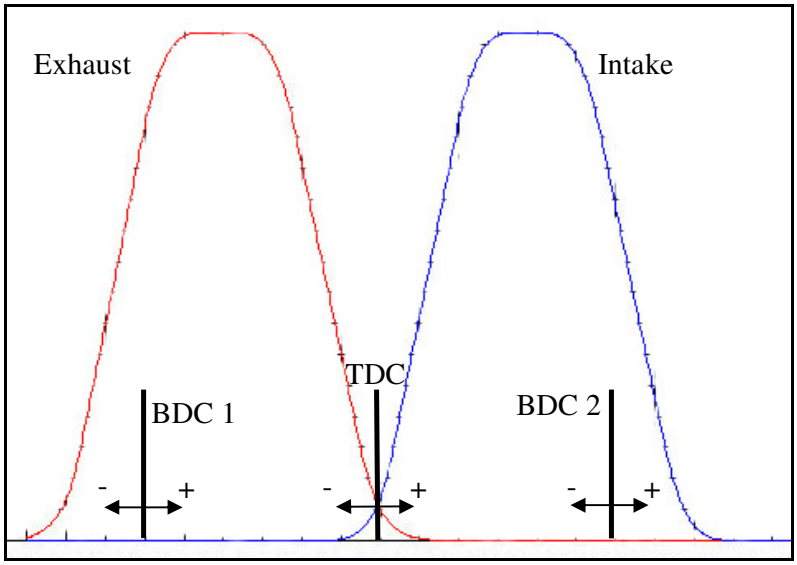

Figure 1.5. Valve timing reference points and corresponding sign conventions.

The abbreviated valve timings are Exhaust Valve Opening, Exhaust Valve Closing, Intake Valve Opening and Intake Valve Closing. Another essential parameter is the valve overlap, i.e. the phase when both intake and exhaust valves are open simultaneously. The size of the valve overlap is given by

$$OL = \theta_{EVC} - \theta_{IVO} \tag{1.1}$$

From this definition, it is evident that *OL* can assume positive (denoted PVO) and negative (denoted NVO) values and the implications from this are discussed in later chapters.

A few thermodynamic quantities need to be defined as well; the pressure-volume-diagram in figure 1.6 provides the basis for these definitions. From now on, if nothing else is stated, combustion TDC occurs at crank angle 360 and is denoted TDC_{firing}. All values referring to pressure levels are considered to be absolute values.

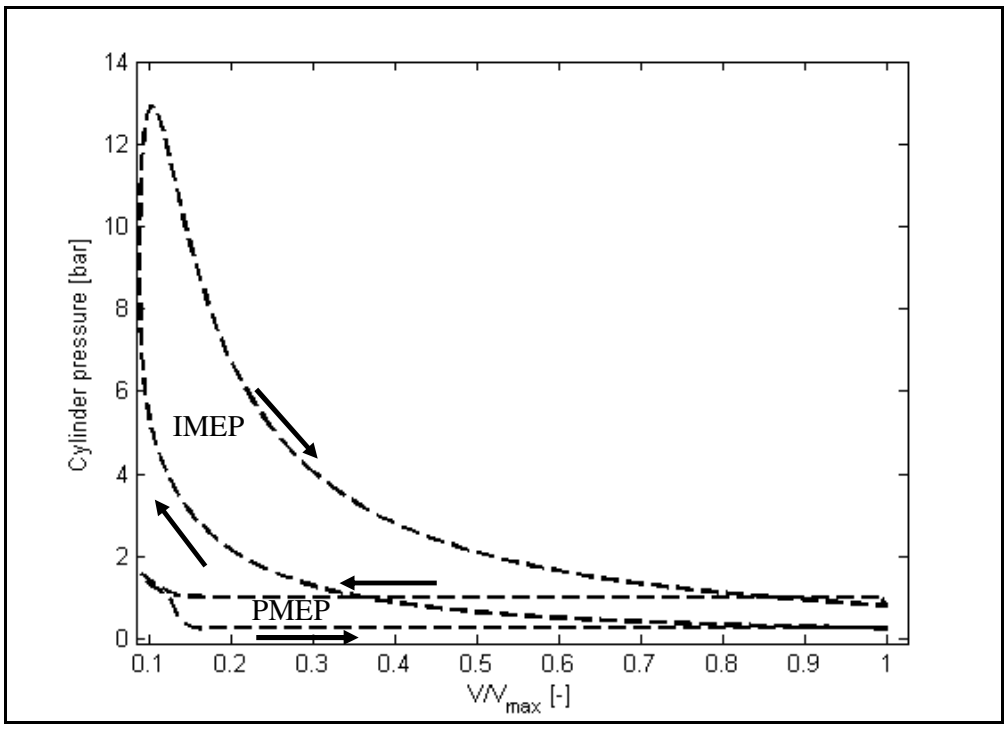

Figure 1.6. Cylinder pressure plotted against normalized cylinder volume with definitions of IMEP and PMEP marked along with arrows marking the four strokes.

The Indicated Mean Effective Pressure (IMEP) is the work produced during the compression and expansion strokes, i.e.

$$IMEP = \frac{1}{V_d} \int_{180}^{540} pdV \tag{1.2}$$

where p is the cylinder pressure, V is the cylinder volume and V_d is the displaced volume. The Pumping Mean Effective Pressure (PMEP) is the work produced during the exhaust and intake strokes, i.e.

$$PMEP = \frac{1}{V_d} \int_{0}^{180} pdV + \frac{1}{V_d} \int_{540}^{720} pdV \tag{1.3}$$

PMEP can, for forced induction engine configurations, become positive but for the experiments in this report, PMEP will always be negative, thereby describing an efficiency loss.

For the entire four-stroke cycle, the Net Mean Effective Pressure (NMEP) is defined as

$$NMEP = IMEP + PMEP \tag{1.4}$$

and from the definition it is evident that a higher NMEP value is equivalent to a higher overall engine efficiency. The term XMEP will occasionally be used in this report and this simply refers to any possible mean effective pressure (i.e. IMEP, PMEP, NMEP, FMEP, etc.) and from the context in each case it should be clear which one is intended.

2. Valve actuation systems

A number of various valvetrain systems exist today. The most common arrangement in today's automotive industry is to use one camshaft for the intake valves and one camshaft for the exhaust valves. Car makers that want to offer higher levels of performance (and of course higher prices) allow some type of cam phasing, which means that the entire valve lift profiles can be moved relative to each other. The mechanical constraints typically limit the variation range to around 50 CAD (Crank Angle Degrees). While the number of valvetrain systems capable of phasing the lift curves steadily increases, very few systems currently in production are able to handle variable lift heights. There are, however, exceptions and a couple of them are listed below.

2.1 Existing systems

For each new model year, more advanced valve actuation systems with higher degree of flexibility appear to reach mass production. Early versions of Honda's *V-Tec* system offered increased high-end performance suitable for the characteristically high Honda engine speeds. BMW's *Valvetronic* system is considered one of the most advanced systems currently in mass production, enabling almost completely unthrottled operation. Fiat's *MultiAir* system was recently introduced and is similar to the BMW system but with a different operating principle. More advanced systems for research purposes include the hydraulically controlled *Lotus AVT* system.

2.1.1 Honda V-Tec

Hondas *V-Tec* system (Variable valve Timing and lift Electronic Control) was introduced in the late 1980's and essentially consists of a camshaft with two different cam lobes, figure 2.1. During low and moderate engine speeds and loads, the valves are operated with relatively short opening durations and low lifts. As speed and load increases, hydraulic pressure locks the high-speed and the low-speed lobe together, causing the valve to follow the profile imposed by the high-speed lobe (i.e. longer duration and higher lift). It is advantageous to link duration and valve lift to each other in order to reduce the mechanical load on the valves, i.e. it could be difficult to combine short durations and high lifts with this mechanical installation. The switching between the two modes is done via a hydraulic unit which is electronically controlled through a solenoid.

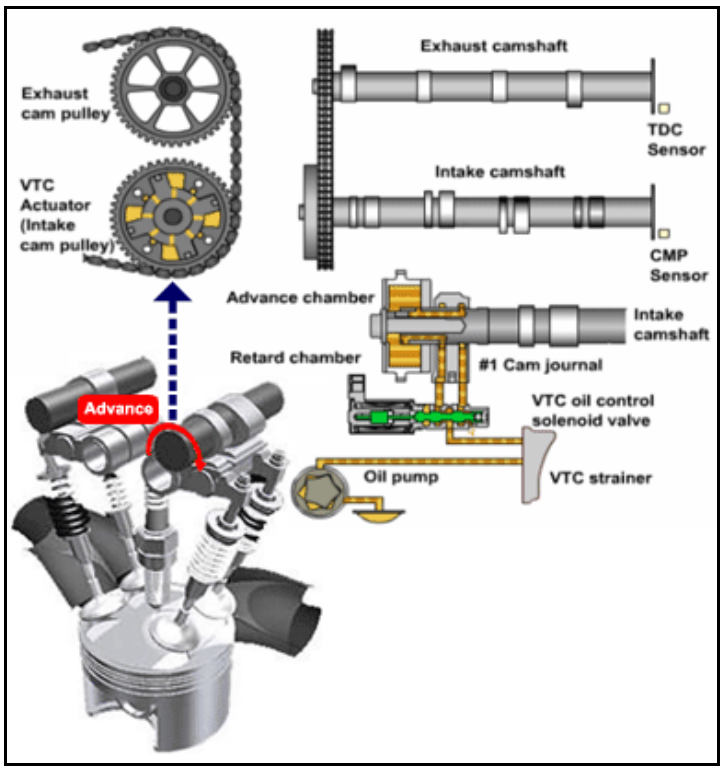

Figure 2.1. Sketch of a *V-Tec* valvetrain system, in this case only the intake camshaft is equipped with two separate lobes, the solenoid control strategy is based on engine speed and load.

Various development modifications of this configuration have been introduced over the years, including cam shafts with three different cam lobe profiles.

2.1.2 BMW Valvetronic

The BMW valvetrain system was introduced in 2001 for a handful of different engine configurations. The system is able to continuously vary both intake valve lift height and phasing and is especially useful since it enables early IVC and thus reduced pumping losses, chapter 2.3.2. Furthermore, the BMW engines can operate almost completely unthrottled but the throttle plate is actually kept since it is used during cold starts and in limp-home safety mode. To make the Valvetronic system work, the cylinder head is equipped with an extra set of rocker arms between the camshaft and the valve stem, figure 2.2. These rocker arms can, thanks to an electronically controlled additional camshaft, pivot freely. The mechanism makes sure that valve duration is a function of lift height, thereby avoiding excessive and possibly harmful valve accelerations and seating velocities. This lift mechanism is combined with a phaser, which makes the choice of IVO and IVC almost independent of each other. The individual intake valve lifts can also be offset relative to each other in order to increase air charge motion even more around idling speed.

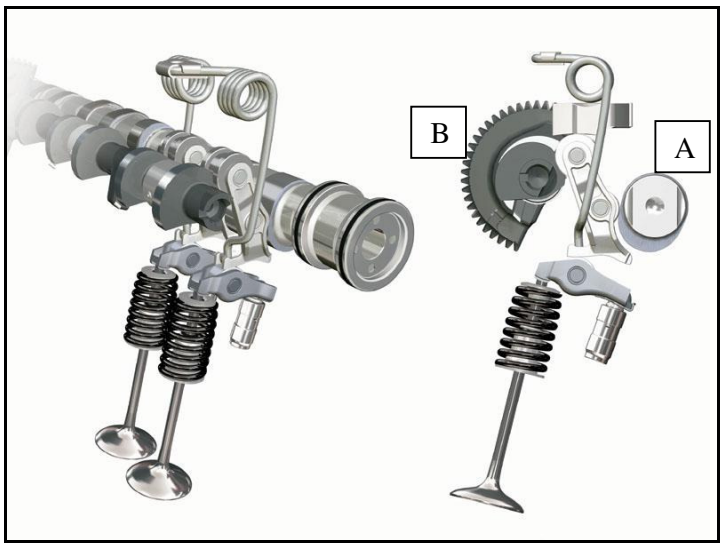

Figure 2.2. The engine intake side uses the *Valvetronic* system; the movements of the original camshaft (A) and the eccentric camshaft (B) are combined to generate continuously variable valve lifts.

Since the *Valvetronic* system requires stronger valve springs than the same engine configuration with fixed cam shafts, a small efficiency drop at higher engine speeds will occur. Because of this, the high performance (high speed) BMW models currently run without the *Valvetronic* system.

2.1.3 Fiat MultiAir

Fiat introduced the *MultiAir* system in 2009 and it has currently been implemented on a couple of vehicle models. A *MultiAir* engine is based on a traditional mechanical exhaust camshaft. This is connected to the intake valves via a hydraulic unit, figure 2.3. Since the oil is practically incompressible it works as a rigid element, thereby causing the intake valves to be synchronized with the exhaust valves when nothing is done. Through the use of an electronically controlled solenoid valve, however, the oil volume can be regulated and by timing this solenoid valve opening the intake valve timings become decoupled from the exhaust camshaft. The solenoid control is also sufficiently fast to enable multiple valve lifts, which could be used to induce turbulence at lower engine loads.

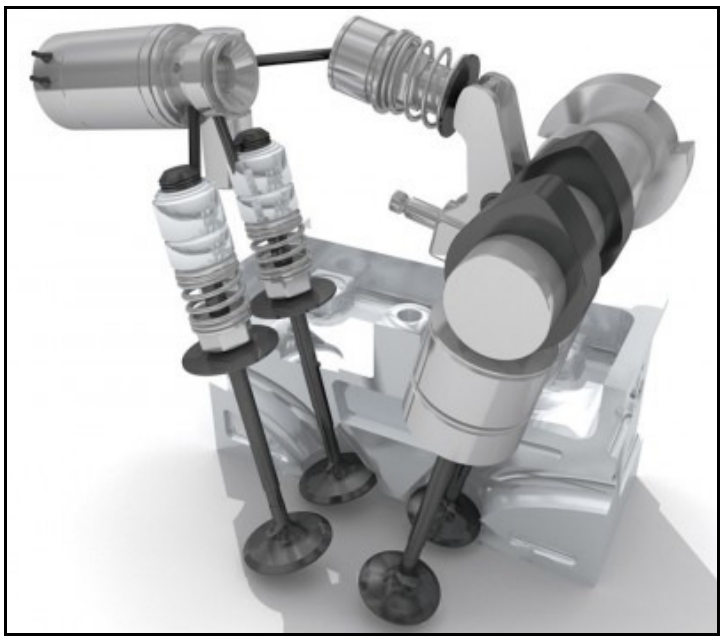

Figure 2.3. *MultiAir* valvetrain installation; the single camshaft is mechanically connected to the exhaust valves and the hydraulic unit incorporates the intake valves into the assembly.

2.1.4 Lotus AVT

The *Lotus AVT* (Active Valve Train research system) is a fully variable valvetrain system that, similarly to the *Cargine* system, is primarily used for research and development purposes rather than mass production (although *Cargine* are aiming for mass production). Instead of camshafts, hydraulically operated actuators and electro-hydraulic servo valves are installed above the valves. It is also equipped with position transducers, which makes the entire valvetrain assembly very similar to the one developed by *Cargine*. The major difference is the use of hydraulics instead of pneumatics to control the actuator and valve motion and, because of the reasons discussed in chapter 2.2, hydraulics are generally a preferable working fluid.

2.1.5 Cargine Free Valve Technology

The valvetrain system used in this project comes from *Cargine Engineering* and will be more thoroughly described in chapter 2.2. The pneumatics used to actuate the valves imposes certain limitations on the variability range, which cannot be seen in e.g. the *Lotus* system. Based on feedback from position sensors fitted to the valves, independent variation of lift height, opening and closing of each valve is achieved. The system behaviour is engine speed dependent since all control signals are approximately constant in time. The control signal implementation also limits the lift height variation range to a certain extent, valve lifts below 3 mm are difficult to maintain stable.

2.1.6 System comparison

These systems all have their own specific advantages and disadvantages and a few of them are listed in table 2.1. The flexibility and complexity ratings are based on subjective thoughts.

Table 2.1. Overview of valvetrain system differences, numbers are approximate and may deviate for certain engine specifications.

System	Approximate phasing range	Approximate lift range	Flexibility	Complexity	Special features
V-Tec	Long dur. 260 Short dur. 210	High 10 mm Low 7 mm	Very limited, only two or three settings	Simple and easily controllable	Noticeable mode switch
Valvetronic	Possible phasing around 60 CAD relative to crankshaft	0.3-9.9 mm	Adjustable intake and exhaust valves, large variation span	Slightly complex installation, advanced control	Completely unthrottled operation
MultiAir	Duration from 60 to 260 CAD	1-8 mm	Only intake valves adjustable, large variation span	Simple installation, advanced control	Multiple valve lifts possible
Lotus AVT	Limited by collision occurrences	Limited by collision occurrences	Practically unlimited	Advanced installation and advanced control	Possible to specify custom lift curve appearances
Cargine	± 100 CA from piston turning point (i.e. TDC/BDC)	3-9 mm	Limited by counteracting cylinder pressure and safety system	Mechanically simple, sometimes difficult to achieve stable operation due to controllability problems	Highly engine speed dependent behaviour

2.2 Free Valve Technology

The *Free Valve Technology* system, figure 2.4, has been developed by *Cargine Engineering* and the working principles of the system are extensively described in e.g. [1] and [2]. Hence, the hardware will not be meticulously described here. However, the system has a few key features, which are essential to account for during the model development.

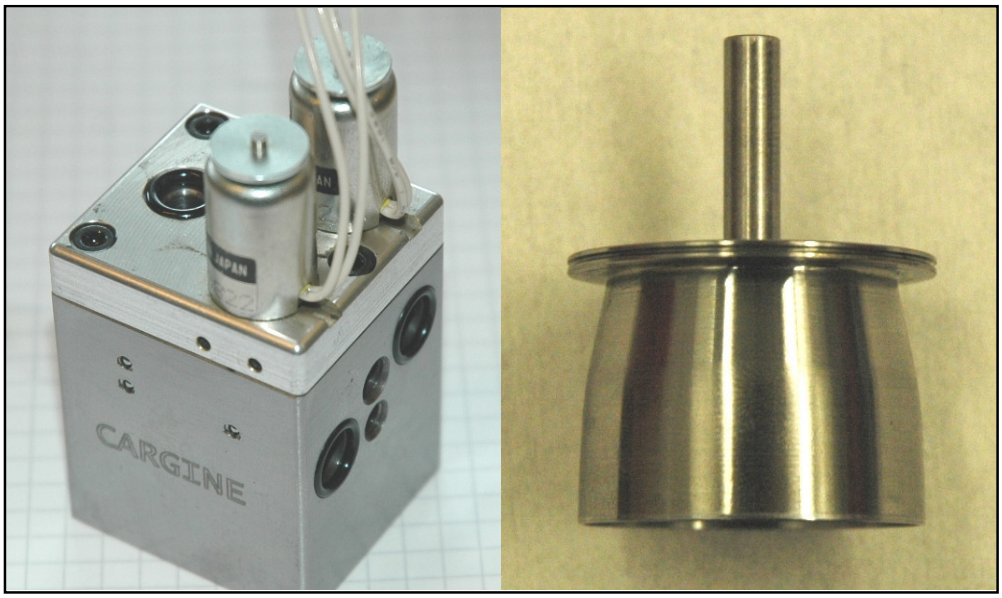

Figure 2.4. Actuator assembly (left) and the slightly conical actuator piston (right) [1].

At higher loads, the pressure compensation implemented at EVO is insufficient, since the air supply pressure to the actuators is limited. For medium and high loads (more than 5 bar IMEP), a supply pressure of 6 bar has been used. This makes early EVO possible, although the requested lift height may not be achieved. Increasing supply pressure, however, causes the valve lifts to become slightly less stable, most likely because the test cell is currently equipped with narrow flow paths. This could impose a restriction in the flow field resulting in air pressure pulsations which might explain the oscillatory behavior. Higher supply pressure also increases power consumption (and consequently parasitic losses), see chapter 2.3.10 for details. For lower loads, a supply pressure of 4 bar has been used. At the moment, this supply pressure control is not implemented in *Raptor*, but this could be done e.g. in order to always use the lowest supply pressure necessary to obtain desired valve behaviour. This implementation would also require some test bed hardware changes and has therefore not been considered for this work.

All electrical solenoid signals used to control the oil and air flow in and out of the actuators are approximately constant in time, which means that there is a strong dependence on engine speed. The algorithms for execution of the control signals developed in [1] have essentially been left unchanged, as well as all calibration parameters concerning electrical delays and air evacuation delays. The control signals for the two solenoids are shown in figure 2.5.

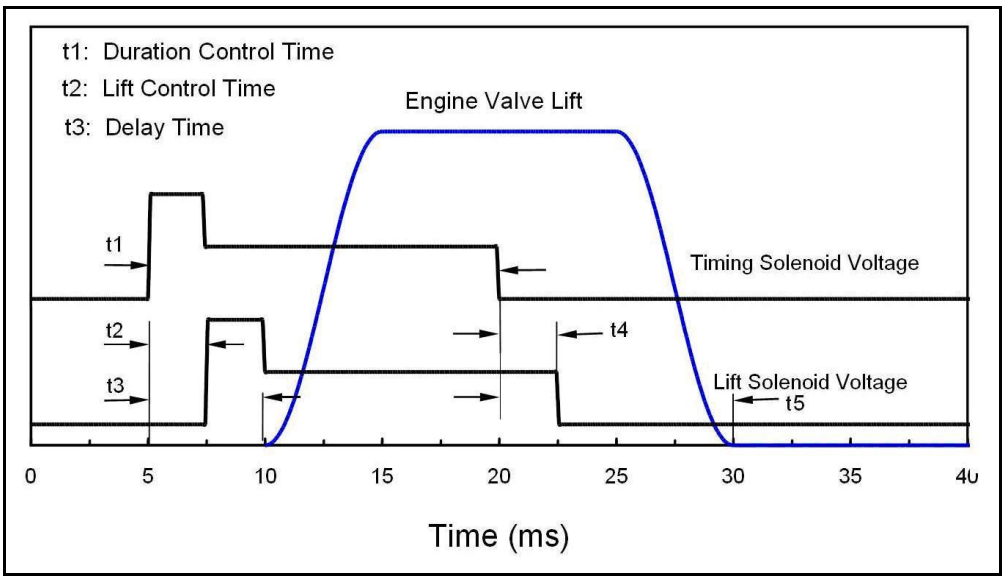

Figure 2.5. Control signals (voltage) for the two solenoids for a generic valve lift [1].

The engine speed dependence imposes certain limitations on the valve variability:

- As engine speed increases, low valve lifts are impossible because the lift control time t_2 decreases and, as a consequence, unstable valve lifts are unavoidable
- At higher engine speeds short valve durations are difficult to obtain because the air charging and air discharging phases will coincide and hence be active simultaneously, causing unstable valve operation
- For higher engine speeds, the entire valve lift profile will change appearance drastically, figure 2.6, which of course also affects the gas exchange behavior and efficiency.

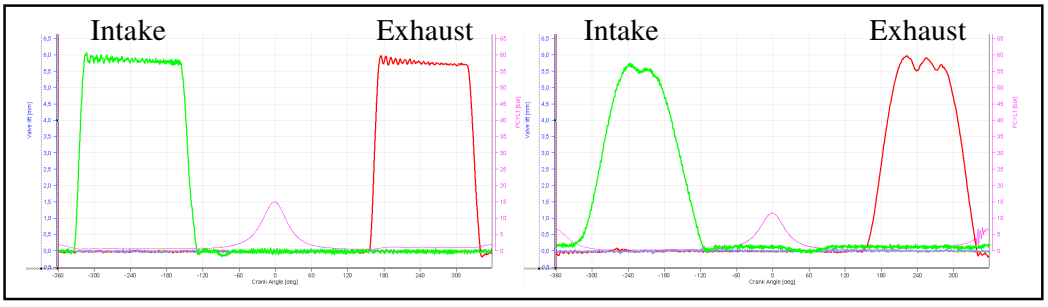

Figure 2.6. Intake and exhaust valve lift at 800 rpm (left) and 3000 rpm (right). Requested timings and lift heights are identical, but the curves look very different. The purple line is measured in-cylinder pressure.

From now on, the valvetrain system will be abbreviated EPVA, Electronically controlled Pneumatic/hydraulic Valve Actuation system.

2.3 Variable valve actuation characteristics

With the valve variability available, new possible engine operation modes become accessible. A few valve settings are considered so special that they are actually associated with special engine cycles, such as Atkinson and Miller cycles. Several other engine parameters can be affected solely by clever usage of the valve variability and a few features are specific for the electro-pneumatic system used in this work. The most important characteristics and operating modes are listed below.

2.3.1 Increased torque and power output

Both intake and exhaust systems can be thought of as a number of control volumes. In each of these control volumes, the pulsating, unsteady gas flow will give rise to standing wave oscillations, figure 2.7. For steady state engine operation, these oscillations will have a well defined frequency, which will be influenced by the valve timings as well as other operating parameters. For mechanically constrained valvetrains, the intake and exhaust valve timings must be a compromise between combustion stability at low engine speeds and high power output at high engine speeds. Increased freedom in deciding of the valve timings will enable better utilization of the pulsating gas flows across the entire engine operating range. To quantify this performance increase, a good reference term is the volumetric efficiency, which relates the inducted air volume to the volume displaced by the piston motion. In other words,

$$\eta_{vol} = \frac{\dot{m}_a}{\frac{1}{2}\rho_{a,i} V_d N} \tag{2.1}$$

where $\dot{m}_a$ is the air mass flow rate through the intake system, V_d is the displacement volume, N is the engine speed and $\rho_{a,i}$ is the inlet air density. For naturally aspirated engines, this may be approximated by the atmospheric density, implying that the volumetric efficiency defines the performance of the entire induction system. For a forced induction engine configuration it is more relevant to use the actual inlet air density (computed from the ideal gas law), in which case the volumetric efficiency is only an indication of the inlet port and valve performance.

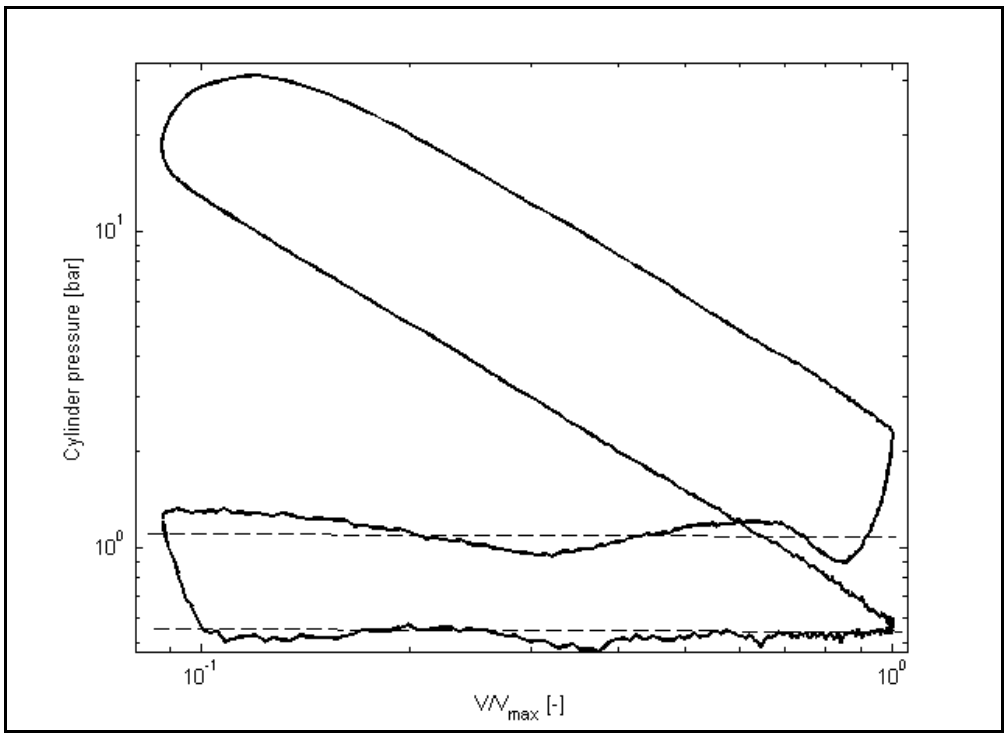

Figure 2.7. Pressure trace showing a clear pressure oscillation during the exhaust stroke. For comparison, the measured exhaust and intake manifold pressures (averaged) are also drawn (dashed).

However, maximizing the volumetric efficiency is not always desirable. For low and medium engine loads, it is advantageous to reduce the volumetric efficiency by altering the inlet valve settings. This enables partly or fully unthrottled engine operation.

2.3.2 Unthrottled engine operation

For a conventionally configured Otto engine, the load is controlled by restricting the air flow into the engine using a throttle. At part and low load this throttle plate causes a near vacuum in the intake manifold with pumping losses as an unavoidable consequence. This problem becomes more noticeable as load decreases and absolute intake manifold pressures of 20 kPa (absolute) or less are a possibility. By removing the throttle plate and controlling the air entering the cylinder by controlling the intake valves, the intake manifold pressure can be kept close to atmospheric levels regardless of operating points, thereby reducing overall pumping losses. Figure 2.8 shows a gas exchange stroke where intake valve opening has been delayed. Early intake valve closing will also aid in reducing pumping losses.

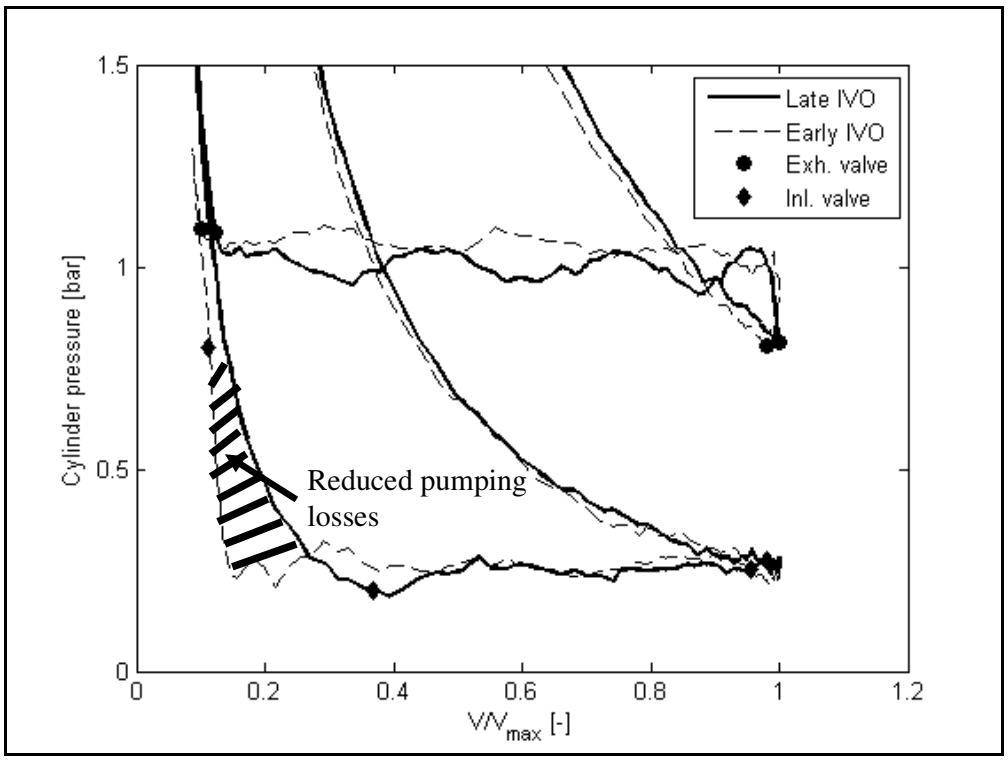

Figure 2.8. Late IVO means 60 CAD ATDC and early IVO means 15 CAD ATDC. Pumping losses are 0.64 and 0.75 bar respectively.

2.3.3 Variable compression and expansion ratio

Using very simplified thermodynamic theory, i.e. assuming that combustion takes place instantaneously at TDC_{firing} and compression and expansion both occur isentropically (without heat exchange) it can be shown that the overall engine efficiency can be calculated as

$$\eta_{tot} = 1 - \frac{1}{r_c^{\gamma-1}} \tag{2.2}$$

where r_c is the compression ratio and γ is the ratio of specific heats. From the equation it can be seen that a higher compression ratio gives higher efficiency. However, a higher compression ratio also increases the risk of knock, which means that a dynamic compression ratio (dynamic IVC, figure 2.9) that can be altered as speed, load and possibly even fuel quality varies would be advantageous. A dynamic compression ratio means that for each IVC timing occurring either before or after BDC2, the effective compression ratio will be smaller than the geometric one since the volume ratio decreases.

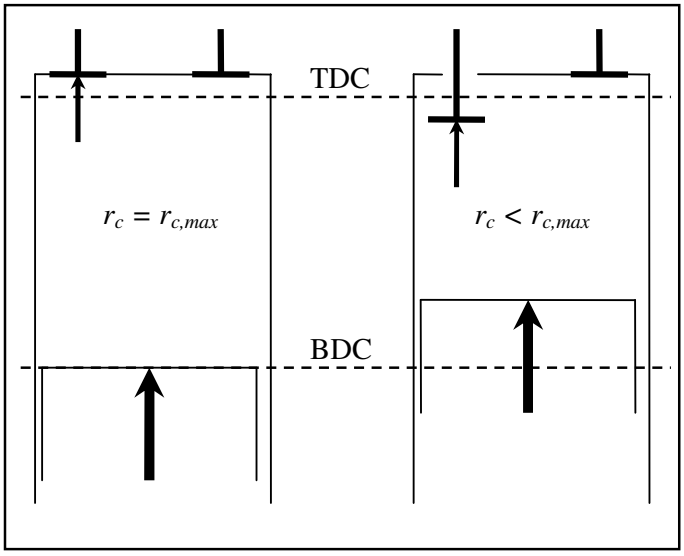

Figure 2.9. Schematic illustration of variable IVC timing on compression ratio. Left picture has IVC at BDC2 which gives maximum compression ratio. To the right, IVC occurs after BDC2, which effectively gives a lower compression ratio.

The same situation applies during the expansion stroke, where the default EVO timing is usually placed to give maximum power, i.e. optimized for high engine speeds. Early EVO aids in evacuation of the exhaust gases before the piston approaches TDC, known as blowdown. As engine speed decreases, EVO occurs much too early to extract full expansion work from the piston. This dilemma can also be counteracted by using a flexible valvetrain system.

2.3.4 Internal EGR control

In CI (Compression Ignition) and direct injected SI (Spark Ignition) engines operating under stratified conditions, the three-way catalytic converter is ineffective due to the overall lean combustion. Therefore, other emission control techniques must be used and the simplest one is EGR (Exhaust Gas Recirculation) control. For this purpose, it is conventional to use an external EGR system to transfer the hot exhaust gases back to the intake manifold. By adjusting valve timings appropriately, a similar effect can be achieved without the need for an external EGR system. Early EVC and short inlet valve duration will contribute to increasing the residual gas fraction. EGR control is particularly helpful when it comes to reducing NO_x emissions.

2.3.5 Idling stability

As a consequence of increasing the residual gas fraction, idling stability is negatively affected. By compromising between the internal EGR and idling stability requirements, the valves can be adjusted to satisfy both requests simultaneously.

2.3.6 Air charge motion

Combustion stability is strongly connected to the burn rate. This is affected by e.g. the residual gas amount and the air charge motion within the cylinder. SI engines rely heavily on turbulent flame propagation and the turbulence intensity can be adjusted by altering the intake valve settings. By deactivating one out of two intake valves, the air will enter the cylinder via a flow path that induces swirl and tumble motion, figure 2.10. Another way to increase turbulence is to

postpone IVO until well after TDC. When the piston is traveling downwards at higher engine speeds, this will increase air intake speed, thereby increasing turbulence. When the engine speed is low, this effect isn't that obvious, but by reducing the valve lift, the air will enter the cylinder through a smaller orifice, generating a similarly increased turbulence effect. This is seen in figure 2.11, where the left picture corresponds to low valve lift at low engine speed and the right picture corresponds to postponed IVO at high engine speed.

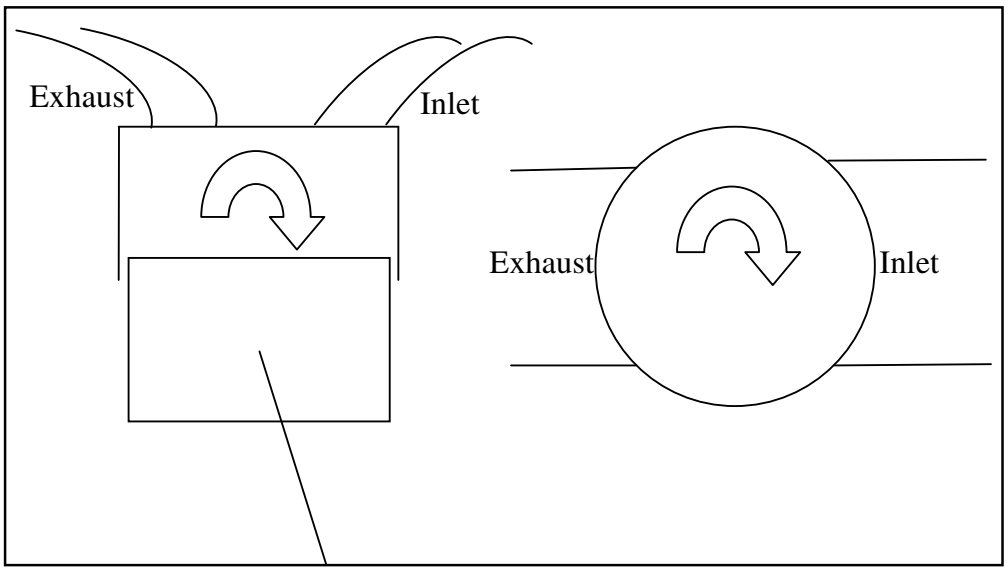

Figure 2.10. Definition of tumble (left) and swirl (right) air charge motion with corresponding schematic engine side and top view respectively.

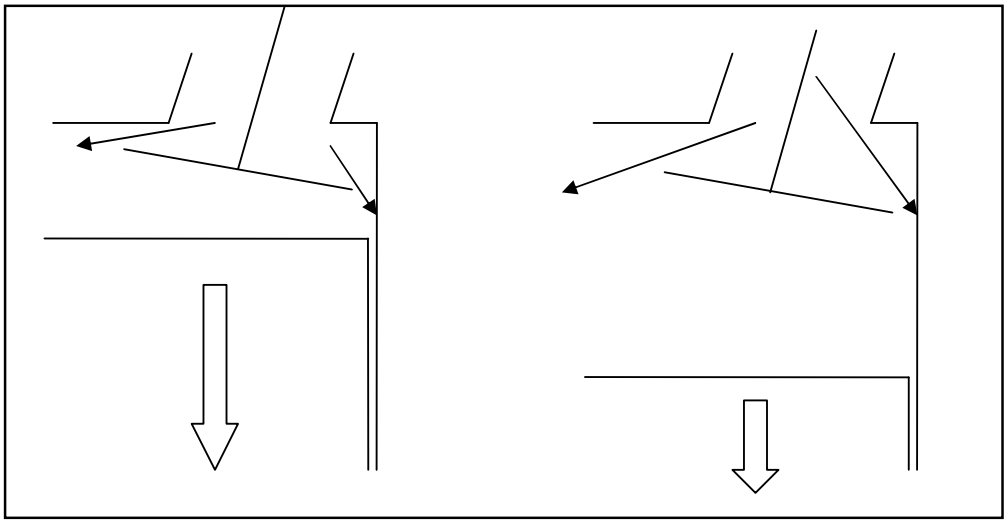

Figure 2.11. At low engine speeds (left), a lower valve lift creates a narrower flow restriction leading to turbulent air charge motion. At higher engine speeds (right), inlet valve opening can be delayed until the piston has a higher downward speed, thereby inducing higher gas velocity and increased turbulence.

According to [3, p195], tumble motion is difficult to achieve when only one intake valve is used. This is because the air flow through the single valve strives towards the ulterior cylinder wall and commences a swirling motion. If two intake valves are used, it is easier to initiate a flow that

hits the cylinder wall and deflects downward. If this is timed relative to the piston motion, a tumbling air charge motion will occur.

2.3.7 HCCI combustion

A lot of research and development effort has been put into the concept of HCCI (Homogeneous Charge Compression Ignition) combustion. The basic operating principle is that a premixed, homogeneous air/fuel mixture enters the combustion chamber, where it is ignited solely via compression heat, figure 2.12. The theoretical advantages are obvious; a rapid, almost instantaneous, combustion keeps the combustion temperature relatively low which reduces NO_x formation, while at the same time generating the high efficiency associated with other CAI (Controlled Auto Ignition) engines, i.e. the Diesel engine. The key control problem is to determine the actual ignition point, something that can be done by varying the compression ratio or changing the residual gas amount. Both these tasks are easily taken care of if the valve timings can be varied.

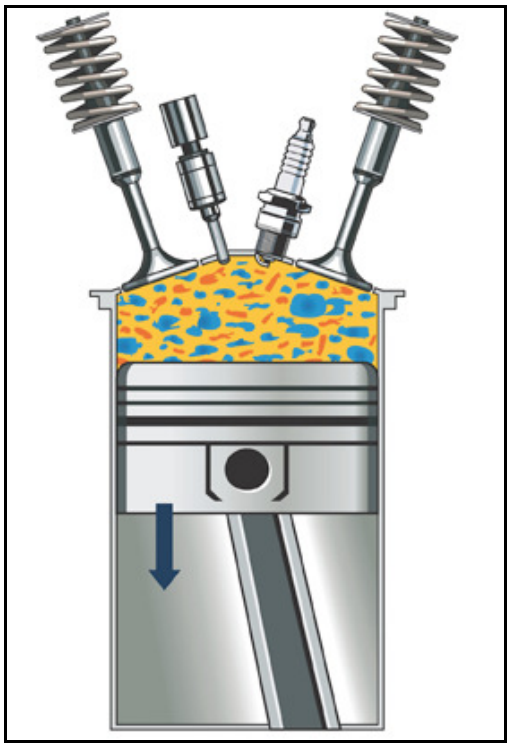

Figure 2.12. Schematic view of spark plug assisted HCCI combustion. The mixture burns uniformly and rapidly across a large area of the combustion chamber.

2.3.8 Cylinder deactivation

The valve control system used in this work is sufficiently fast to deactivate individual valves for time periods as short as one engine cycle. By cutting off fuel injection and spark ignition, individual cycles can be skipped completely. On a multi cylinder engine, this corresponds to cylinder deactivation and on the single cylinder engine used in these tests it corresponds to switching between different strokes, e.g. 4-, 6- or 8-stroke. Control system functionality for running the single cylinder engine in 8-stroke mode has been implemented in a previous work, but this option has not been used for these tests.

2.3.9 Hardware installation space

It is evident that removal of the camshafts and installation of actuators will force changes in the overall engine architecture. The primary concern is the hoses for oil and air supply and the necessary air pump that delivers the pressurized air. However, *Cargine* claims that these issues are manageable and even that the entire installation is smaller than a corresponding camshaft valvetrain [2].

2.3.10 Energy consumption

One critical concern of the EPVA system is the energy consumption. The pressurized air is released into the ambient atmosphere, meaning that the overall energy recovery is very small, in contrast to conventional camshafts where energy is stored in the valve springs. This downside is, to a certain extent, compensated by the fact that the EPVA system makes use of inlet and expansion air but the overall power consumption is fairly high. This work has not put any effort into analyzing the power consumption in detail, but it is evident that increasing number of valves, increasing lift heights and increasing engine speed are all factors that increase power consumption. To translate this power consumption into an equivalent loss in engine efficiency, it is reasonable to assume adiabatic compression [1], giving the air power P_a as

$$P_a = \frac{1}{\eta_p}\frac{1}{1-\gamma}\dot{m}_a RT\left[\left(\frac{p_a}{p_{atm}}\right)^{\frac{\gamma-1}{\gamma}} - 1\right] \tag{2.3}$$

where η_p is the pumping efficiency (assumed to be 50%), γ is the specific heat ratio, $\dot{m}_a$ is the air mass flow supplied to the valve actuators, R is the gas constant for air, T is the air temperature, p_a is the supply pressure and p_{atm} is the ambient pressure. Based on measurements, it can be seen that power consumption increases almost linearly with both increasing engine speed and increasing valve lift height. A graphical representation of this phenomenon can be done by studying the estimated air power consumption P_a as function of total lift height (intake and exhaust valve together) and engine speed, figure 2.13.

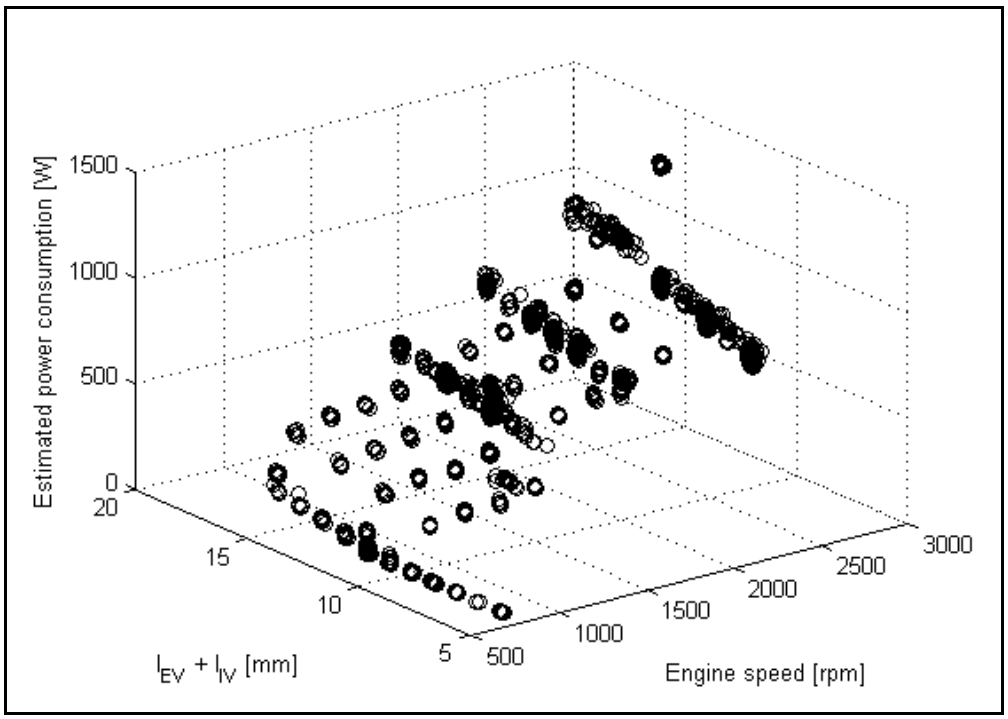

Figure 2.13. Estimated air power consumption plotted versus engine speed and total valve lift height.

It can be seen that power consumption increases as lift height and engine speed increases. At low engine speeds and lift heights, the power consumption approaches zero, because the air mass meter used to track the air supply has too poor resolution. When the term $\dot{m}_a$ in equation 2.3 above approaches zero, the power consumption will therefore do the same. This power consumption can be easily translated to friction losses in terms of losses in mean effective pressure according to

$$p_{AirMEP} = \frac{4\pi P_a}{V_d N \frac{2\pi}{60}} \tag{2.4}$$

The importance of these losses can be understood by looking at the air power MEP, p_{AirMEP}, in relation to IMEP for all operating points, figure 2.14.

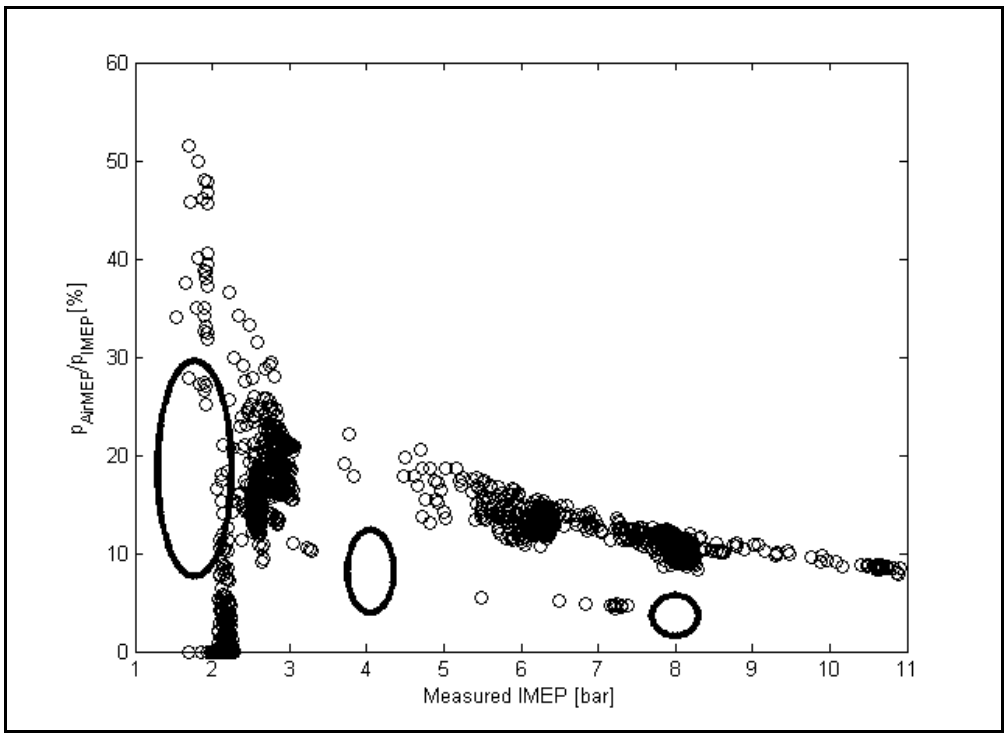

Figure 2.14. Relative torque loss due to powering of the valve air supply as function of engine load. Ellipses indicate approximate friction losses in conventional camshaft valvetrains.

It can be seen the parasitic losses in most cases are substantial. As will be discussed in later chapters, valve lift height has little or no significant impact on combustion performance and it is therefore preferable to keep the lift heights as low as possible to minimize torque losses. At higher loads, one might expect that the relative parasitic losses would be even smaller, but for these operating points the supply pressure must be increased to enable e.g. early EVO, which causes power consumption to rise. The large variation range around 2 bar IMEP comes from the fact that this load point has been tested for several engine speeds. It is also worth noting that all operating points in figure 2.14 are run with two valves. Increasing to three or four valves will naturally increase power consumption accordingly.

Intuitively, it would also be interesting to compare these losses against the ones found in a more conventional production valvetrain. In [6, p738], a few different mechanical valvetrain configurations are listed and depending on engine speed they can also be sorted in the figure above (large black ellipses). It has been difficult to find friction data for a real comparison and these numbers should only be considered a rough indication. An upcoming project within AVL will evaluate the air power consumption in more detail.

2.3.11 Sensitive to varying ambient conditions

Since the actuators rely on an accurate oil supply, large variations in ambient temperature are difficult to handle. This is because oil viscosity increases for decreasing temperatures, which might cause the valves to operate abnormally. Furthermore, as explained in chapter 2.2, the air supply to the actuators might be unsteady, leading to unsteady valve behaviour. This of course contributes to the cyclic combustion variations as well.

3. Experimental setup and measurements

All tests and measurements have been conducted at AVL SPEAB's premises in Södertälje. Only one engine hardware setup has been used and all measurements were planned and organized in advance. The entire measurement schedule with 1800 operating points took just over a week to go through, which largely is thanks to the automatic script explained below.

3.1 Engine and test bed equipment

The test cell is equipped with an AVL Smoke Meter, a Horiba exhaust gas analyzer and an AVL IndiCom data acquisition system. The engine itself comes from the British engineering company *Ricardo* and is a *Hydra Mk3*. The cylinder head is a modified head from a *GM LNF* 2.0 l 4 valve DOHC (Double Over-Head Camshaft) engine and the engine is equipped with both port and direct fuel injection. For the experiments conducted during this work, only direct fuel injection has been used. Table 3.1 shows engine and fuel data associated with the conducted measurements.

Table 3.1. Engine geometry and thermodynamic fuel data.

Parameter	Symbol	Value
Cylinder bore [mm]	B	86
Stroke [mm]	L	94.6
Connecting rod length [mm]	l	156.5
Geometric compression ratio [-]	r_c	11.41
Pin offset [mm]	x_{off}	-0.8
Displacement volume [cm^3]	V_d	549.5
Fuel (lower) heating value [J/kg]	q_{HV}	$43 \cdot 10^6$
Intake valve diameter [mm]	d_{IV}	35
Exhaust valve diameter [mm]	d_{EV}	29

3.2 Control units and actuators

The cell control system enables control of throttle angle (i.e. engine load), engine speed and fuel pressure. The in-house developed *Raptor* controls the engine operation and some actuators related to the cell. The process of integrating *Raptor* more into the cell environment is ongoing. This will hopefully aid in further improvement of the entire measurement process efficiency. To be able to use the highly versatile control system in an efficient way, a GUI (Graphical User Interface) has been designed specifically for this cell, figure 3.1. This panel lets the cell operator control the entire engine operation while maintaining a good overview of all engine parameters, i.e. pressures, temperatures, etc. A short user manual for managing the user interface and the measurement system is included in appendix B.

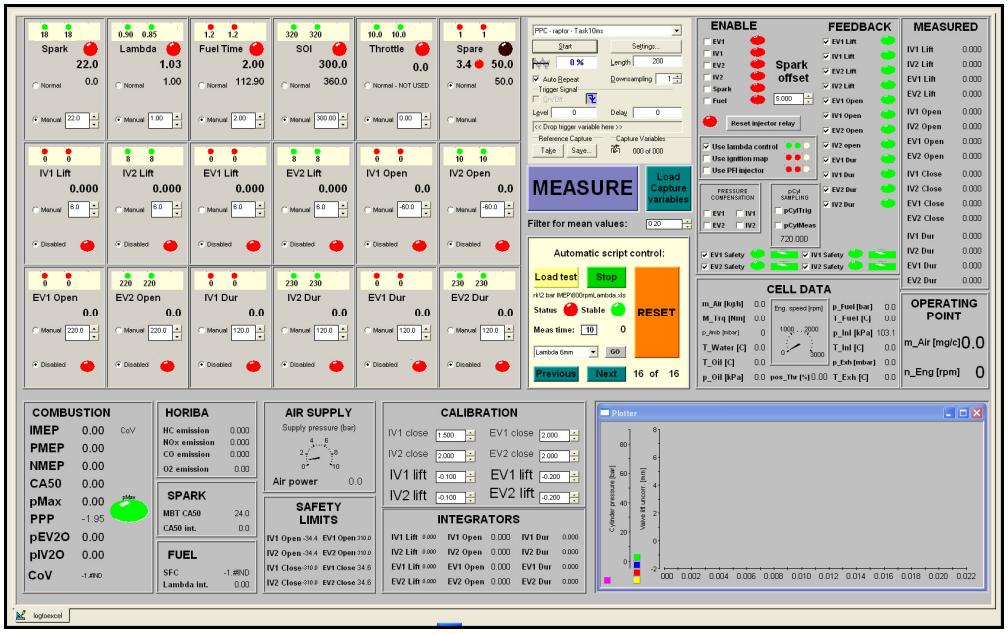

Figure 3.1. The *ControlDesk* designed GUI with controllable operating parameters, measurement control and feedback switches as well as some general output information.

Raptor is connected to the engine via an ECU (Engine Control Unit) from *dSPACE GmbH*. The standard ECU tasks are taken care of by a *MicroAutoBox* (MABX), which possesses greater computational performance than a regular ECU, as well as a comprehensive automotive I/O. To handle all signal conditioning, the MABX is assisted by a RapidPro unit. This can easily be expanded with additional power stages and imposes little or no practical limitation on computational resources. Figure 3.2 shows the *dSPACE* system including all interconnections.

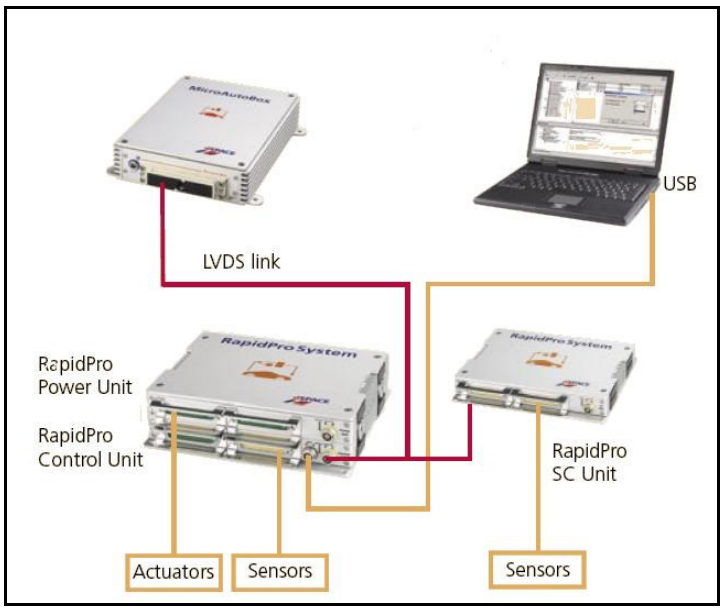

Figure 3.2. The *dSPACE* package connects the signal conditioning unit to the MABX and the *RapidPro* power stages. This interfaces with a standard PC via a USB link.

Raptor enables control of spark timing, fuel timing, and valve settings. Functionality for controlling external EGR, boost pressure, etc. exists but has not been used during these tests. The entire *Raptor* system is *Simulink* based and each subsystem has specific tasks. The main subsystems needed to run the single cylinder engine are:

- 'SensorCalc' – where all measured and calculated input signals are treated
- 'Fuel' – where lambda control, injection timing, etc. are embedded
- 'Spark' – where e.g. MBT (Maximum Brake Torque) timing is controlled
- 'AirRealization' – where the free valve control system is embedded.

The entire cylinder pressure vector is analyzed after each combustion event with respect to mean effective pressures, burn rate, etc. This analysis is then used to adjust e.g. spark timing towards MBT (based on estimated CA50 position), using closed loop control. This also reduces the need for time consuming map calibration, instead it is possible to directly let *Raptor* adjust the needed spark advance based on the previous cylinder pressure trace. The implementation of this combustion analysis module is done in C code, which makes it sufficiently fast.

Figure 3.3 shows an overview of the *Raptor* ECM (Engine Control Module).

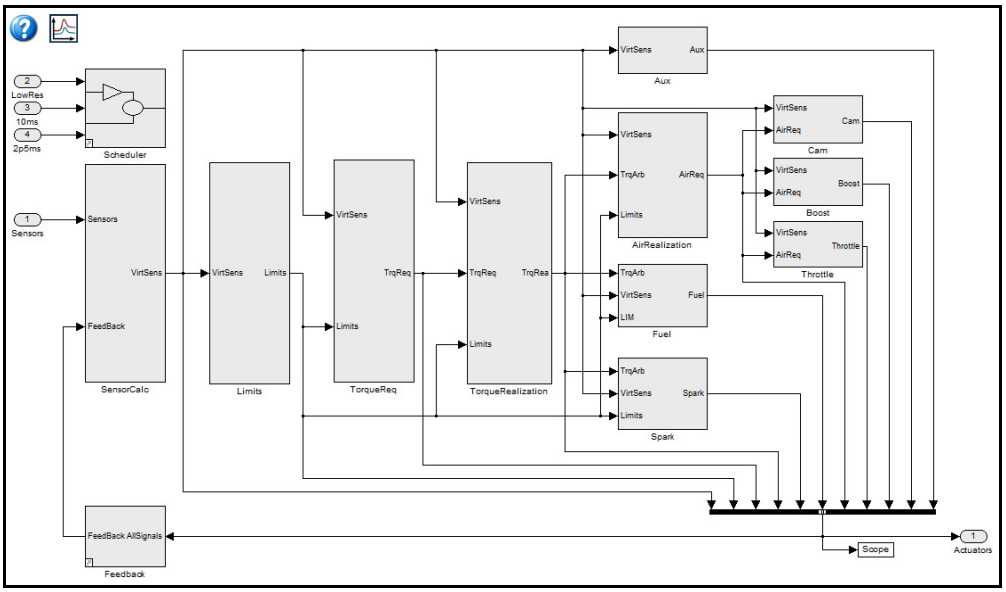

Figure 3.3. The *Raptor* ECM with subsystems. The different blocks handle sensor signals, limitations, torque requests/realizations, air mass/fuel/spark control, and several other tasks.

The actuators controlling the valves have been thoroughly described in [1] and will not be given any additional attention here.

3.3 Auxiliaries

Apart from the equipment described above, several other systems are required to function together with the cell equipment, particularly for controlling the valve system.

3.3.1 Position sensors

To track the valve movement, non-contact position sensors from *MicroStrain* (model NC-DVRT -1.0) have been used. They are mounted normally to the actuator piston and measure the distance to the slightly conically shaped piston, figure 2.4.

Due to manufacturing imperfections, the piston is not perfectly rotationally symmetric, which means that calibration (assuming linear voltage output) becomes a bit complicated. The sampling of the lift height measurement, however, was changed to be made every crank angle degree. Thanks to this, the measurement accuracy is deemed good enough to be reliable.

3.3.2 Oil and air supply

Pneumatics for actuating the valves comes from the air pressure system in the building. The supply pressure during measurements has varied between 4 and 8 bar and a *Kistler* pressure sensor monitors the actual supply pressure. For additional monitoring of the air flow, a thermal gas flow meter from *Manger+Wittmann* was used. The air mass measurement is necessary in order to be able to estimate the power consumption equivalent to parasitic engine losses that an in-vehicle installation would result in (chapter 2.3.10).

3.4 Measurements

The main target for the measurement series was to cover as much of the engine operating map (with respect to speed and load) as possible. Due to practical limitations this meant an engine load ranging from 2 to 11 bar IMEP and a speed range from 800 to 3000 rpm. Certain compromises have been made to stay within the stable valve operating range and Figure 3.4 shows the evaluated operating points.

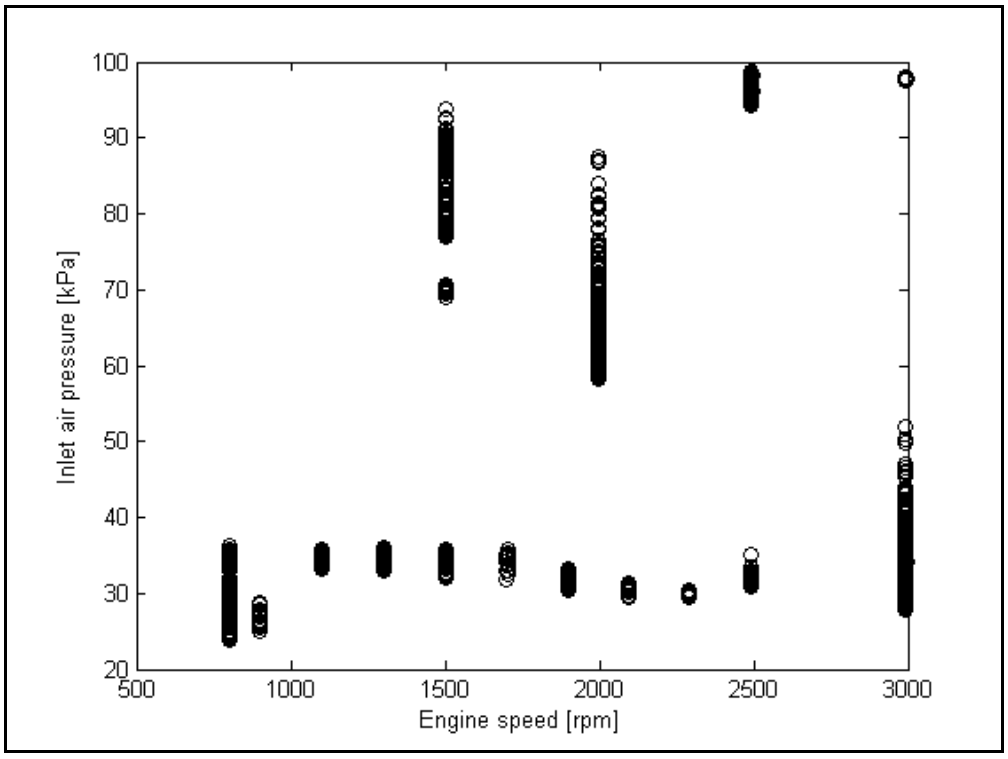

Figure 3.4. Overview of all tested engine operating points during the project.

Higher engine speeds than 3000 rpm have unfortunately not been tested due to temporary test bed restrictions. In the low speed/high load region, knock proneness increases and because it was deemed necessary to test a large amount of operating points in a short amount of time without any knock control implemented in the ECU, this region of the operating map was avoided.

Although emphasis is on modeling the cylinder pressure trace implied by the variations in valve settings, other parameters such as fuel pressure, injection timing, spark timing and lambda value should be included in the algorithm. This means that these controllable operating variables should be altered as well. Table 3.2 shows the entire range of variation for these parameters.

Table 3.2. Parameter range of variation for the controllable engine variables.

Variable and unit	Variation interval
λ [-]	[0.85 … 1.20]
l_{EV} [mm]	[2.9 … 8.1]
l_{IV} [mm]	[2.9 … 8.2]
N [rpm]	[800 … 3000]
p_{inl} [kPa]	[24 … 99]
p_{fuel} [bar]	[14 … 70]
θ_{EVC} [°ATDC]	[-61 … 22]
θ_{EVO} [°ABDC1]	[-60 … 60]
θ_{IVC} [°ABDC2]	[-65 … 62]
θ_{IVO} [°ATDC]	[-21 … 61]
φ_{spk} [°BTDC$_{\text{firing}}$]	[5 … 50]
φ_{SOI} [°BTDC$_{\text{firing}}$]	[200 … 350]

Figure 1.2 illustrates the enormous variation possibilities when all four valves are used. To actually take all air flow phenomena etc. into account when the valves can be arbitrarily offset against each other would require extensive CFD (Computational Fluid Dynamics) analysis. Therefore, as previously stated, it is considered enough to focus on two operating valves within the available time frame of this project.

From now on, if nothing else is stated, all numerical values extracted from measurements (except for the cylinder pressure) are mean values formed during the entire measurement time (10 seconds).

3.4.1 Cylinder pressure measurements

The key variable in the measurement process is of course the in-cylinder pressure. This is the only parameter that needs to be measured with high resolution (i.e. one sample per crank angle), which creates a somewhat difficult situation. Although the *dSPACE* system is versatile, the data compression is rather poor, and to store high resolution cylinder pressure data sets during the entire measurement time consumes large amounts of disk space. A memory consuming data set is also difficult to handle during post-processing and analysis. Therefore, a simple *Simulink* model for adapting a mean cylinder pressure trace has been implemented. The model is initialized with the first measured pressure trace and as soon as the data logging is triggered to start, 5% of the difference between the (continuously updated) mean value and the current pressure trace is added, according to

$$\begin{aligned} p_{cyl,mean} &= p_{cyl,meas} && t = 0 \\ p_{cyl,mean} &= p_{cyl,mean} + 0.05\left(p_{cyl,meas} - p_{cyl,mean}\right) && 0 < t \le t_{meas,final} \end{aligned} \tag{3.1}$$

This of course imposes certain limitations on engine operation. An accurate mean value can only be determined for steady state engine operation and consequently if the combustion variability is

too large, the mean value pressure trace is difficult to analyze. For a more detailed discussion around this, see chapter 8.3.2. The long-term plan is to expand the measurement system via *Raptor*, making extensive high resolution measurements possible. As a first solution, this could be done by for example letting the automatic script (chapter 4.5) trigger a parallel measurement in the *IndiCom* system. This would then automatically give synchronized file names, etc. and scripts for converting *IndiCom* data to e.g. *Matlab* format already exists.

4. Control system and test bed development

The first part of this thesis work was to modify and improve the existing valve control system in certain areas that had previously been identified as system weaknesses in [1]. The entire control system needed for the valvetrain is shown in figure 4.1.

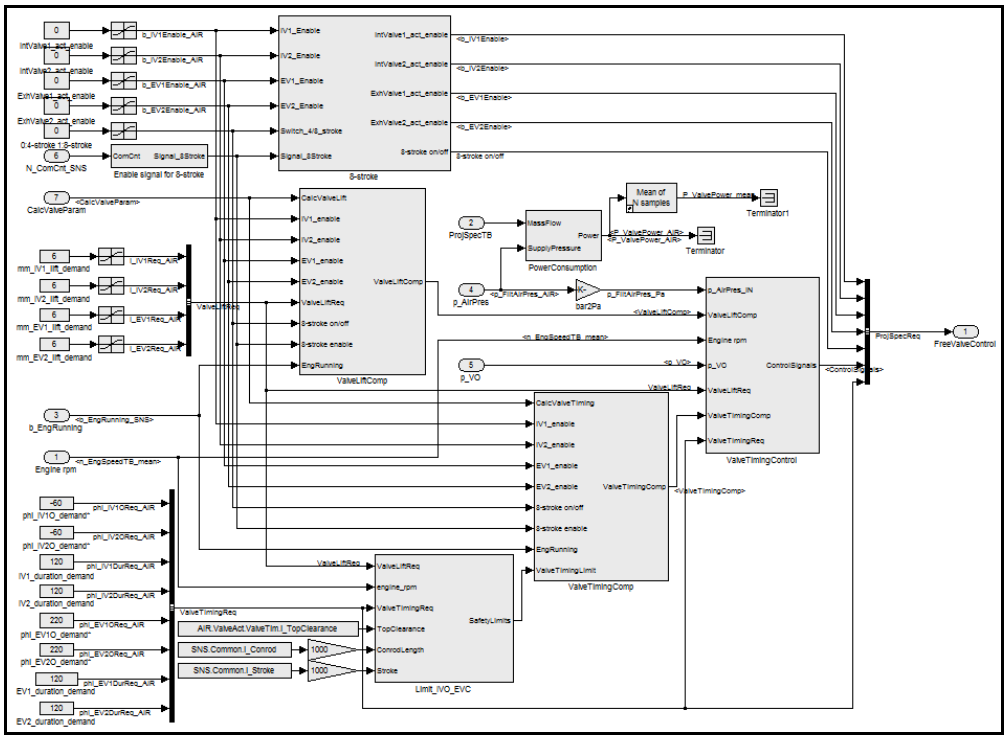

Figure 4.1. Valve control system the way it is currently implemented in *Simulink*.

Each subsystem in the picture handles a separate task. Furthermost to the left are user inputs, the variables that are linked to the *ControlDesk* GUI. The '8-stroke' subsystem has not been active during these tests, but contains logic for valve activation and deactivation. All requests are passed through feedback compensators that use error integration to fulfill the requests. The safety system (explained below) limits valve timings based on engine operating point and valve lift height. These signals are passed through to the 'ValveTimingControl' block that converts everything to solenoid control signals.

4.1 Collision detection and safety system

With the engine equipped with valve variability, the collision risk between valve and piston becomes a real issue. During the initial installation and development phase the engine ran with a compression ratio of 1:5.5 and the safety system was very conservative, positive valve overlap was never allowed. This was an inevitable consequence of not including the engine speed dependence. However, as discussed in chapter 2.2, the actual valve lifts depend strongly on engine speed and the safety system logic needs to be modified accordingly.

Assuming once again that all solenoid signals are constant in time, a linear dependence on engine speed can be expected. To determine this correlation, a number of engine speeds with fixed valve timings and lifts were studied and a constant delay between maximum lift and

detected IVO/EVC of approximately 3.5 ms was found. As an additional precaution, the actual delay was then said to be 3 ms (denoted t_{delay}), which enables up to 40 degrees valve overlap at 3000 rpm and 6 mm lift height for example.

Since knowledge about the actual engine and valve installation geometry exists, it is easy to determine for which crank angle collision will occur at the current lift height. The geometric nomenclature is defined in figure 4.2.

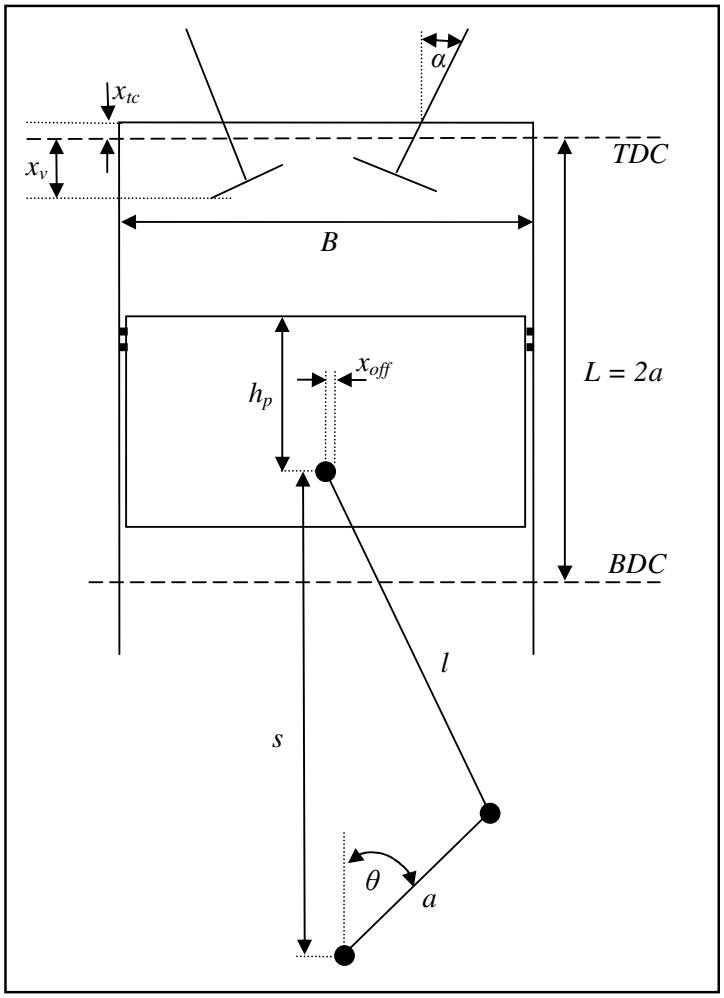

Figure 4.2. Schematic engine crank and valve geometry with nomenclature.

The logic for intake and exhaust valves is identical, except for the fact that the angle relative to the piston crown normal, α, is 16° on the intake side and 18° on the exhaust side. However, since the intake valves have a greater diameter, α is taken as 18° on both intake and exhaust side. Based on this, the valve lift protruding the top clearance x_{tc} can be calculated as

$$x_v = x\cos\alpha - x_{tc} \tag{4.1}$$

where x is the actual valve lift. The distance from crank shaft center to piston pin center (neglecting the pin offset x_{off}) is given by

$$s = a\cos\theta + \sqrt{l^2 - (a\sin\theta)^2} \tag{4.2}$$

For a given valve lift, the maximum allowable piston crown position can be written

$$s_{\lim} = S - h_p - x_v \tag{4.3}$$

where S is the total height from crank shaft to closed valve, i.e. $S = l + a + h_p + x_{tc}$, and combining these two gives

$$s_{\lim} = l + a + 2x_{tc} - x\cos\alpha \tag{4.4}$$

This is then the maximum allowable position of the piston crown to avoid collision with the valve at the given valve lift x.

Rearranging with respect to crank angle gives

$$\theta = \arctan\left(\pm \frac{\left[2(as_{\lim})^2 + 2(al)^2 + 2(ls_{\lim})^2 - a^4 - l^4 - s_{\lim}^4 \right]^{1/2}}{as_{\lim}} \right) \tag{4.5}$$

which is the crank angle corresponding to collision. Due to the crank angle definition used in the valve control system, the negative value is used for IVO and the positive value for EVC. The safety function described above assumes instantaneous valve opening, i.e. maximum lift is reached immediately when the valve opens. The allowable crank angle in equation 4.5 must therefore include an offset as

$$\theta = \arctan\left(\pm \frac{\left[2(as_{\lim})^2 + 2(al)^2 + 2(ls_{\lim})^2 - a^4 - l^4 - s_{\lim}^4 \right]^{1/2}}{as_{\lim}} \right) \mp N \frac{360}{60 \cdot 1000} t_{delay} \tag{4.6}$$

This limitation is then passed through to the compensation algorithm. As an additional safety feature (merely to avoid typing errors from the cell operator), the valve timings in the proximity of TDC_{firing} (IVC and EVO) are limited to a window ranging from 30 CAD before to 30 CAD after TDC_{firing}.

Since no transient tests have been done, it is difficult to say how the safety system handles rapid changes in timing requests. For steady state engine operation it has proven to work well. It is also worth noting that the system still is conservative. The uncertainties involved in the valve position measurements (described in [1]) combined with the fact that the valves appear to have an oscillation amplitude of around 0.5 mm makes a certain amount of safety margins necessary to keep. If the test bed operator is confident of the actual valve behaviour, he or she can switch off the safety system during a run and take full control of the valve timings. Table 4.1 shows a summary of allowed amount of overlap (defined in equation 1.1) for different engine speeds when using equation 4.6 as safety algorithm. In the calculation below, both intake and exhaust valve lifts are kept constant at 7 mm. A brief discussion about weaknesses in the safety system is presented in chapter 9.

Table 4.1. Allowed valve overlap for 7 mm valve lifts as function of engine speed when the collision avoidance system is enabled.

Engine speed [rpm]	800	1000	1200	1400	1600	1800	2000	2200	2400	2600	2800	3000
Max. allowed overlap [CAD]	-40	-33	-26	-19	-11	-4	3	10	17	25	32	39

4.2 Valve lift and timing detection

Since the valve lift curve is sampled every crank angle degree it is easy to analyze the measured data and detect relevant parameters, i.e. valve opening, closing and maximum lift height. A valve is considered open when the lift exceeds 0.3 mm. To detect this angle, the lift height vector is searched in a region around the requested opening point. Due to measurement noise, a hysteresis effect is included, implying that three consecutive samples should be above 0.3 mm. Measurement noise can, for certain engine speeds, have an amplitude of up to 0.2 mm. The first out of these three is then considered to be the actual opening angle, see figure 4.3.

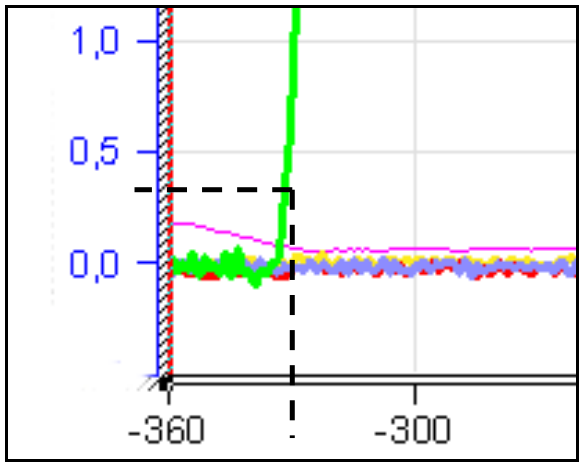

Figure 4.3. Definition of valve opening, due to measurement noise the valve is considered open when the lift height exceeds 0.3 mm.

Valve closing is detected in a similar manner, i.e. three consecutive values need to fall below 0.3 mm and the first out of these three is considered to be the actual closing point.

Since the valve lift profiles are engine speed dependent as well as slightly stochastic in their appearance, the maximum valve lift is considered to be the maximum value of the measured lift height across all crank angle degrees. There are two main reasons for this choice of definition; it provides an additional safety factor to the collision detection system and the seemingly random valve profile behavior does not need to be taken into account. An example of this random profile appearance can be seen in figure 2.6, where the intake valve in the right picture has a relatively smooth peak lift profile, while the maximum exhaust valve lift shows three distinct humps. The possibility of this being a consequence of the position sensor uncertainty can unfortunately not be completely discarded either.

4.3 Valve timing feedback

Although an open-loop system is quite useful, some sort of feedback implementation is necessary to compensate for algorithm errors and hardware deviations. Feedback in the form of error integration had previously been implemented on the lift height signal and the same fundamental system architecture is used to handle the timing requests, figure 4.4.

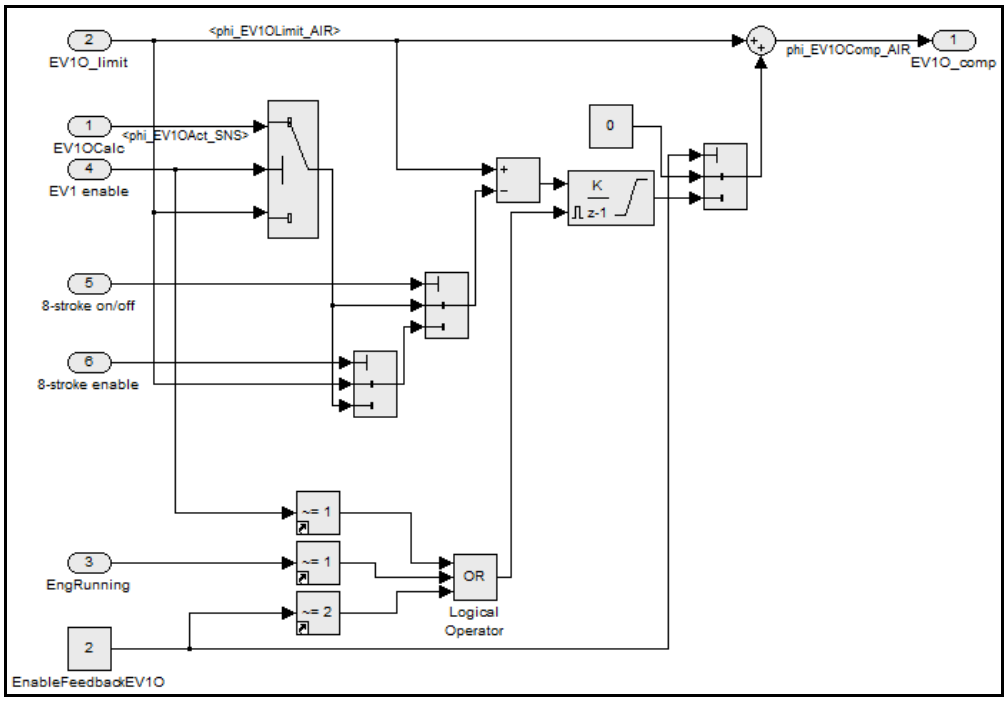

Figure 4.4. *Simulink* model of exhaust valve opening feedback.

The low-gain (i.e. slow) integrator outputs the error between detected and requested valve timing and adds it to the input signal (provided of course that the signal has firstly been limited in the safety system). For the purpose of these tests, the integrators have been made deliberately slow to reduce oscillatory behavior. This is obviously not ideal for transient tests, where step response performance is crucial, but since the actuators show large differences between one another and the algorithms for air charging etc. aren't individually tuned to an extent that would be necessary, this simple control strategy is considered sufficient at the moment.

4.4 Pressure compensation

Valve opening is always counteracted by the in-cylinder pressure, particularly at EVO but sometimes also at IVO when early EVC with subsequent recompression might be used for HCCI combustion or other reasons. Therefore a simple pressure compensation algorithm should be developed. During valve opening, the forces acting on the valve are as shown in figure 4.5.

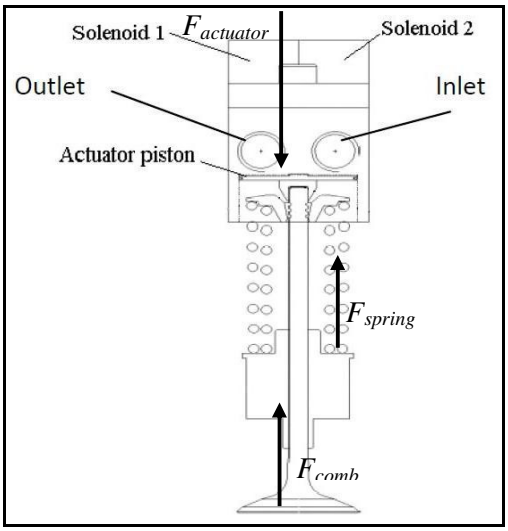

Figure 4.5. Forces acting on the valve during opening [1].

The pressure resulting from combustion, p_{EVO}, can be estimated from the combustion analysis module implemented in *Raptor*. This module analyses the measured pressure trace and calculates the necessary offset correction according to equation 5.23. The implementation is done as C code and calculations have been verified against data provided from the *IndiCom* system and show good accuracy. This offset corrected pressure, along with knowledge about the surface area of the valve and the actuator piston, can be used to determine the extra amount of air pressure (and, through the ideal gas law, air mass) that is needed to overcome p_{EVO}. The equations were originally implemented during the work presented in [1] and have only been modified slightly. The first step is to determine the initial air mass inside the actuator due to the dead volume distance. This air mass can be written

$$m_0 = \frac{p_{atm} x_0 A_{AP}}{R T_{amb}} \tag{4.7}$$

where x_0 is the dead volume height of the actuator (approximately 0.5 mm), A_{AP} is the actuator piston area and T_{amb} is the ambient air temperature. One source of valve opening resistance is the return spring, the air mass needed to overcome this is

$$m_{spring} = \frac{k(x_{pc}^2 + l_{EV}^2)}{R T_{amb}} \tag{4.8}$$

where k is the spring constant, x_{pc} is the spring precompression length and l_{EV} is the valve lift. To overcome the pressure resulting from combustion, an extra air mass as

$$m_{comb} = \frac{p_{comb} x_0 A_{AP}}{RT_{amb}},\ p_{comb} = p_{EVO} \frac{A_{EV}}{A_{AP}} \tag{4.9}$$

is required and the total air mass needed to meet the requested valve lift is given by

$$m_{tot} = m_{comb} + m_{spring} - m_0 \tag{4.10}$$

There is of course a physical limitation for how much extra air that can be used for filling the actuator volume, and the only solution to overcome the cylinder pressure is then to increase supply pressure to the actuators. For a detailed discussion around the control algorithms and air power consumption, see chapter 9.

4.5 Automatic script and test bed time delays

In the multi cylinder test cells at AVL SPEAB, a script for running automated test sequences has been developed. This allows offline definition of several hundred operating points in a regular *Excel* file, *ControlDesk* then loads the file and sets up all parameters in the way they are defined in the test sequence. While the engine is running, *ControlDesk* performs necessary setpoint changes and after a predefined stabilization time, the measurement is initiated. The script stores all mean value variables in an *Excel* file and parallel to this starts a high resolution *MATLAB* log file. This file contains data with 10 ms resolution and a cylinder pressure trace adapted as the mean value pressure during the measurement time. Figure 4.6 shows the chain of events from test sequence definition to the produced data log files.

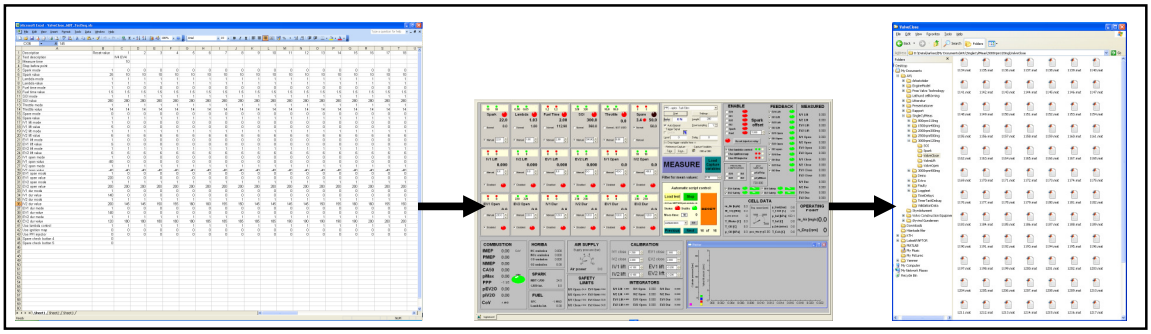

Figure 4.6. Schematic overview of the workflow when using the automatic script; starting with the test sequence in an *Excel* spreadsheet, continuing with the actual engine operation handled by *ControlDesk* and finally the output in compact .mat-files ready for postprocessing.

In order to be able to use the automatic script as efficiently as possible, the response time of measurement instruments must be analyzed. It is vital to know when the engine can be considered to run at steady state after a setpoint change. The most advanced (and most accurate) stability criterion would be to assign tolerances to specific engine variables, e.g. CA50, exhaust gas temperature, HC emissions, etc. This would then mean that the engine operation is considered to be steady when all these values stay within certain predefined boundaries. However, determining these boundaries takes time and for a flexible research installation such as the *Ricardo* engine they might also vary a lot for different hardware setups.

For simplicity, it is therefore assumed that the *Horiba* emission measurements have the longest stabilization time. This assumption is motivated by the fact that the measurement techniques used in the exhaust gas analyzer are indigenously slow and the actual measurement unit is placed

physically far away from the engine which means long flow paths. To test this, a λ setpoint change from 1.0 to 0.9 is done and since the λ control is considered to be fast, the delay from this is negligible compared to the overall stabilization delay. Figure 4.7 shows the measured emissions during the λ setpoint change.

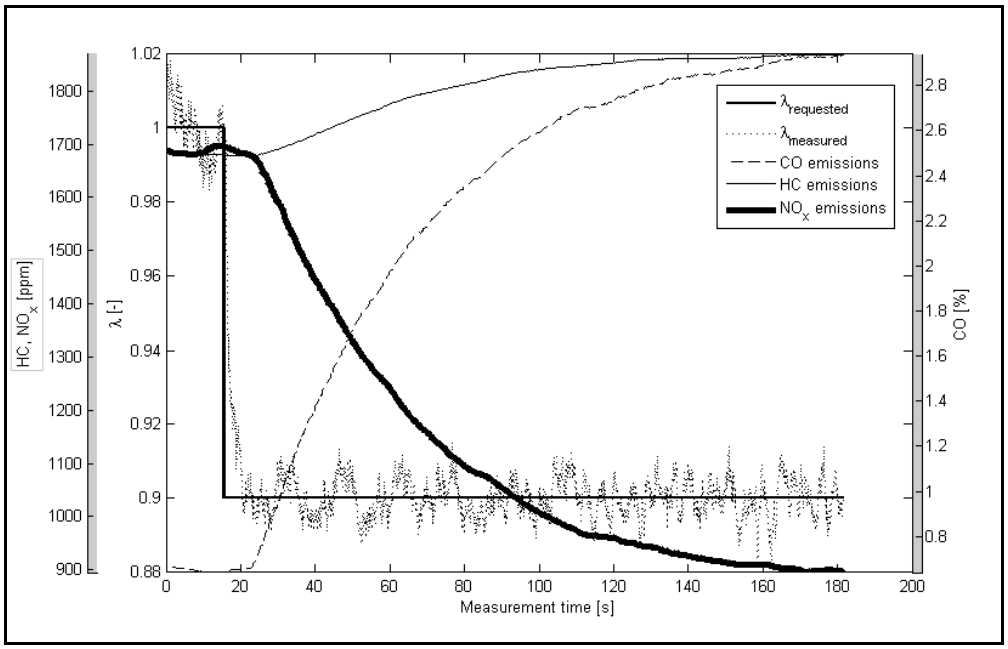

Figure 4.7. Time resolved emission measurements during a λ setpoint change, engine operating at 1500 rpm and inlet air pressure is 30 kPa. Emission levels start reaching their final values after around 3 minutes.

Since the exhaust gas flow paths have a strong influence on the practical time delay, one parameter that affects the measurement delay time is the air mass flow across the engine. This, in turn, depends on engine speed and engine load and figure 4.8 illustrates this dependence during the same λ setpoint change as described above. The time τ_{delay} is defined as the time from the λ setpoint change until 90% of the "final" emission value has been reached.

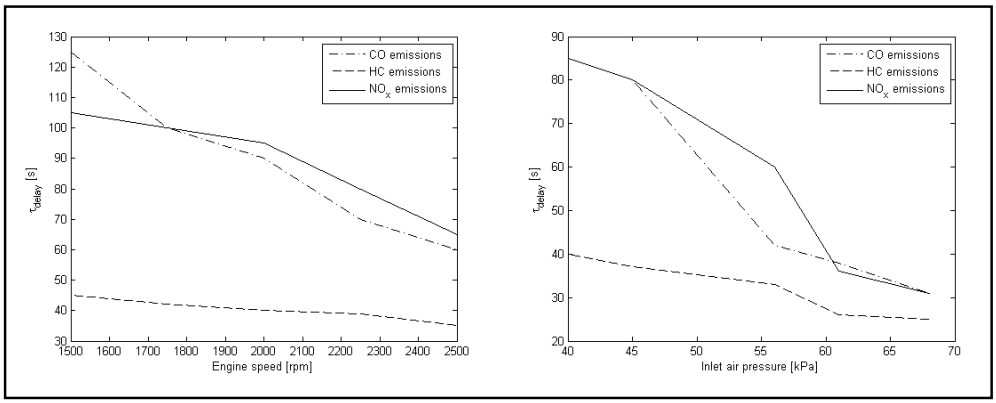

Figure 4.8. Stabilization time for emission measurements as function of engine speed (left) and inlet pressure (right). The slightly irregular appearance comes from the fact that it is difficult to define the final emission value as well as the low number of data points.

Because all tests and setpoint changes are planned in advance, it is easy to make sure that consecutive operating points differ as little as possible from each other. In practice, this means that during systematic runs, only one or two input parameters should be changed simultaneously. This allows for a short static stabilization time, which has been defined as 10 seconds during the tests carried out in this work. As a consequence of this, however, the emission measurements cannot be trusted completely and should only be seen as trend indicators. The absolute values have most likely not reached a steady state condition.

5. Cylinder pressure model

In order to be able to predict the engine behavior during a full cycle (two crank angle revolutions), an accurate engine model is essential. The model needs to take the combustion as well as the gas exchange process into account and generate a complete cylinder pressure trace that can later on be used for control applications and various other model alterations. The model development has been ongoing for quite some time before this work was carried out and the complete combustion model is extensively described in [4]. It is worth noting that the model described in [4] only has been validated against a data set recorded using a fixed cam shaft engine configuration.

5.1 Initial analysis and frame of reference

Initially, the model kept its original appearance and the only thing that was done was to replace the old data set with the 1790 new operating points. The result is shown in figure 5.1, where the modeled IMEP, PMEP and CA50 values are compared to the measured values.

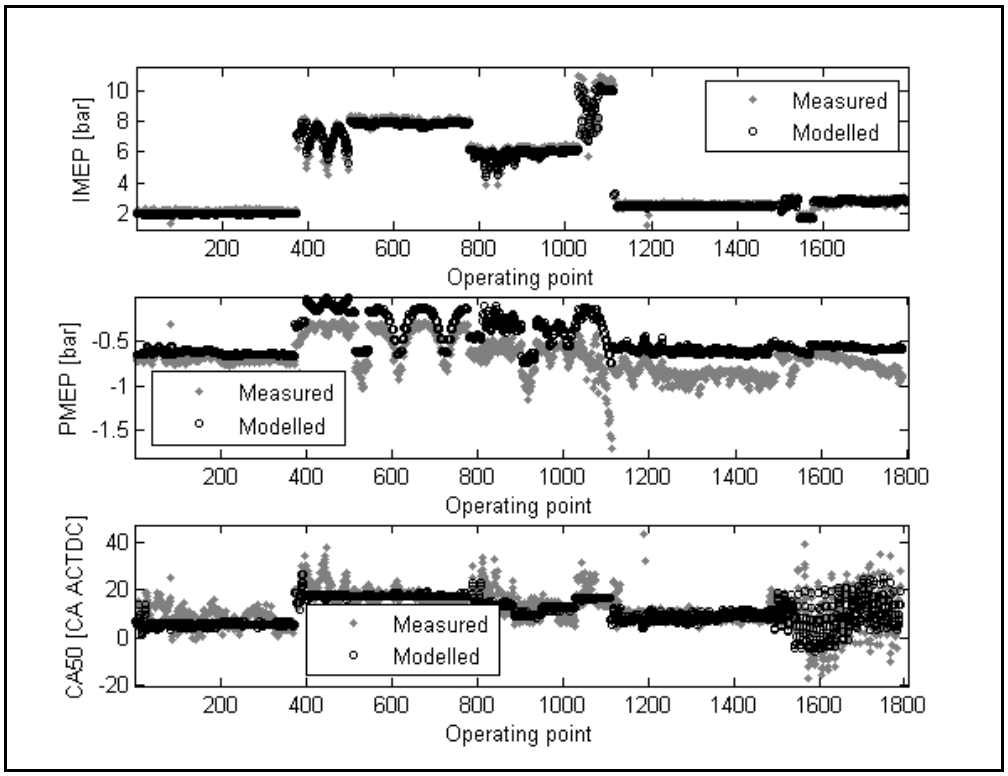

Figure 5.1. Comparison between measured and modelled IMEP, PMEP and CA50 values for all evaluated operating points.

A statistical analysis shows an underestimation of IMEP and PMEP values, but the overall result is a good starting point for further development. The high pressure part of the cycle should be corrected by calibrating the Vibe parameters in order to get a better estimate of the CA50 timing. The low pressure part of the cycle requires a bit more work and this is where the main focus will be.

The logarithmic cylinder pressure trace in figure 5.2 illustrates the areas that are considered to contain the greatest potential for accuracy improvements, namely the recompression

phenomenon around gas exchange TDC (a), the blowdown phases after EVO and IVO (b), the standing wave phenomena during exhaust and intake stroke (c) and the residual gas fraction affecting the combustion part of the cycle and possibly γ during compression and expansion (d).

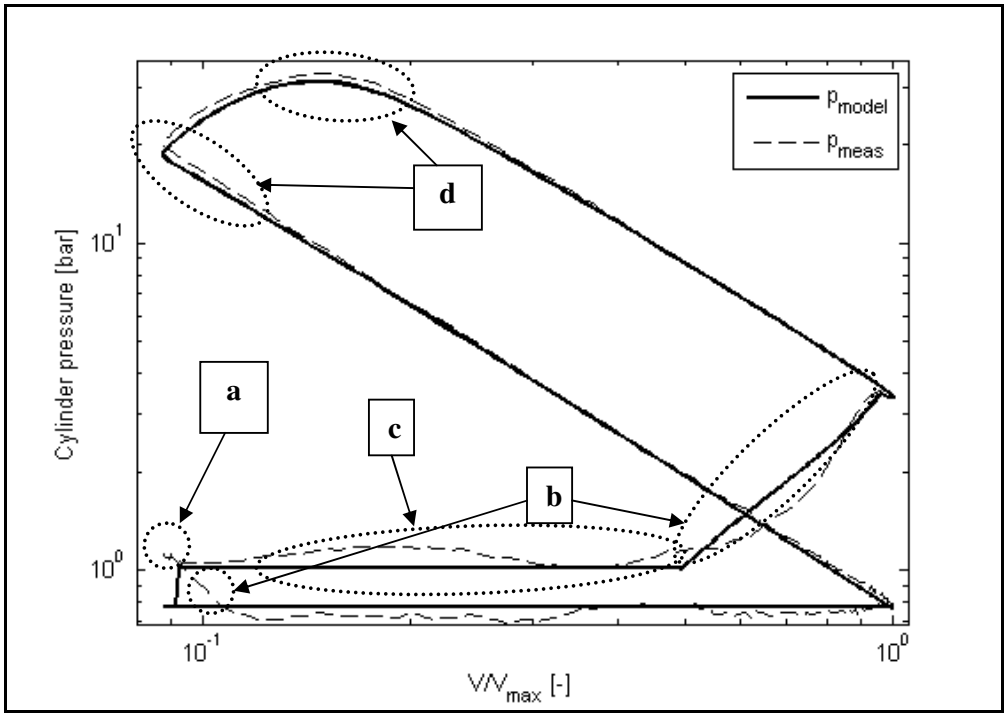

Figure 5.2. Measured and modelled cylinder pressure trace plotted with possible areas for model improvements marked.

Since the high pressure part of the cycle (compression and expansion strokes) have been tuned during extensive modelling prior to this work, this will essentially be left unchanged. Focus will be on capturing the dynamics during the gas exchange process, i.e. from EVO until IVC. For reading convenience, the most fundamental equations concerning the high pressure cycle are summarized in appendix C. The complete combustion model for the high pressure cycle is extensively described in [4].

5.2 Thermodynamic model

The combustion model in its original appearance is not primarily intended for real-time applications, but rather for high accuracy. The best choice is then to use a differential equation model. This will mean that the model executes comparatively slow, but the accuracy of the governing equations is well documented. The starting point for the combustion model is the first law of thermodynamics

$$dQ = dU + dW \tag{5.1}$$

where dQ is heat released, dU is the change in (sensible) internal energy and dW is the net work produced during the process. Figure 5.3 illustrates these processes along with typical flow directions.

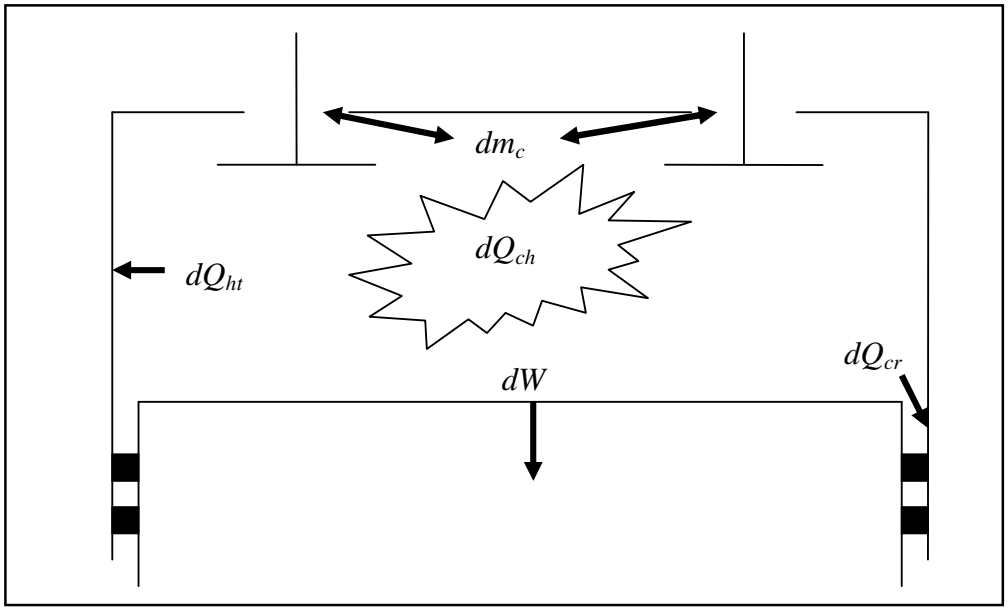

Figure 5.3. Graphical representation of the first law of thermodynamics. The system of interest in this case is of course the combustion chamber including the flow across valves, the gas leakage past the piston rings and the energy lost due to convective and radiative heat transfer.

This equation describing the energy conservation during the combustion process can be implemented as the gross heat release equation [5], which is then easily implemented into a standard differential equation solver. As mentioned before, the high pressure cycle only needs a few minor adjustments which will be briefly explained in chapter 5.5, so from now on the focus will be on the gas exchange behaviour. This is done by extending the differential equation to include the mass flow across the valves and thereby also the change in internal energy. An overview of these extended equations is given on the following pages.

5.3 Gas exchange modelling

With the well defined system boundaries and energy fluxes depicted in figure 5.3, the energy conservation equation can be expanded and rewritten into an expression for the actual pressure. The complete derivation of this expression is given in [5]. The sensible internal energy dU and the extracted work dW is given by

$$\begin{aligned} dU &= mc_v dT \\ dW &= pdV \end{aligned} \tag{5.2}$$

Using the differentiated ideal gas law and known relationships for the specific heats, the complete expression for the heat released during the engine cycle becomes

$$dQ_{ch} = \frac{1}{\gamma - 1} Vdp + \frac{\gamma}{\gamma - 1} pdV + \left(u - \frac{RT}{\gamma - 1} \right) dm_c + dQ_{ht} + dQ_{cr} \tag{5.3}$$

where u is the mass specific internal energy and dm_c is the change in cylinder charge mass. The heat transfer and crevice losses dQ_{ht} and dQ_{cr} are already modelled and the specific heat ratio γ has also been modelled and validated in [4]. The remaining terms are the internal energy and the change in air charge mass. By rewriting as a pressure differential and including the charge mass change in the temperature differential, one obtains

$$dp = \frac{dQ_{ch} - \frac{\gamma}{\gamma - 1} pdV - dm_c \left(u - \frac{RT}{\gamma - 1} \right) - dQ_{ht}}{\frac{1}{\gamma - 1} V + dQ_{cr}} \tag{5.4}$$

$$dT = \frac{1}{Rm_c} \left(Vdp + pdV - RTdm_c \right) \tag{5.5}$$

where m_c is the initial (i.e. at the time for valve opening) in-cylinder charge mass. The internal energy u is calculated as suggested in [5] as

$$u = \int_{T_0}^{T} c_v dT = \int_{T_0}^{T} \frac{R}{\gamma - 1} dT \tag{5.6}$$

where the temperature ranges *from* in-cylinder *to* exhaust manifold temperature at EVO and *from* exhaust manifold *to* intake manifold temperature at IVO. The mass flow (in crank angle domain) is calculated in [6, p226] as

$$dm_c = \frac{pC_D A_{nom}}{\sqrt{RT_0}} \left(\frac{p}{p_0} \right)^{\frac{1}{\gamma}} \left\{ \frac{2\gamma}{\gamma - 1} \left[1 - \left(\frac{p}{p_0} \right)^{\frac{\gamma - 1}{\gamma}} \right] \right\}^{\frac{1}{2}} \frac{60}{2\pi N} \tag{5.7}$$

where C_D is the flow discharge coefficient and A_{nom} is the nominal flow area. If the air flows across the exhaust valve, p_0 is the cylinder pressure and p the exhaust manifold pressure and

equivalently if the air flows across the intake valve; p_o is the intake manifold pressure and p is the cylinder pressure. The same subscript logic applies for T_0. Implementing this equation in the ode45 solver presents a problem. One requirement needed to assure the uniqueness of an ODE solution is that the equation satisfies the Lipschitz continuity theorem ([7] and [8]), meaning that dm_c must be continuously differentiable. The derivative of this function tends toward infinity when the pressure ratio p/p_0 approaches 1. This is equivalent to saying that the pressure difference across the valve, Δp, approaches 0. In a region defined by $0.99 < p/p_0 < 1.01$, the mass flow rate is approximated with a linear function. This does not influence the final result in any noticeable way, but it does speed up the simulation.

Equation 5.7 is valid if the flow is unchoked – for choked flow, it must be rewritten as

$$dm_c = \frac{pC_D A_{nom}}{\sqrt{RT_0}} \gamma^{1/2} \left(\frac{2}{\gamma+1} \right)^{\frac{\gamma+1}{2(\gamma-1)}} \frac{60}{2\pi N} \tag{5.8}$$

The flow becomes choked when the pressure ratio across the restriction drops below a certain value. This limit is defined by

$$p_{cr} = \frac{p}{p_0} \leq \left(\frac{2}{\gamma+1} \right)^{\frac{\gamma+1}{2(\gamma-1)}} \tag{5.9}$$

and if a more general form is used for writing the mass flow, namely

$$dm_c = \frac{pC_D A_{nom}}{\sqrt{RT_0}} \frac{60}{2\pi N} \Psi(p_r) \tag{5.10}$$

where p_r is the pressure ratio across the restriction, the flow can be graphically represented according to figure 5.4.

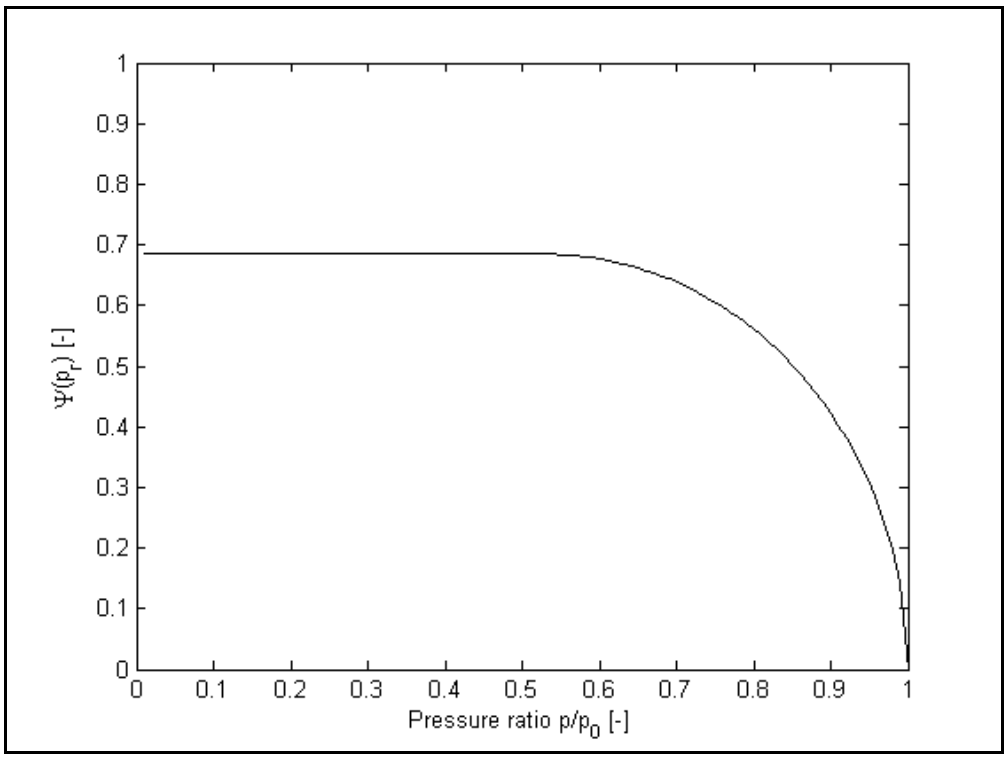

Figure 5.4. The term $\Psi(p_r)$ visualized assuming constant $\gamma = 1.4$. The flow is choked (reaches sonic velocity) when the pressure ratio drops below approximately 0.53.

The concept of choked and unchoked flow can be understood by considering a de Laval nozzle, figure 5.5.

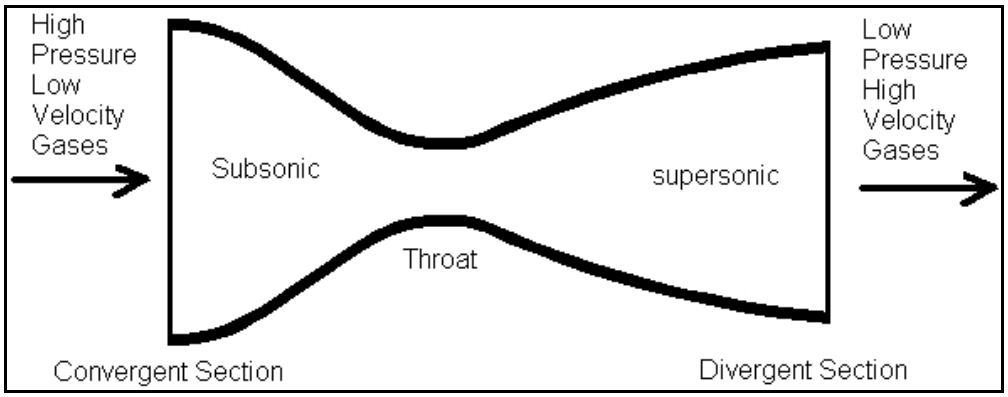

Figure 5.5. A generic de Laval nozzle with the characteristic area restriction.

Under normal conditions, the downstream pressure is smaller than the upstream pressure, which consequently gives the flow direction. Since conservation of mass applies, the fluid flow velocity must increase when passing the flow restriction (with smaller area). For the gas mixture in the engine, choked flow occurs when the flow velocity reaches sonic speed. During these conditions, the mass flow rate no longer depends on the downstream conditions and its magnitude can only be altered by changing the upstream conditions, i.e. the in-cylinder pressure and temperature for the case of exhaust gas flow for example.

5.3.1 Valve lift model

The nominal flow area A_{nom} needs to be a function of the valve lift and for this purpose, since no crank angle resolved measurements of the valve lifts are available, the valve lift needs to be modelled numerically. Tests for various engine speeds suggest that both valve opening (time from opening until maximum lift is reached) and valve closing (time from maximum lift to closed valve) are approximately constant in time, implying that there is a linear dependence on engine speed. It is also clear that the time delay from zero to maximum lift must depend on the actual value of the maximum lift. A reasonable assumption, which is also done in *Raptor*, is that each actuator has constant opening and closing velocity, implying that there is also a linear dependence on valve lift. Since the valve actuators display large differences between each other, these delays are manually tuned to fit the measured data set. Based on this knowledge, it is considered adequate to divide the valve lift into three parts; a linear increase, a dwell period with maximum lift and a linear decrease. Figure 5.6 shows the modelled valve lifts for low and high engine speed.

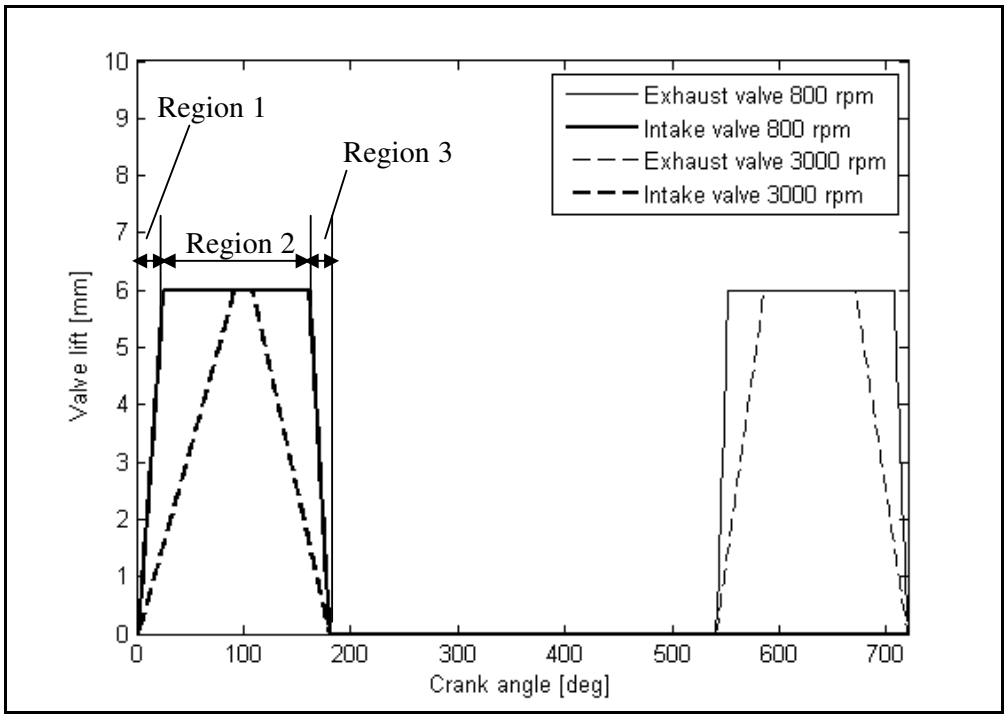

Figure 5.6. Modelled intake and exhaust valve lifts at low and high engine speed. It can be seen that the exhaust valve actuator is noticeably quicker, hence the longer maximum lift duration. The three regions are assigned individual discharge coefficients.

A method for estimating the nominal flow area (sometimes denoted valve curtain area) based on this lift height is suggested in [9, p32] and is easily determined as the cylindrical surface area formed around the open valve, figure 5.7.

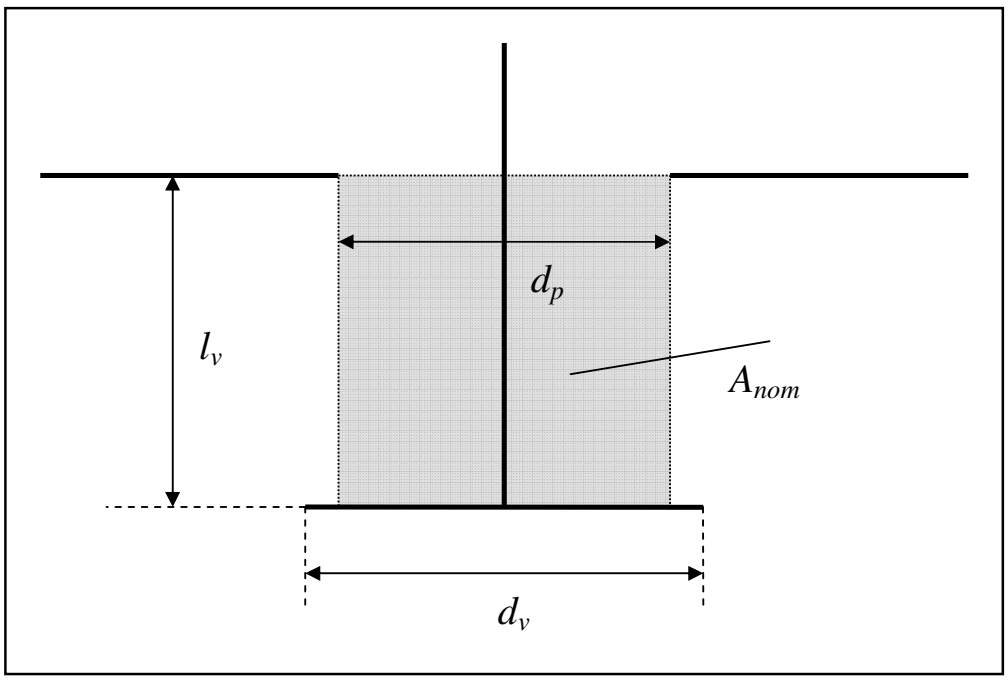

Figure 5.7. Nominal flow area around an open valve. This will vary linearly with lift height.

The port diameter d_p is, according to [6, p221], considered to be approximately 85-90% of the valve diameter, thus rendering the full expression for the geometric flow area as

$$A_{nom} = \pi \frac{d_v}{1.15} l_v \tag{5.11}$$

The discharge coefficient can be shown to have a valve lift dependency as well, [6, p227], and different flow regimes are suggested. It is therefore necessary to assign an individual discharge coefficient to each of the two valve lift regimes depicted in figure 5.6. The numerical values are determined by fitting the flow model to the measured data set for all tested lift heights. Table 5.1 summarizes the numerical values for opening and closing velocities as well as discharge coefficients.

Table 5.1. Numerical inputs in valve lift model.

Parameter	Value
Intake valve opening velocity	1.4 mm/ms
Intake valve closing velocity	1.5 mm/ms
Discharge coefficient region 1, intake	0.55
Discharge coefficient region 2, intake	0.65
Discharge coefficient region 3, intake	0.55
Exhaust valve opening velocity	2.4 mm/ms
Exhaust valve closing velocity	2.2 mm/ms
Discharge coefficient region 1, exhaust	0.50
Discharge coefficient region 2, exhaust	0.60
Discharge coefficient region 3, exhaust	0.50

The physical meaning of the discharge coefficient can be understood from the definition described in [6, p226]. The product of C_D and A_{nom} forms the effective flow area A_{eff}. Therefore, C_D can be thought of as a flow resistance factor where a low value corresponds to a high resistance. Ideally, flow rig measurements should be used to determine this coefficient, but the measurement process is complex and outside the scope of this work and a sufficient level of accuracy is achieved by using the two lift and flow regions described above.

5.3.2 Alternative model

While the use of a differential equation model for the gas exchange process significantly improves accuracy, it also increases the calculation time. If computational resources are a limiting factor, it might be preferable to use polynomial interpolation between valve opening and manifold pressure. The blowdown duration can then be adapted using a least-square fit technique to depend on engine speed, load, valve opening and lift. Figure 5.8 shows the duration in crank angle degrees from EVO until exhaust manifold pressure is reached along with the polynomial that provides the best fit in a least-square sense.

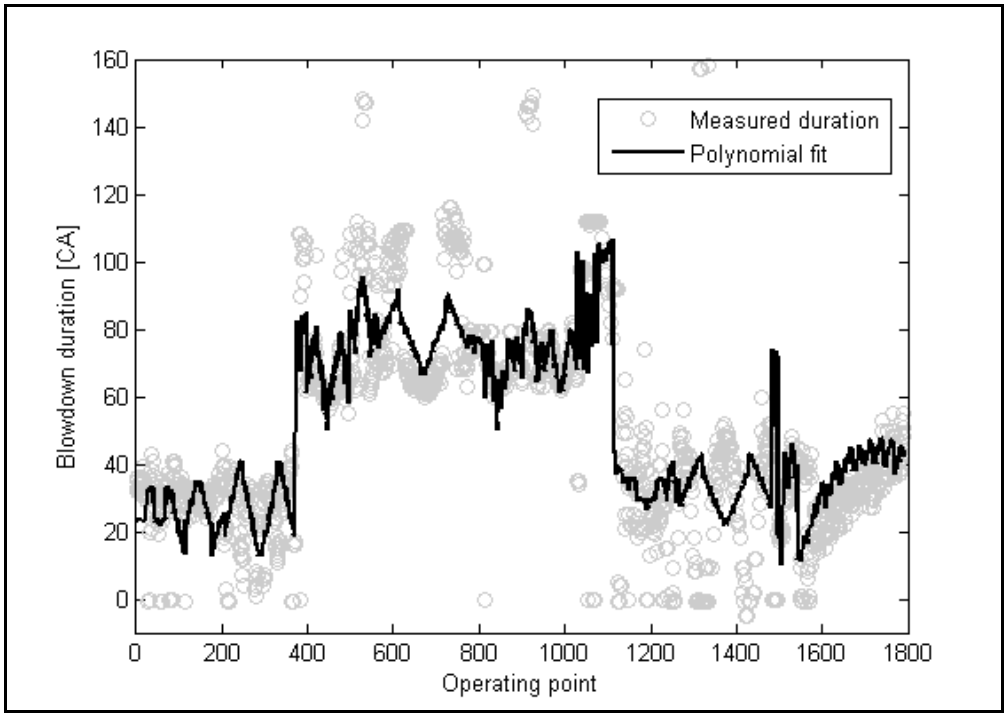

Figure 5.8. Exhaust blowdown duration and fitted polynomial for all operating points. Mean error between polynomially adapted and detected duration is 14 crank angle degrees.

Some points indicate 0 CAD from valve opening until cylinder pressure has dropped to exhaust manifold pressure. This could either be due to the fact EVO occurs so late that cylinder pressure has already dropped close to manifold pressure, or it could be because the analysis script is slightly sensitive to measurement noise and sharp pressure gradient. The accuracy of this method is particularly poor as engine speed and load increases, and for the purpose of this project, the differential equation model is preferred.

5.4 Residual gas estimation

By varying the valve timings, the mixture composition during the closed part of the cycle can be drastically changed. Since the residual gas mass fraction, x_{rg}, will affect the intake port temperature at IVC, the burn rate and many other important model parameters, it is important to have a reasonable estimate of this fraction. One approach is to consider the gas states in intake and exhaust manifold and model the residual gas mass fraction as

$$x_{rg} = \left\{ 1 + \frac{T_{exh}}{T_{inl}} \left[r_c \frac{p_{inl}}{p_{exh}} - \left(\frac{p_{inl}}{p_{exh}} \right)^{\frac{\gamma-1}{\gamma}} \right] \right\}^{-1} \tag{5.12}$$

where subscripts *exh* and *inl* denote exhaust and intake manifold conditions respectively and γ is assumed to be equal to 1.35. This model is sufficient for relatively moderate residual gas fractions, but with the possibility of e.g. closing the exhaust valve very early or shorten the intake valve duration considerably, all burned residuals will not be evacuated from one cycle to the next and a better model is needed.

Since the implemented model of mass flow across the valves has proven to work quite well, it is possible to use the ideal gas law and get a reasonable estimate of the charge mass at any given crank angle. Neglecting the effect of scavenging during overlap, the residual gas mass fraction can be calculated as

$$\begin{aligned} x_{rg,0} &= \frac{m_{EVC}}{m_{IVC}} = \frac{\frac{p_{EVC}V_{EVC}}{287T_{EVC}}}{\frac{p_{IVC}V_{IVC}}{287T_{IVC}}}, \text{ during NVO} \\ x_{rg,0} &= \frac{m_{IVO}}{m_{IVC}} = \frac{\frac{p_{IVO}V_{IVO}}{287T_{IVO}}}{\frac{p_{IVC}V_{IVC}}{287T_{IVC}}}, \text{ during PVO} \end{aligned} \tag{5.13}$$

Figure 5.9 shows the estimated residual gas fraction plotted against EVC timing and inlet air pressure. The numerical values are difficult to verify via measurements, but the trends are intuitively correct; earlier closure of the exhaust valve traps more exhaust residuals and for low load and excessive throttling, evacuation of exhaust gases will also become poorer.

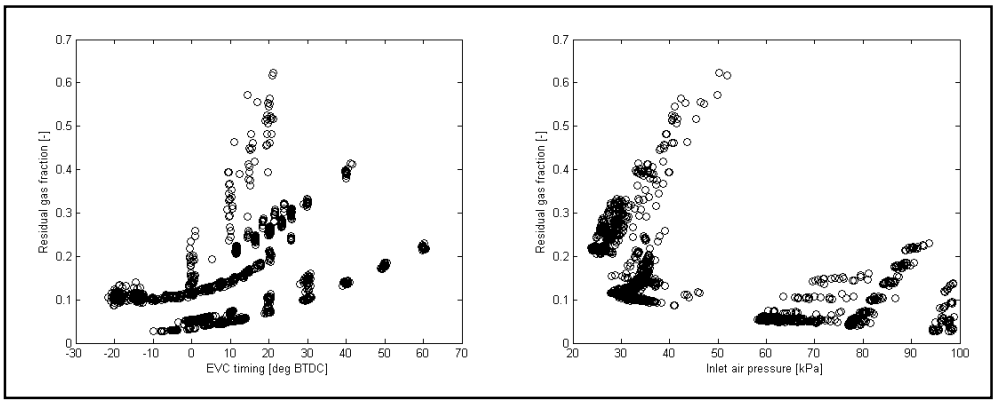

Figure 5.9. Estimated residual gas fraction plotted against EVC timing and intake manifold pressure.

The internal exhaust residuals will influence the cylinder temperature throughout the cycle and a way to model this is to raise the gas temperature at IVC using linear interpolation as

$$T_{IVC} = T_{inl}(1 - x_{rg}) + T_{exh} x_{rg} \tag{5.14}$$

Based on previous research, the measured inlet air temperature (measured in the intake manifold) shows a slight inaccuracy due to heat transfer phenomena. For this purpose, a corrected intake temperature is introduced according to

$$T_{inl,corr} = T_{inl} + 0.56\left(T_{coolant} - T_{inl}\right)\left(\frac{10^3 m_{fuel} Z_{st} \lambda N}{60 \cdot 2}\right)^{-0.34} \tag{5.15}$$

The difference between measured and corrected inlet air temperature is depicted in figure 5.10. It is worth noting that the corrected temperature is based on regression parameters determined at AVL during previous measurements. The relative physical location between the measured and the corrected temperature is not well defined, but since equation 5.15 has previously been used with good results [4] it is included here as well.

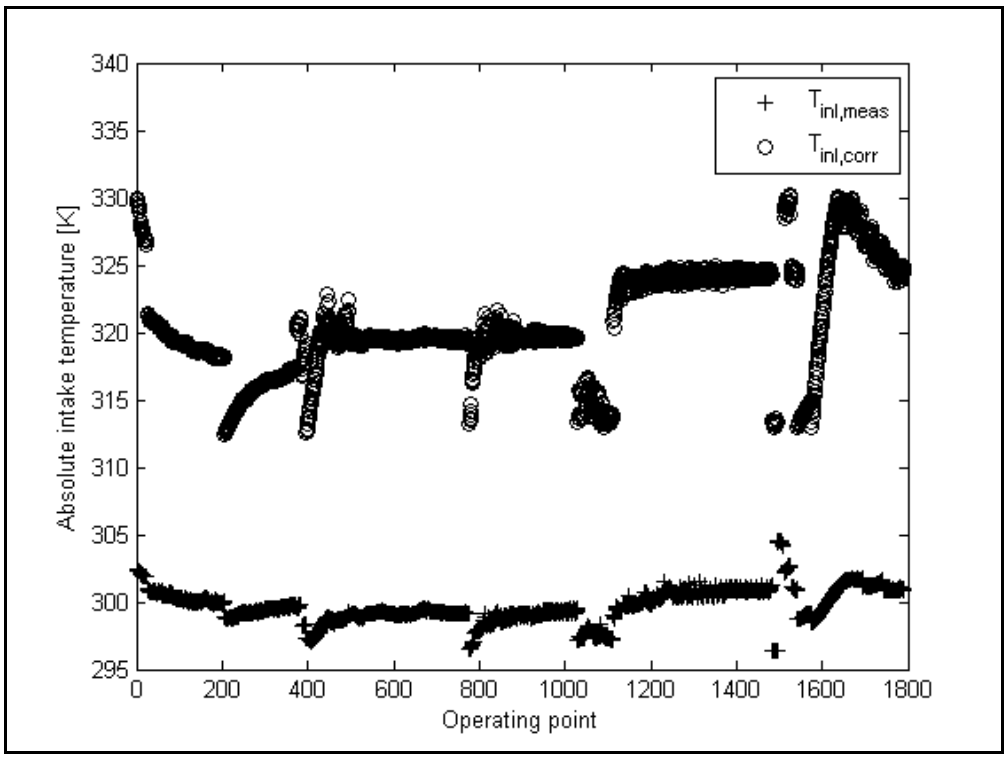

Figure 5.10. Comparison between measured and corrected inlet air temperature for all operating points.

It is evident that this residual gas model approach requires an iterative process, since the residual gas fraction influences the temperature (and pressure), which in turn affects the residual gas fraction. Although these iterations are time consuming, they are also deemed necessary in order to obtain sufficient overall model accuracy. The steps involved in this iteration are described below.

5.4.1 Iterative modelling approach

The entire combustion model is run with the simplified model in equation 5.12, the residual gas fraction is updated based on the calculated charge masses and the model is run once again with the new residual gas fraction. This approach is relatively slow but provides accurate results; figure 5.11 shows a schematic flowchart of the process.

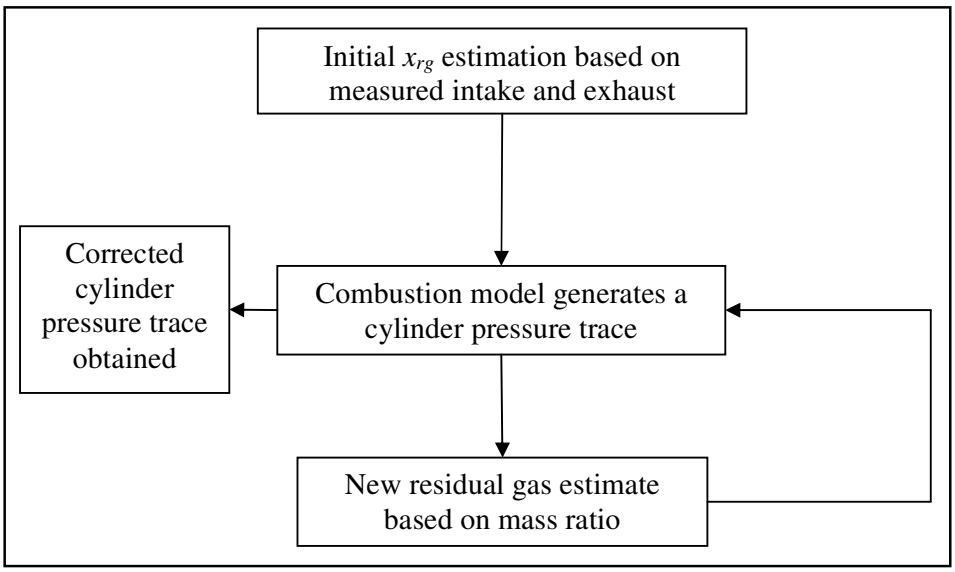

Figure 5.11. Flowchart for determining residual gas fraction.

5.5 Combustion modelling

The methodology described in the paragraphs below had also been implemented in the model prior to this work and only needed to be recalibrated to obtain the correct regression parameters. The compression and expansion processes are modelled as two separate polytropic processes; see chapter 5.6.1. To connect the two asymptotes, a model for the actual combustion event is required. The model has to capture the instantaneous combustion rate, which is why the Vibe function is desirable. It describes the fuel mass fraction burned across the entire combustion duration interval as

$$x_b(\theta) = 1 - e^{-a\left(\frac{\theta-\theta_0}{\Delta\theta}\right)^{m+1}} \tag{5.16}$$

In [10], a method based on laminar burning velocity correlations is suggested for determining the shape factor m and the burn duration $\Delta\theta$. The angle θ_0 is taken as the crank angle where spark timing occurs and a is defined as

$$a = -\ln(1 - x_{b,EOC}) = -\ln(1 - 0.999) = 6.90 \tag{5.17}$$

As described in [4] and [11], it turns out that the correlation functions obtained in [12] are difficult to use for extrapolation and therefore a simplified regression model has been used.

The regression model is based on the double logarithm method suggested by Vibe, and by taking the natural logarithm of equation 5.16 twice and rearranging the terms, one obtains

$$\ln\left[\frac{\ln(1-x_b(\theta))}{\ln 0.001}\right] = (m+1)\left[\ln(\theta-\theta_0)-\ln(\Delta\theta)\right] \tag{5.18}$$

The measured data can then be fitted to a linear function $y = kx + b$ (known as the transformed heat release concept in [12]) and the Vibe parameters are calculated as

$$\begin{aligned} m &= k-1 \\ \Delta\theta &= e^{-b/k} \end{aligned} \tag{5.19}$$

Regression analysis based on least-square fit is performed and a good fit is achieved with

$$\begin{aligned} m = a_1 + a_2 x_{rg} + a_3 x_{rg} p_{inl} + a_4 x_{rg} N + a_5 N + a_6 N^2 + a_7 \varphi_{spk} + a_8 \varphi_{spk}^2 + \\ + a_9 p_{inl} + a_{10} p_{inl}^2 + a_{11}\lambda + a_{12} OL + a_{13} OL^2 + a_{14} r_{c,real} + a_{15} l_{IV}^2 \end{aligned} \tag{5.20}$$

$$\begin{aligned} \Delta\theta = a_1 + a_2 x_{rg} + a_3 x_{rg}^2 + a_4 x_{rg} N^2 + a_5 N + a_6 N^2 + a_7 \varphi_{spk} + a_8 \varphi_{spk}^2 + \\ + a_9 p_{inl} + a_{10} p_{inl}^2 + a_{11}\lambda + a_{12} OL + a_{13} OL^2 + a_{14} l_{IV}^2 \end{aligned} \tag{5.21}$$

In this context, $r_{c,real}$ refers to the actual compression ratio, i.e. the one based on IVC timing instead of the volume ratio between BDC and TDC.

For m, the standard deviation is 0.1632 and the regression coefficient R^2 is 0.9227 and for $\Delta\theta$, the standard deviation is 4.8472 and the regression coefficient is 0.8557.

Figure 5.12 exemplifies the fitted regression accuracy where the estimated and modelled Vibe parameters are plotted against the size of the valve overlap. The regression model does not fully capture the behaviour during really slowly burning cycles, which could be due to uncertainties in the residual gas estimation. However, the general accuracy is deemed good enough.

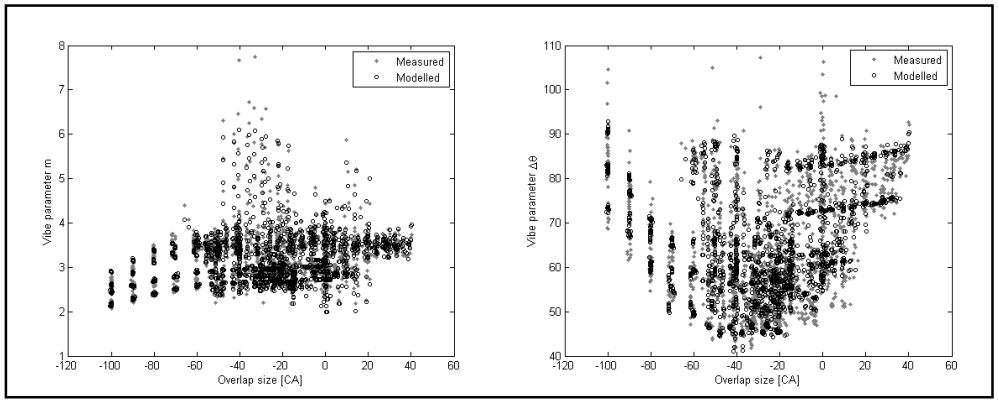

Figure 5.12. Vibe parameters plotted against size of valve overlap.

5.6 Complete 4-stroke cycle simulation

With all thermodynamic relationships and parameters described above available, it is now possible to bind everything together to form the complete four-stroke cycle. For reading convenience, the cycle is divided into four different parts and some additional logic around gas exchange TDC. Below follows a description of each of the four sequences. Since the model is based on MATLAB's ode45 solver, all equations need to be expressed as differentials.

5.6.1 IVC to SOC

After the intake valve has closed, the polytropic relationship

$$pV^{\gamma} = \text{constant} \tag{5.22}$$

is used to align the measured pressure trace correctly. This technique is referred to as pegging and needs to be done because the cylinder pressure transducer is unable to measure absolute pressure and therefore only detects pressure changes. The pressure offset correction is determined as

$$\left(p_1 + p_{off}\right)V_1^{\gamma} = \left(p_2 + p_{off}\right)V_2^{\gamma} \rightarrow p_{off} = \frac{p_2V_2^{\gamma} - p_1V_1^{\gamma}}{V_1^{\gamma} - V_2^{\gamma}} \tag{5.23}$$

Equations 5.22 and 5.23 are only used to remove the offset error from the measurement and are not integrated into the simulation. Figure 5.13 shows the compression process after IVC. The logarithmic pressure trace has a linear slope, where the inclination corresponds to the specific heat ratio.

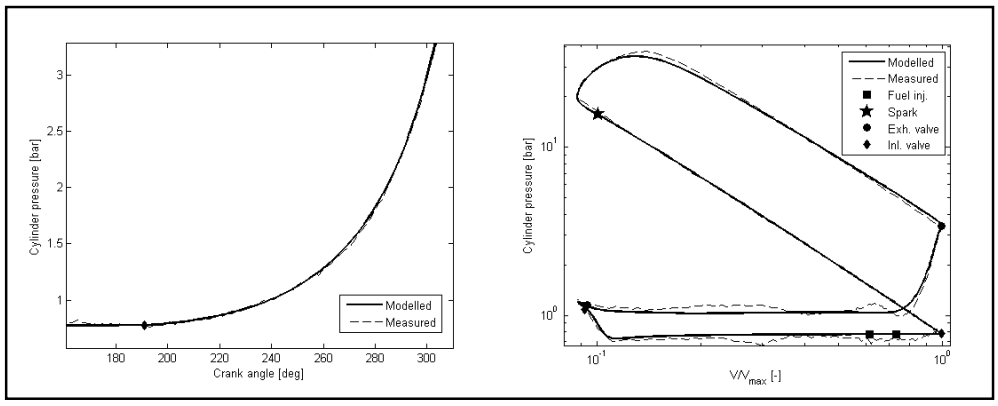

Figure 5.13. Compression process shown as crank angle resolved (left) and logarithmic (right) cylinder pressure trace. The diamond indicates IVC timing after which the pegging calculation is triggered.

For simulating this part of the engine cycle, the temperature and pressure differentials described by equations 5.4 and 5.5 are used. The only difference is that the system is now considered closed (because the valves are closed), i.e. the term dm_c is equal to zero. This part of the cycle was already implemented in the model described in [4].

5.6.2 SOC to EVO

Combustion is, according to the methodology described in chapter 5.5, initiated at the crank angle for spark timing. The burn rate is modelled as

$$dx_b = \frac{a(m+1)}{\Delta\theta}\left(\frac{\theta-\theta_0}{\Delta\theta}\right)^m e^{-a\left(\frac{\theta-\theta_0}{\Delta\theta}\right)^{m+1}} \tag{5.24}$$

which is nothing else than the differentiated Vibe function and the corresponding heat release is

$$dQ_{ch} = dx_b q_{HV} \tag{5.25}$$

The transition between unburned and burned gases influences the specific heat ratio and is modelled as

$$\gamma = (1 - PR(\theta))\gamma_u + PR(\theta)\gamma_b \tag{5.26}$$

where subscripts *u* and *b* denote unburned and burned gases respectively. In this context, *PR(θ)* is the Vibe function defined in equation 5.16. This part of the model was also implemented in [4].

5.6.3 EVO to EVC

When the exhaust valve opens, the blowdown process commences and the cylinder pressure will approach the pressure in the exhaust manifold. Figure 5.14 shows an example of this process.

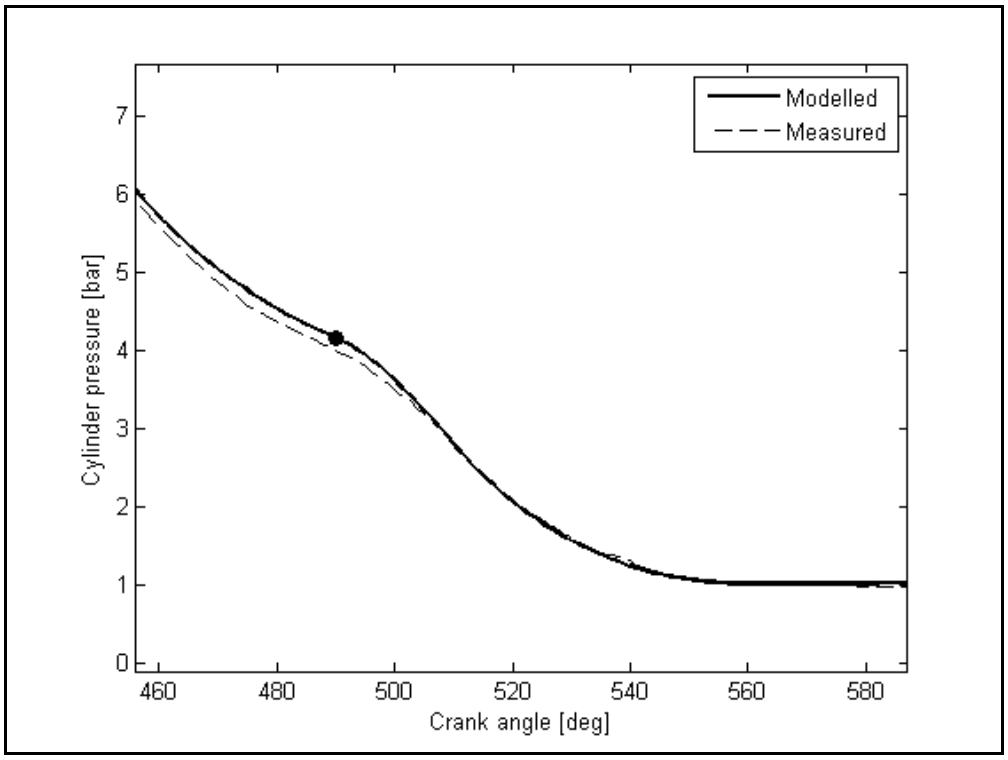

Figure 5.14. Blowdown process after EVO, marked with a circle. The transition appearance from in-cylinder to exhaust conditions depends primarily on engine speed and load.

Using the schematic valve lift profile described in chapter 5.3.1, the mass flow can be included in the differential equation as suggested in chapter 5.3. To account for possible backflow, i.e. when the cylinder pressure drops below exhaust manifold (atmospheric) pressure, the mass flow equation is extended with a *sign* function (figure 5.15) and due to the sign convention in the original heat release equation, a minus sign should also be added, giving

$$dm_c = -\frac{pC_D A_{nom}}{\sqrt{RT_0}}\left(\frac{p}{p_0}\right)^{\frac{1}{\gamma}}\left\{\frac{2\gamma}{\gamma-1}\left[1-\left(\frac{p}{p_0}\right)^{\frac{\gamma-1}{\gamma}}\right]\right\}^{\frac{1}{2}}\frac{60}{2\pi N}\operatorname{sgn}(p_0-p) \tag{5.27}$$

This equation relates the air flow rate to the pressure at the flow restriction (assumed equal to the static pressure just downstream of the restriction), as well as the upstream stagnation pressure and temperature.

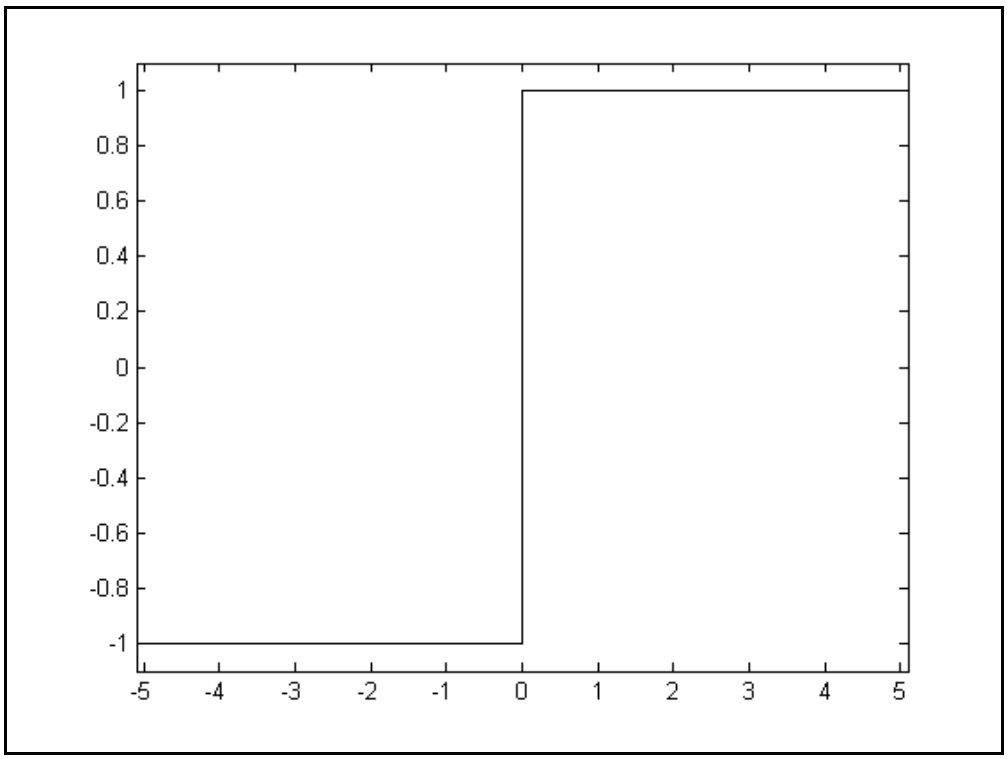

Figure 5.15. The *sign* function, close to $x = 0$ it will switch value repeatedly causing numerical difficulties in the ode45 solution.

5.6.4 IVO to IVC

When the intake valve opens and the induction of fresh air begins, a new blowdown process where the cylinder pressure approaches the intake manifold pressure commences. The same differential equations are used, but due to the sign convention regarding flow in to and out of the combustion chamber, the mass flow must be written as

$$dm_c = \frac{pC_D A_{nom}}{\sqrt{RT_0}} \left(\frac{p}{p_0}\right)^{\frac{1}{\gamma}} \left\{ \frac{2\gamma}{\gamma - 1} \left[1 - \left(\frac{p}{p_0}\right)^{\frac{\gamma-1}{\gamma}} \right] \right\}^{\frac{1}{2}} \frac{60}{2\pi N} \operatorname{sgn}(p_0 - p) \tag{5.28}$$

Due to numerical simulation speed in the ode45 solver, the *sign* function is problematic. Because the upstream/downstream pressure difference continuously alters between positive and negative values, the differential equation solver automatically reduces the solution time step in order to achieve the desired convergence tolerances. Thus, the *sign* function is only used when the relative pressure difference between upstream and downstream conditions exceeds 2%. This causes a slight degeneration in accuracy but increases simulation speed significantly. Figure 5.16 shows an example of the *sign* function constantly altering flow direction during the intake stroke.

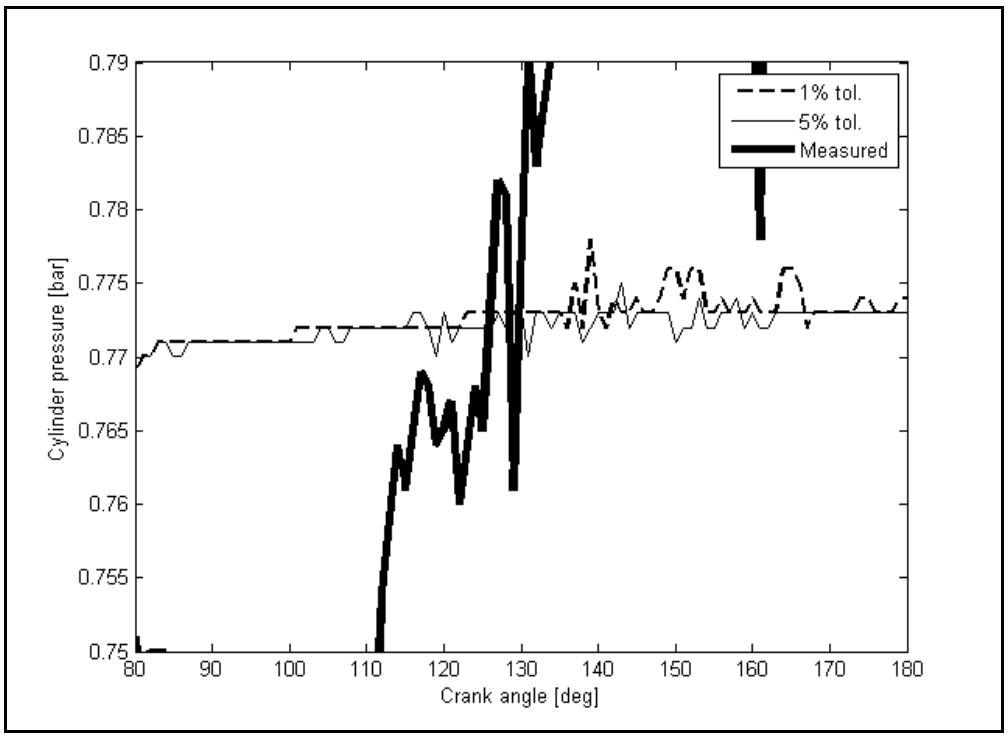

Figure 5.16. Alternating flow direction reduces simulation speed. A certain operating point is simulated using a 1% and a 5% backflow tolerance limit (thin lines). For the 1% limit, simulation time was around 7 seconds. Increasing to 5% reduced simulation time to around 4 seconds.

It can be seen that an increased sign tolerance smoothens the pressure trace in a noticeable way. This is a sequence extracted from part of the intake stroke (between 80 and 180 CAD after gas exchange TDC) and the two simulated pressure traces show different behaviour. If the sign tolerance is set to 1%, the ode45 solver will be forced to reduce solution step size, causing a rougher shape of the pressure trace. The resulting complete cylinder pressure trace will be closer to the measured one, but at the cost of computational time. However, introducing a tolerance as high as 5% causes convergence problems. Because of this, as mentioned above, a tolerance window of 2% has been used during simulations. In other words, the sign function modelling the backflow phenomenon is only taken into consideration when the relative pressure difference between upstream and downstream conditions exceeds 2%.

5.6.5 Valve overlap

During valve overlap there are two different possibilities. The engine could be run with NVO, i.e. the exhaust valve closes before the intake valve opens and a small, but not insignificant recompression occurs around gas exchange TDC. For this situation, the polytropic model is used one additional time between EVC and IVO. An example of this recompression phenomenon is shown in figure 5.17.

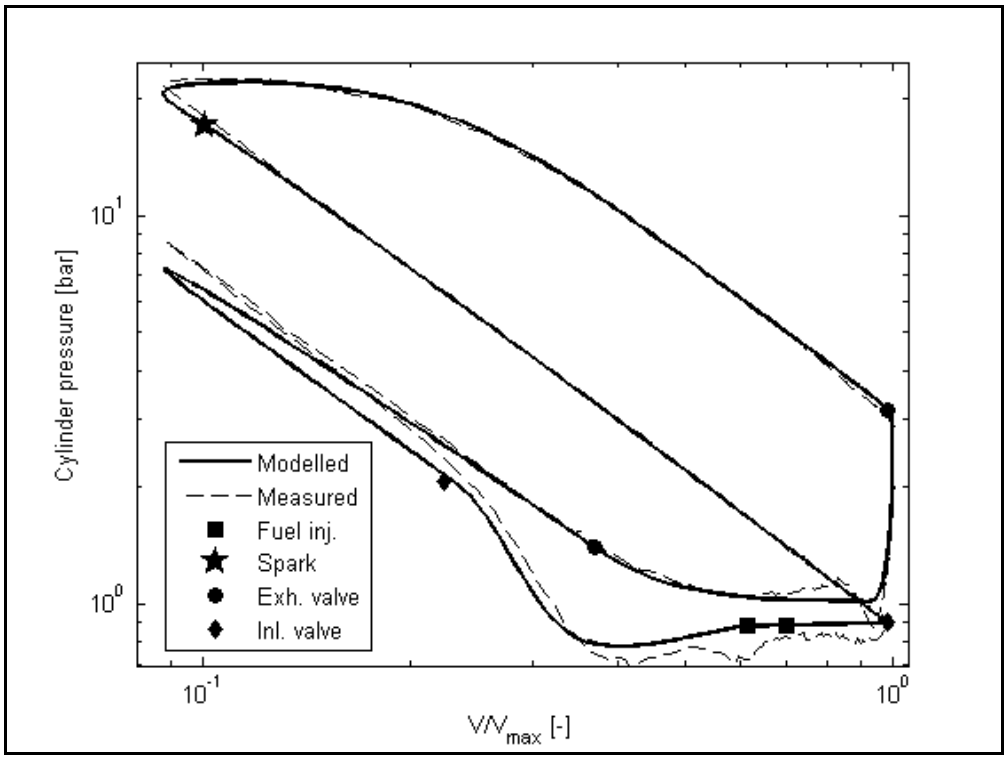

Figure 5.17. Cylinder pressure trace with EVC 60 degrees BTDC and IVO 40 degrees ATDC.

The other possibility is more typical for conventional valvetrain assemblies, namely positive valve overlap, see figure 1.4. During the overlap sequence, the flow direction of the gas mixture is controlled by the pressure ratio between intake and exhaust manifold. From IVO to EVC, the flow direction is thus controlled by this pressure ratio and with the backflow logic described in equations 5.27 and 5.28, an operating point with PVO looks like in figure 5.18.

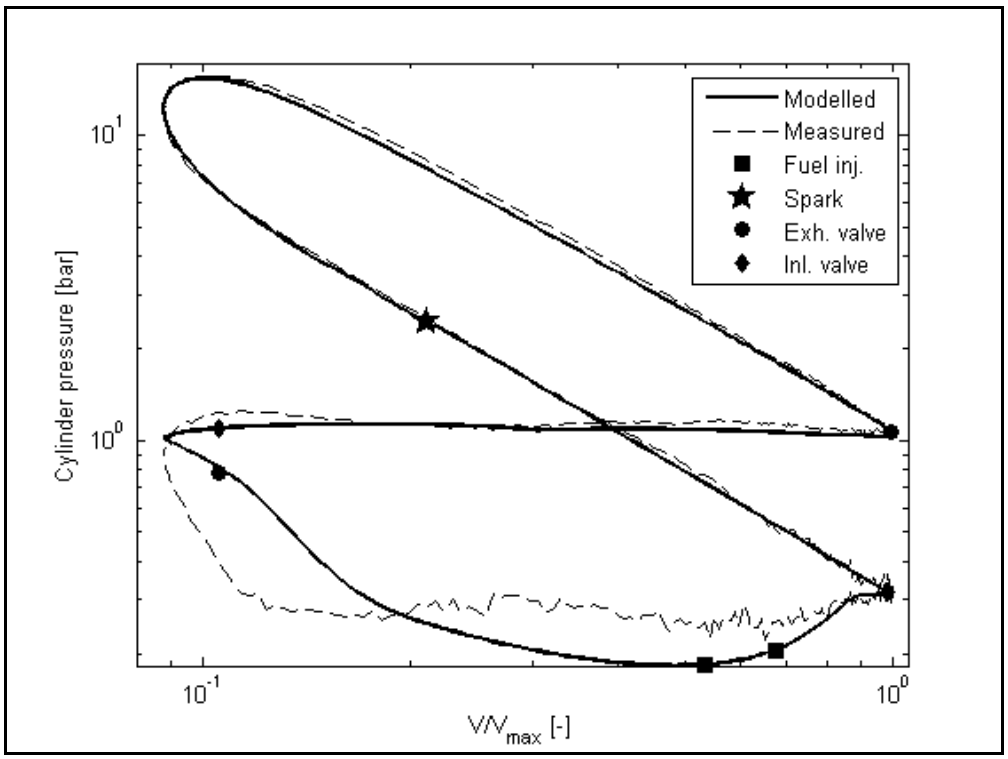

Figure 5.18. Cylinder pressure trace with EVC 15 degrees ATDC and IVO 15 degrees BTDC.

Unfortunately, because of the fast opening and closing response of the valves and the margins implemented in the safety system, positive valve overlap is only possible for higher engine speeds. Below approximately 2000 rpm, PVO is not allowed even for low valve lifts, which of course is a practical limitation imposed on the useable range of the flexible valvetrain.

6. Optimization algorithm

The model described above estimates the 4-stroke cylinder pressure trace with good accuracy, and it is reasonable to assume that the model can be used to generate the optimal cylinder pressure trace for a given operating point. This algorithm is broken down into several steps and to execute the implementation correctly, it is first necessary to define what is considered to be the optimal engine operation.

6.1 Target function

Optimized engine operation in this context refers to maximum overall efficiency. This means that for each given engine speed and fuel amount injected, the maximum engine torque should be output.

6.2 Limitations

Since not all parameters are included in the model, certain simplifications need to be made regarding the optimization objective function.

6.2.1 Fuel injection strategy

The model was originally developed for an engine with port fuel injection. During this work, only homogeneous direct injection has been used and no model alterations have been made to accommodate for this. As long as the injection takes place sufficiently early (implying homogeneous air/fuel mixture) this assumption is valid. In order to run the engine at stratified conditions, i.e. with fuel injection taking place during the compression stroke and possibly also after closing of the intake valve, the model must be significantly modified. The heterogeneous mixture is of particular interest during part load, since it allows much leaner gas mixtures. However, another issue that can't be overlooked is the issue of wall wetting. With a centrally placed fuel injector and the possibility to alter fuel pressure and injection timing, the risk of wall wetting becomes apparent. This affects emissions of CO and unburned hydrocarbons significantly, and since the emission measurements during these tests cannot be trusted, it is difficult to draw any conclusions regarding fuel injection strategy. Figure 6.1 illustrates the issue of possible wall wetting in an engine with direct fuel injection.

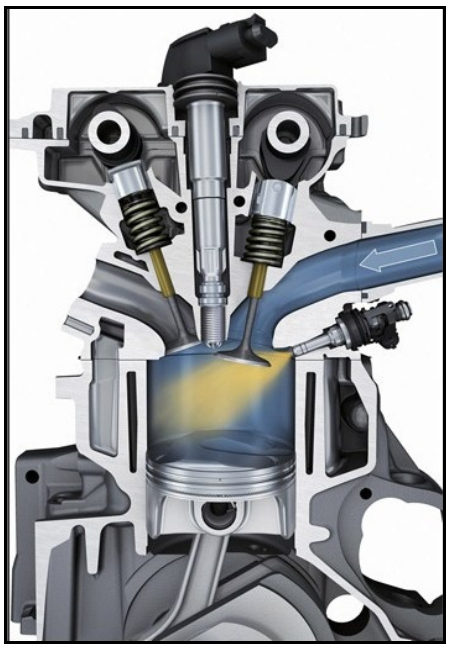

Figure 6.1. Example of a direct fuel injection configuration. High injection pressure combined with early SOI elevates the risk of wall wetting considerably.

6.2.2 Spark timing strategy

The combustion model does not currently have a knock model such as an Arrhenius equation (knock integral) implemented and to achieve maximum torque output the only possible spark timing is then MBT timing. On one hand, too early initiation of the spark during the compression stroke causes an efficiency loss, since the work transfer is from the piston to the cylinder gases. On the other hand, excessively retarding spark timing causes the combustion to complete too far into the expansion stroke, thereby resulting in lost expansion work because the peak cylinder pressure occurs long after TDC. A good general setpoint recommendation regarding combustion phasing is to adjust spark timing such that CA50 occurs approximately 8° $ATDC_{firing}$. If the engine is knock limited, spark timing needs to be further retarded. An illustration of the useful work dependence on spark timing can be seen in figure 6.2.

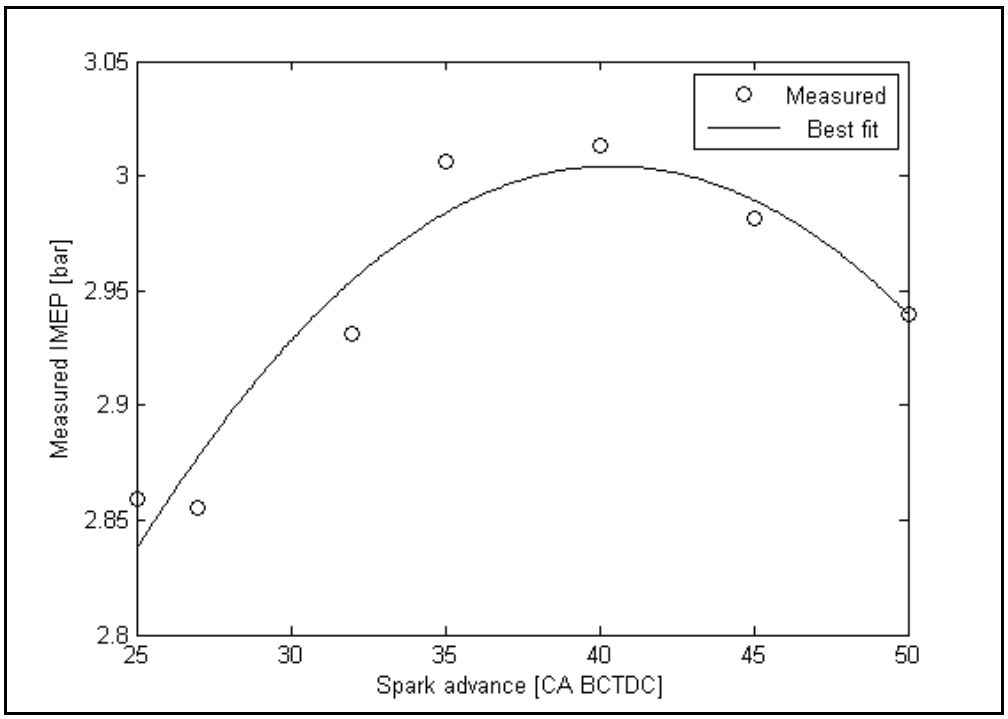

Figure 6.2. Spark hook for the engine operating at 2500 rpm, 33 kPa inlet pressure and stoichiometric combustion.

6.2.3 Additional limitations

Since the time consuming emission measurements have been disregarded during this work, it is difficult to draw any decisive conclusions regarding optimal mixture composition. Since most SI engines in production operate with homogeneous air/fuel mixtures and therefore still use a three-way catalytic converter for exhaust gas aftertreatment, the optimization is only carried out for λ = 1, where the catalytic converter efficiency is at its highest.

6.3 The actual optimization routine

With a cylinder pressure model that displays high prediction accuracy regarding mean effective pressures, burn rate, etc., it is reasonable to assume that it can be used to evaluate different valve timing strategies. Mathematically and computationally efficient optimization algorithms are slightly outside the scope of this work, and the simplest method is therefore to loop through possible valve timing combinations (and including the limitations regarding spark timing and fuel injection settings described above). The combustion model will then generate a cylinder pressure trace (giving IMEP and PMEP) and if this is done for each point, the result is a level curve where XMEP is presented as function of the valve timings.

The algorithm is initialized by defining engine speed, injected fuel mass and λ value, which then consequently gives the air mass according to

$$m_{air} = m_{fuel} \lambda Z_{st} \tag{6.1}$$

The combustion model also needs to be fed a reasonable starting guess for the inlet pressure. This is approximated as a load dependency fitted to measurement data according to figure 6.3.

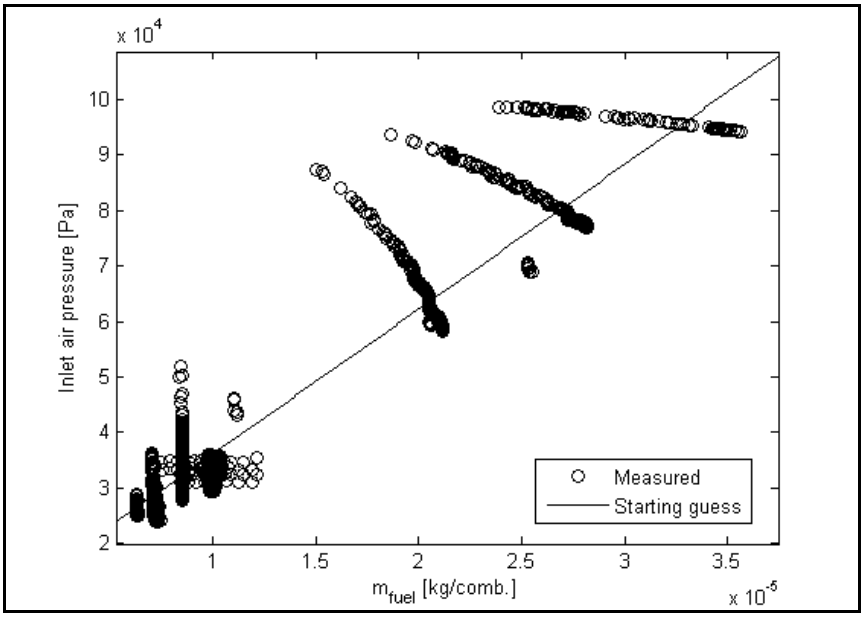

Figure 6.3. Inlet pressure and the fitted correlation $p_{in} = 2.6 \cdot 10^9 \cdot m_{fuel} + 1 \cdot 10^4$.

For the combustion calculations, a clear influence can also be seen from the exhaust gas temperature. As the model needs to be as parameterized as possible, this temperature also needs to be described by a correlation function. Based on measurement data, a least square fit is performed, giving

$$T_{exh} = 421 + 0.37N - 5.75 \cdot 10^{-5} N^2 - 7.23\varphi_{spk} + 0.09\varphi_{spk}^2 + 4.36 \cdot 10^6 m_{fuel} \tag{6.2}$$

This correlation results in an exhaust gas temperature varying with engine speed as depicted in figure 6.4. It is worth noting that the equation is only valid for stoichiometric combustion. If fuel

rich combustion is the case, the excess fuel will aid in cooling the exhaust gases, which is not captured by this simple regression model.

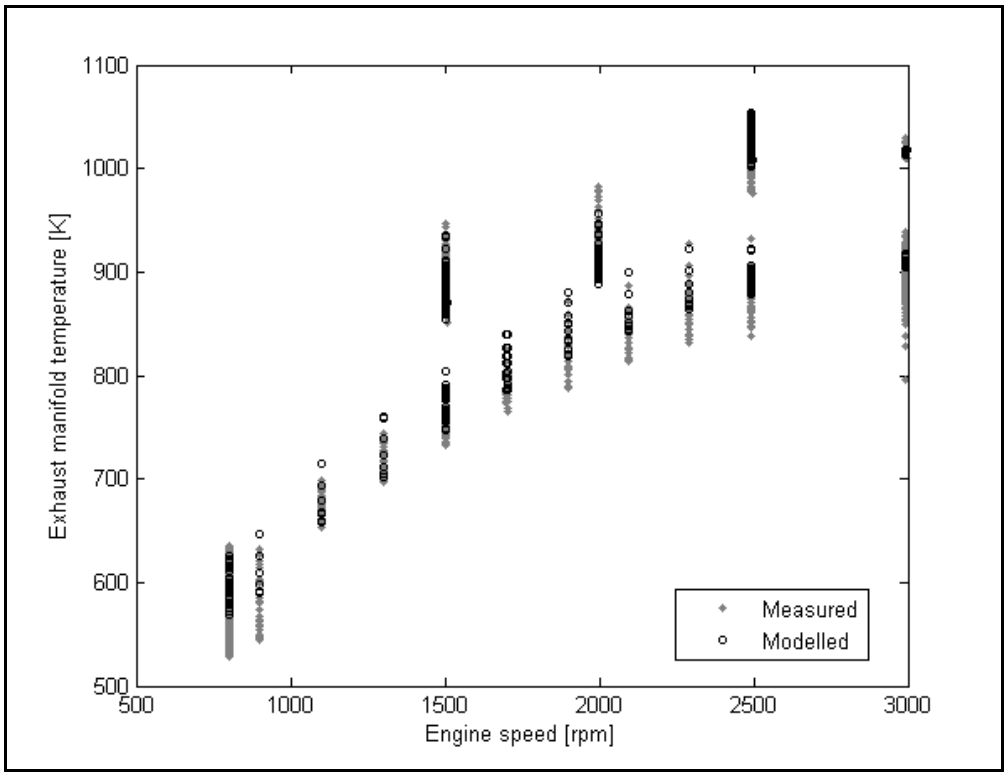

Figure 6.4. Comparison between modelled and measured exhaust gas temperature for different engine speeds.

With a starting point for the inlet pressure and the exhaust gas temperature, the combustion model can be initiated. Based on the inputs determined above and the user defined operating point, the model is called with fixed valve lift heights and exhaust valve timings. The inlet valve timings are varied across the entire practically useable range. Sweeping the inlet valve timings requires an iterative procedure; the first combustion model function call gives an actual air mass. This is then used to adjust the inlet air pressure until the desired air mass has been obtained. This procedure is repeated until the estimated air charge mass deviates less than +/- 5% of the nominal value. At the same time, the modelled cylinder pressure trace is used to analyze the combustion phasing in order to identify optimum spark timing.

Based on the chosen setpoint for CA50 (normally 8 CAD $ATDC_{firing}$), the spark timing is adjusted in the same iterative loop as the inlet pressure until the estimated CA50 value deviates less than +/- 2 CAD from the setpoint. This procedure executes quickly, and does not normally require additional iterations after the correct air mass has been obtained.

If this procedure would slow the routine down, for example if the residual gas fraction becomes much too high, one alternative way of adjusting the spark timing towards MBT would be to use the regression model in chapter 5.5. However, because the model iterations are necessary in order to correct the inducted air mass, it is easy to use these iterations to adjust spark timing as well without losing computational performance. The intake valve timings that provide the highest NMEP value are stored and the procedure is then repeated for the exhaust valve timings.

To account for the subsequent changes in residual gas fraction, the adjustments of spark timing and inlet pressure remain active during this process as well.

The exhaust valve timings that provide the highest NMEP value are stored and the process is repeated once more for different lift heights as well. Figure 6.5 shows the entire parameter variation sequence executed by the optimization script.

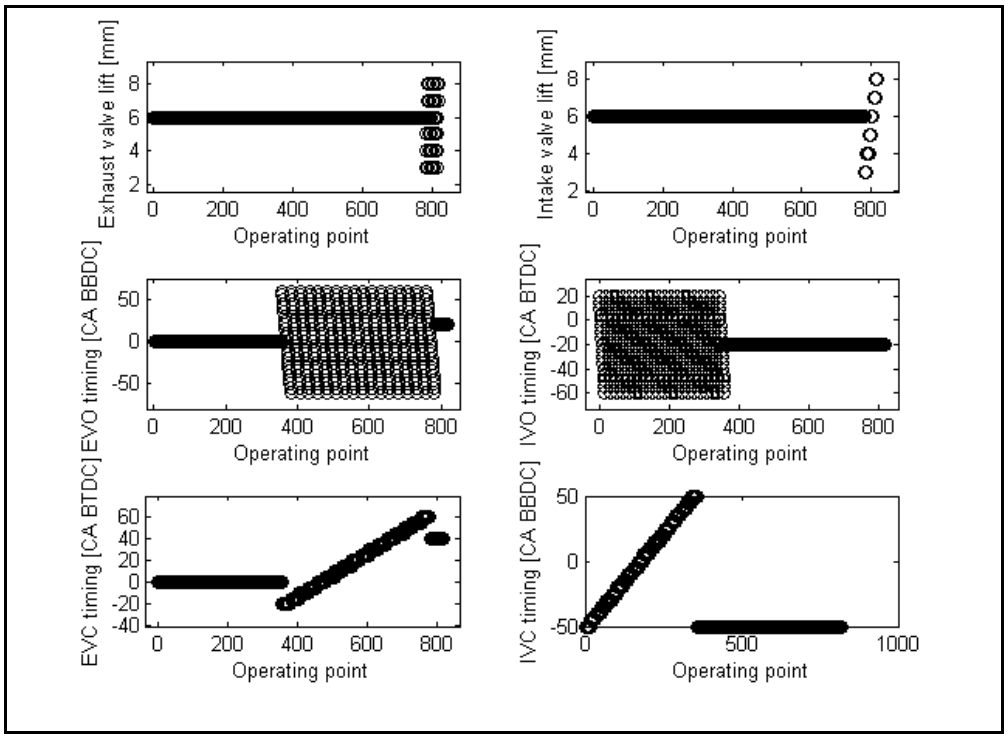

Figure 6.5. Total test sequence used to determine optimal valve settings. Intake and exhaust valve timings are frozen when the optimal settings have been found, assuming that a better point has not been found during the random variation sweep.

When this process is complete, the resulting modelled pressure trace is presented along with recommended parameter setpoints. Figure 6.6 shows an example of an exhaust timing sweep.

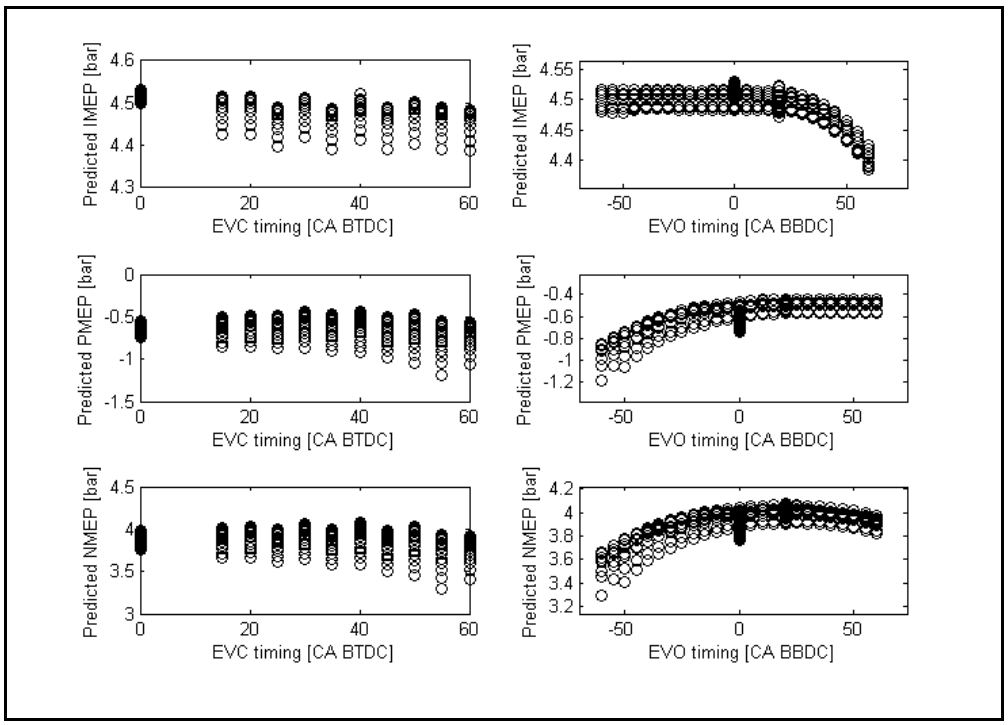

Figure 6.6. Predicted mean effective pressures against exhaust valve parameters, operating point in this case is 1350 rpm and 15 mg/comb. fuel mass flow.

The optimization algorithm could be further improved with respect to computational efficiency. The only time saving implementation that has been done includes a safety system check, meaning that for each requested combination of engine speed, valve lift height and valve timing, the actual cylinder pressure model will only be called if the settings are practically achievable with respect to the test bed safety system. Figure 6.7 shows the flow process as the optimization routine executes.

To handle situations where for example the inlet pressure needs to be raised above atmospheric levels to provide the desired air mass, certain other limitations need to be implemented as well. The estimated residual gas fraction is not allowed to exceed 35%, partly because it is difficult to fit the combustion (Vibe) parameters to higher ratios and partly because such high EGR ratios are considered to cause too large cyclic variations. For combustion phasing of CA50 position, spark timing is not allowed to be advanced more than 50 CAD $BTDC_{firing}$, since this will also increase the risk of erroneous extrapolation in the Vibe parameter regression model.

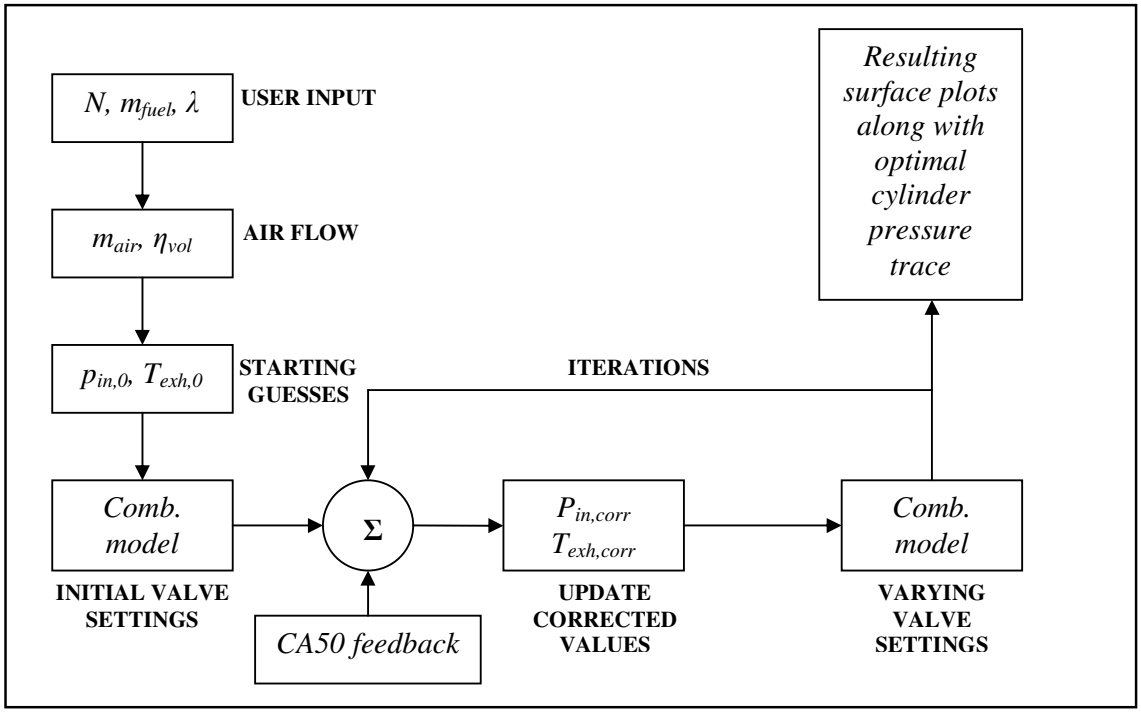

Figure 6.7. Optimization process flowchart from user input to an obtained result.

The procedure described above, where the intake and exhaust valves are treated separately, is unlikely to result in a global maximum efficiency point. This is because the intake and exhaust strokes are not disconnected during real engine operation. It is therefore an erroneous assumption to fix the exhaust valve settings while testing all possible intake valve settings. With more computational power it would be better to alter intake and exhaust valves simultaneously, evaluating all combinations but within the time frame of this project and the requirements on computational performance this optimization strategy is discarded. In an attempt to compensate for this fixation of the exhaust valve, an additional set of data points is run where all valve settings are varied randomly and simultaneously. During the model development and testing done in this work, this random variation has not managed to locate a settings area where higher efficiency has been achieved. This is an indication that the initial parameter testing provides reasonably accurate efficiency estimations. Although, when considering the statements above, the level curves obtained during this simulation should only be interpreted as local optimal setpoints.

7. Results and model validation

As previously discussed, the obtained mean value imposes certain limitations on measurement validity. The first step in the validation process is therefore to decide reasonable discarding tolerances for appropriate variables.

7.1 Discarded data

The valve variability gives the engine operator almost complete freedom when it comes to predefining the gas composition in the cylinder and this composition will in turn have a strong effect on combustion stability. Since the valve behaviour is sensitive to combustion variations they could start oscillating during a measurement and create larger and larger variations. With a static stabilization time of 10 to 15 seconds between setpoints, there is a risk that a measurement is being done when the engine operation is highly unstable. In this case, the mean values given in the log file are not accurate enough to fully describe the engine behaviour. Based on the operator's knowledge of how the valves behave in practice, the following filtering routine has been developed:

1. Eliminate all points where $CoV_{IMEP} > 15$ %
2. Eliminate all points where l_{IV} has a standard deviation > 25 %
3. Eliminate all points where EVC has a standard deviation > 10 %

The Coefficient of Variation (CoV) is a qualitative measure of combustion stability and is computed from the cyclic variations in IMEP as the ratio between standard deviation and mean value, i.e.

$$CoV_{IMEP} = \frac{\sigma_{IMEP}}{\mu_{IMEP}} = \frac{\sqrt{\frac{1}{N_x - 1}\sum_{i=1}^{N_x}\left(x_i - \bar{x}\right)^2}}{\frac{1}{N_x}\sum_{i=1}^{N_x} x_i} \tag{7.1}$$

where N_x is the total number of samples and $\bar{x}$ is the mean value of all samples in the series.

The points that fulfill at least one of the criterions above are considered to be too unstable to provide reliable cylinder pressure data and they are therefore excluded from the analysis. Since the stored cylinder pressure only is a mean value, excessive combustion irregularities will corrupt the pressure trace. For a complete list of all removed measurements from the data set used in this analysis, see appendix D. An example of an excluded cylinder pressure trace is shown in figure 7.1.

For the data set used in this project, 32 out of the 1790 (around 2 %) operating points are discarded.

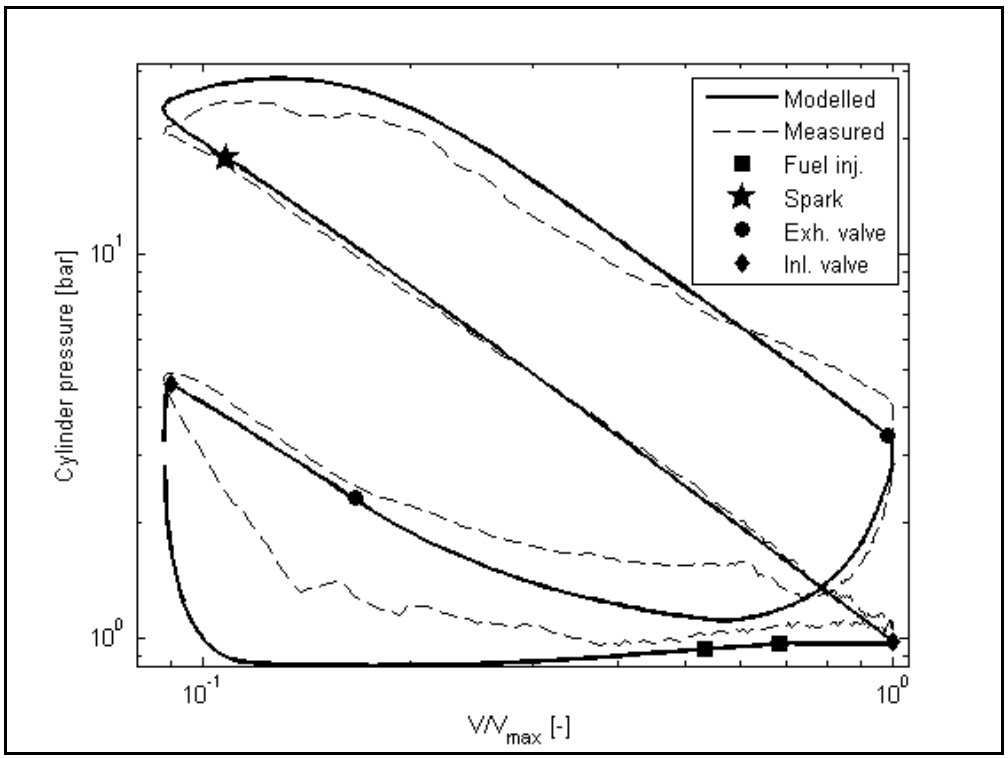

Figure 7.1. Typical appearance of a cylinder pressure that is excluded from the analysis, CoV for this point was around 32%.

7.2 Overall model validation

The cylinder pressure trace can be translated into mean effective pressures as explained in chapter 1.4 and if this comparison is done for all measured operating points, the result looks like in figure 7.2. This should be compared to the original model shown in figure 5.1, where little effort had been put into investigating the impact of the valve settings and the gas exchange behaviour.

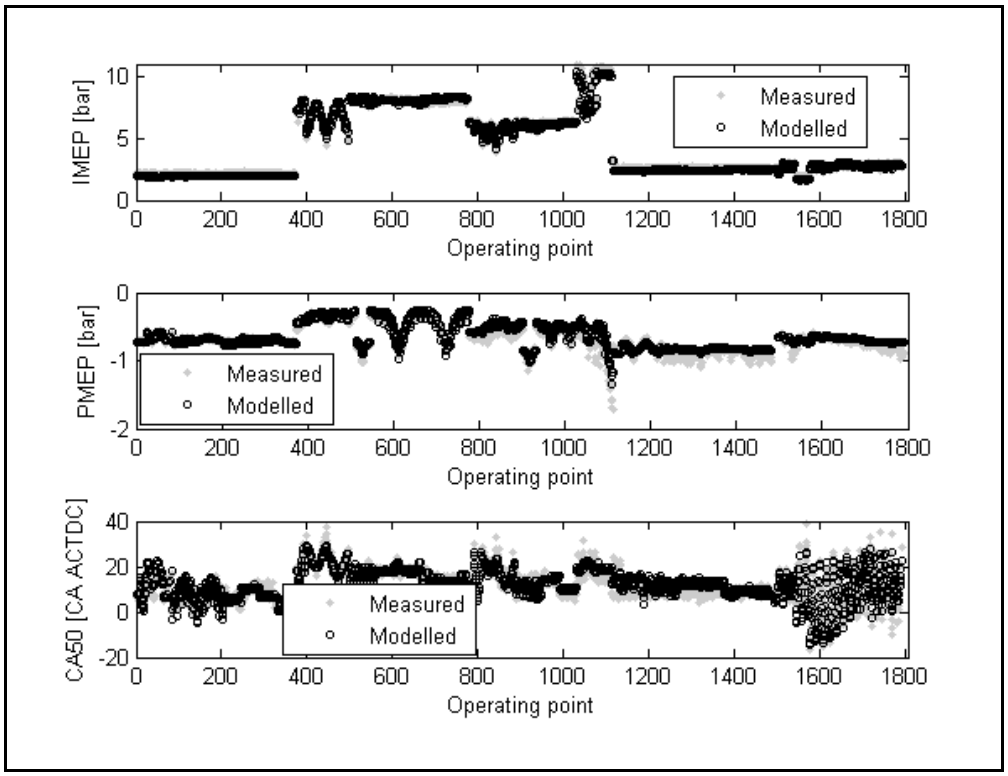

Figure 7.2. Overview of all evaluated operating points using the updated combustion model with improved gas exchange modelling and recalibration of the Vibe parameters.

A statistical analysis is carried out and shown in figure 7.3. The relative IMEP error has a standard deviation of 4.9% and a mean value of -3.6% and the relative PMEP error has a standard deviation of 8.8% and a mean value of -5.6%. In terms of absolute errors, IMEP has a standard deviation of 0.17 bar and a mean value of -0.09 bar. For PMEP errors, the standard deviation is 0.06 bar and the mean value is 0.04 bar. Figure 7.4 shows the corresponding histograms.

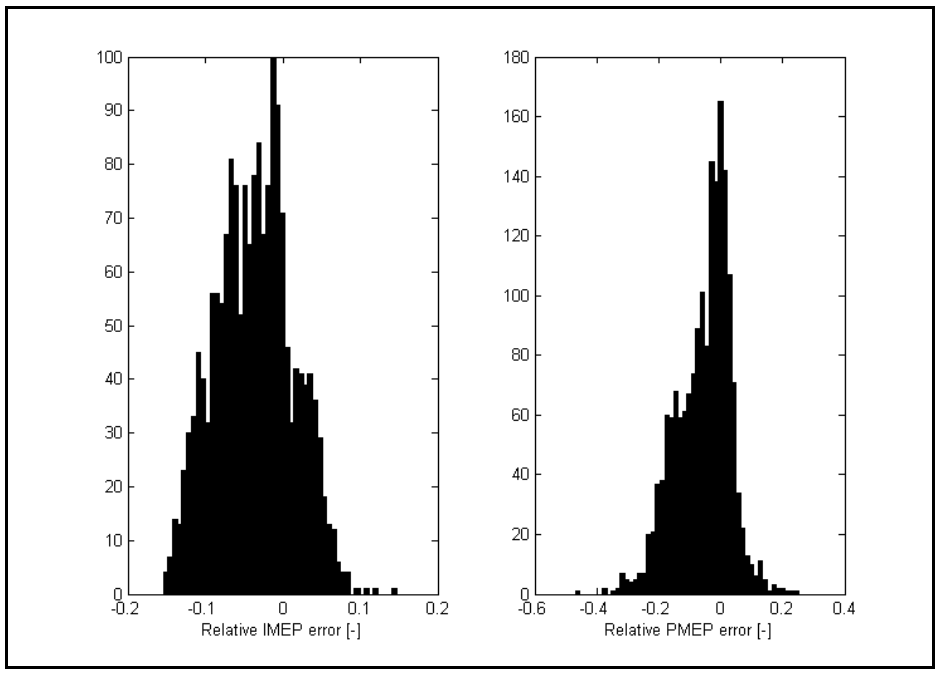

Figure 7.3. Histogram of relative IMEP and PMEP modelling errors.

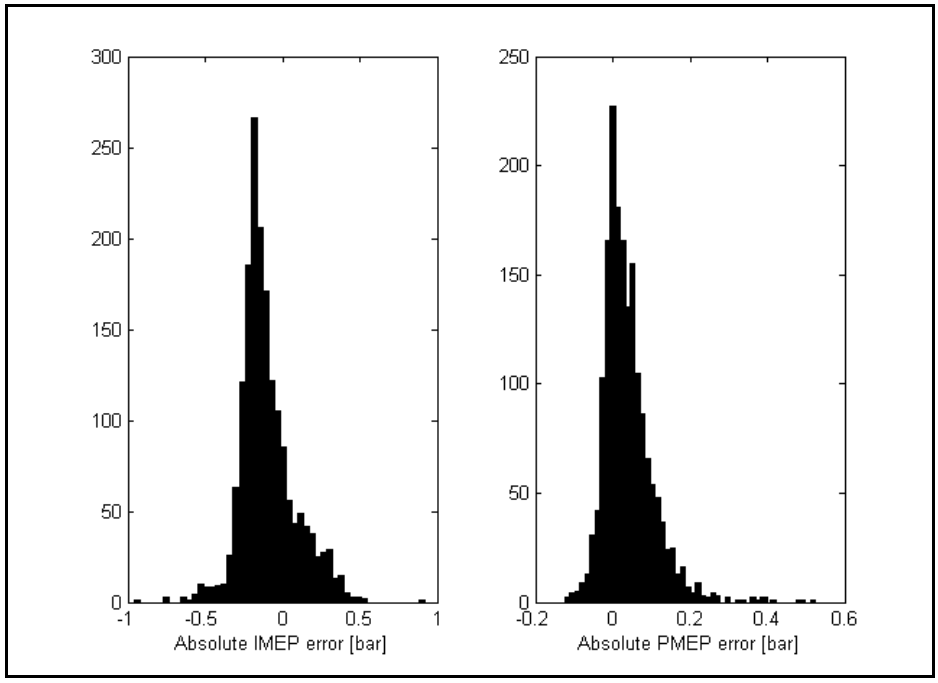

Figure 7.4. Histogram of absolute IMEP and PMEP modeling errors.

A more detailed error analysis can be done by looking at the model error as a function of individual parameters. In general, no obvious trends in modelling errors can be seen with respect to isolated parameter values. This indicates that there are no systematic errors hidden in the model. In figure 7.5, this is exemplified by the CA50 estimation error as function of exhaust valve parameters.

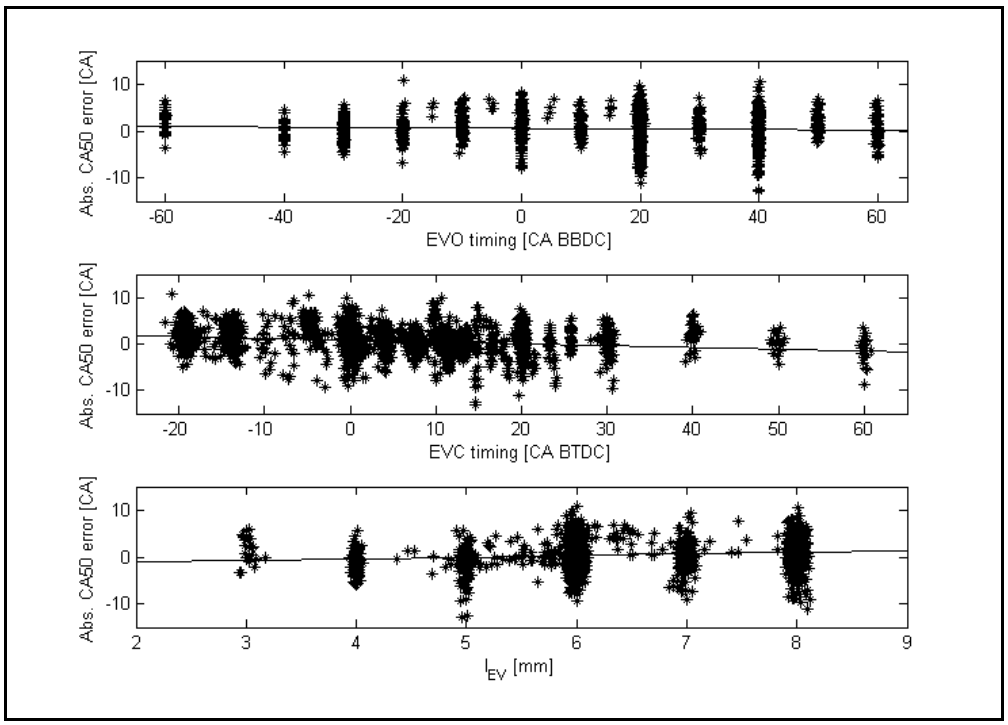

Figure 7.5. Absolute CA50 estimation error as function of exhaust valve timings and lift height along with trend lines.

A slightly negative trend can be observed for retarded (earlier) EVC timings, but this timing has strong influence on the estimated residual gas fraction, which in turn influences the combustion parameters. It is therefore difficult to conclude or determine the actual source of this error trend.

7.3 Evaluation of optimization routine

In an attempt to evaluate the optimization routine, three different engine operating points that have not previously been tested are chosen; 850 rpm and 8 mg/comb. fuel, 1350 rpm and 15 mg/comb. fuel and finally 2800 rpm and 20 mg/comb. fuel. These points are chosen to stay inside the operating map in figure 3.4, but should not coincide with the previously evaluated points. This forces the model to interpolate in the map and is a good measure of prediction accuracy. For these points, the sweep in the optimization routine is performed and the resulting level curves are compared. For the three operating points, a total number of 357 data points have been evaluated. Figure 7.6 shows the resulting NMEP level curves during the intake sweep for the low speed point described above.

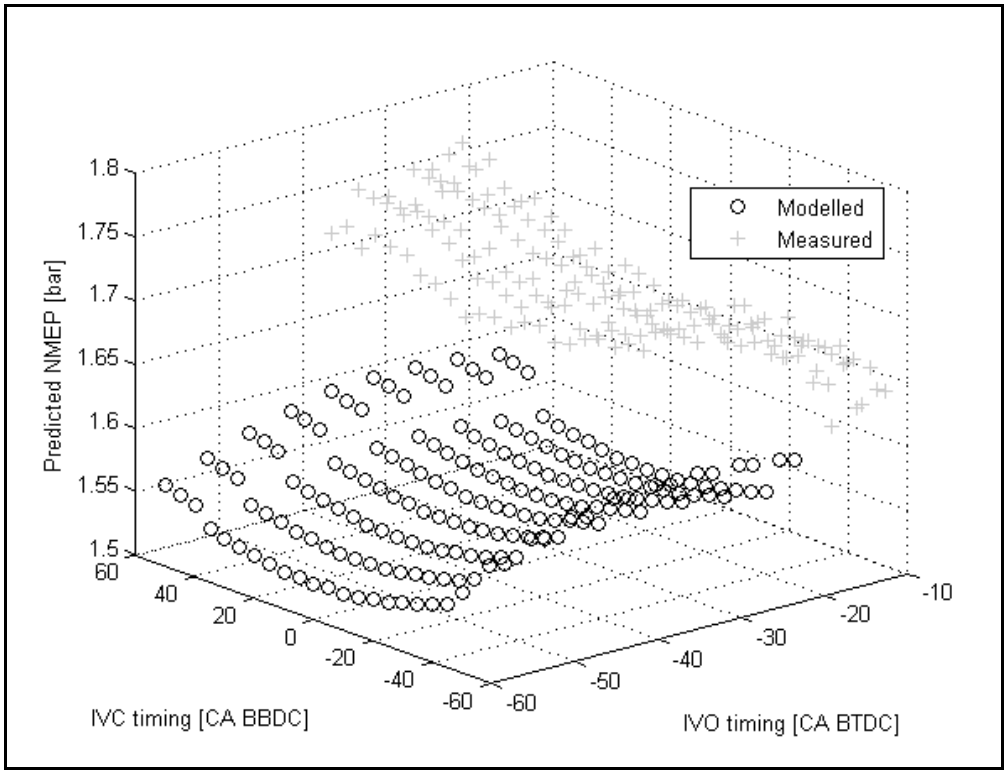

Figure 7.6. NMEP level curves during the simulated intake sweep for 850 rpm 8 mg/comb. fuel.

Apart from the absolute offset seen in the figure, the principal shape and appearance of the level curves seem to be similar. The saddle-like shape can be seen in both the measured and the modelled data set and this is a good indication of a reasonable prediction of the optimal settings. However, when the other operating points are evaluated, this appearance cannot be observed. The measured level curves in these cases are difficult to characterize geometrically and the model predictions does not appear to coincide with the measured mean effective pressures. An extended analysis based on individual cylinder pressure traces is carried out to try to determine the reason for this estimation error. Figure 7.7 shows this analysis as a comparison overview between measured and modelled pressure traces.

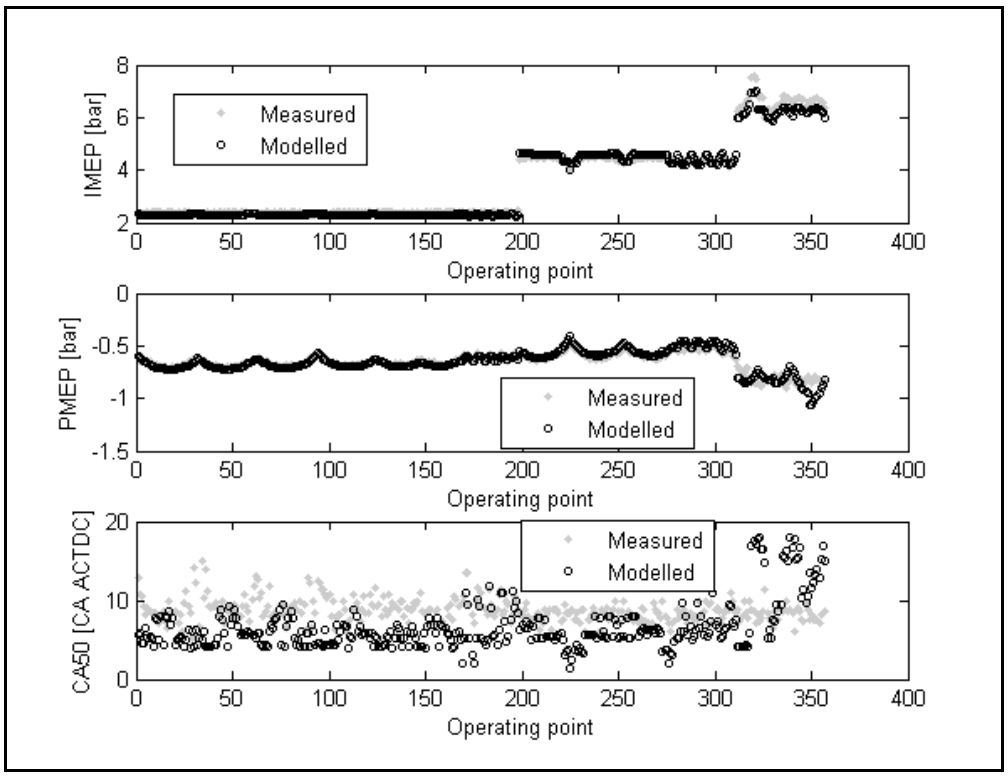

Figure 7.7. Modelled and measured IMEP, PMEP and CA50 values for the operating points tested during the optimization sweep.

In this figure, it is evident that the combustion phasing is no longer accurately modeled. In other words, the regression model used to determine the Vibe parameters is still a bit too sensitive to parameter changes. This can be illustrated by performing the same evaluation once again and just recalibrate the regression coefficients a_1, a_2, etc. in the least square polynomials in equations 5.20 and 5.21. When this is done, the cylinder pressure simulation looks like in figure 7.8.

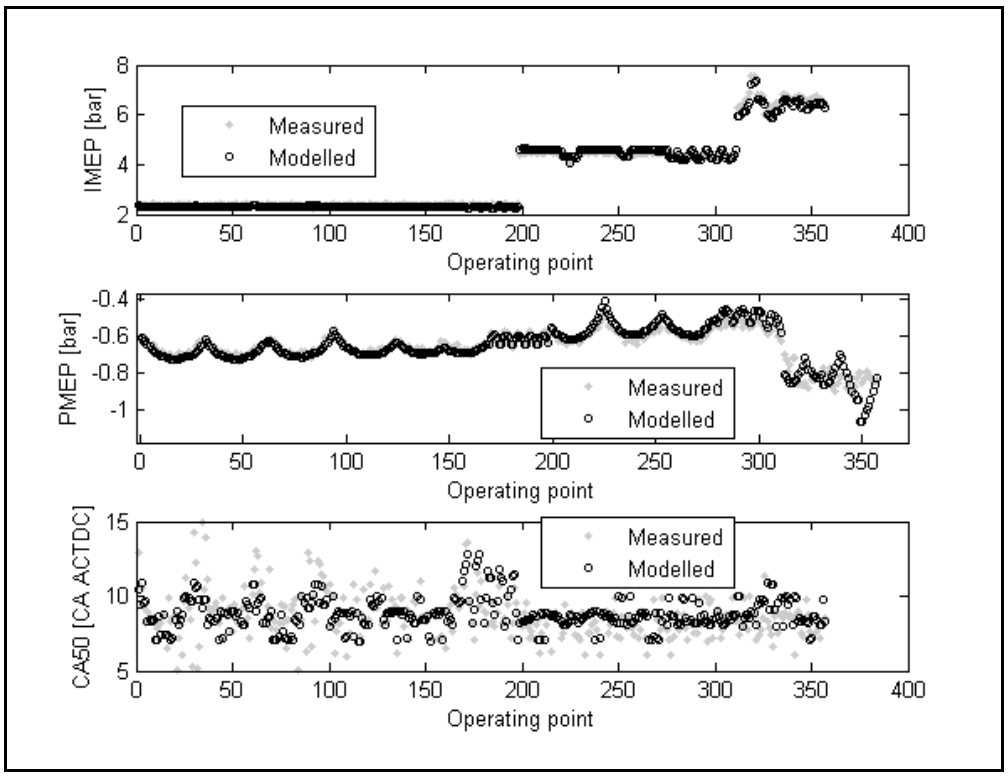

Figure 7.8. Modelled and measured IMEP, PMEP and CA50 with recalibrated Vibe parameters.

Hence, the final conclusion from this part of modeling is that more work needs to be done regarding the actual combustion process, small errors in the combustion burn rate profile will influence these kinds of predictions significantly. The faulty PMEP estimation for the rightmost set of data points comes from the fact that this is done at a high engine speed where the valve behaviour is known to be less consistent.

8. System analysis and discussion

Below follows a general discussion on how the valvetrain system and the combustion model actually have performed based on the measurements that have been carried out.

8.1 Control performance

Since transient performance has been given a lower priority than stability, it is more interesting to analyze the control error (i.e. the difference between requested and actual valve settings) than the step response performance. Figure 8.1 illustrates this control error for the exhaust valve openings, closings and lift heights for all 1790 operating points.

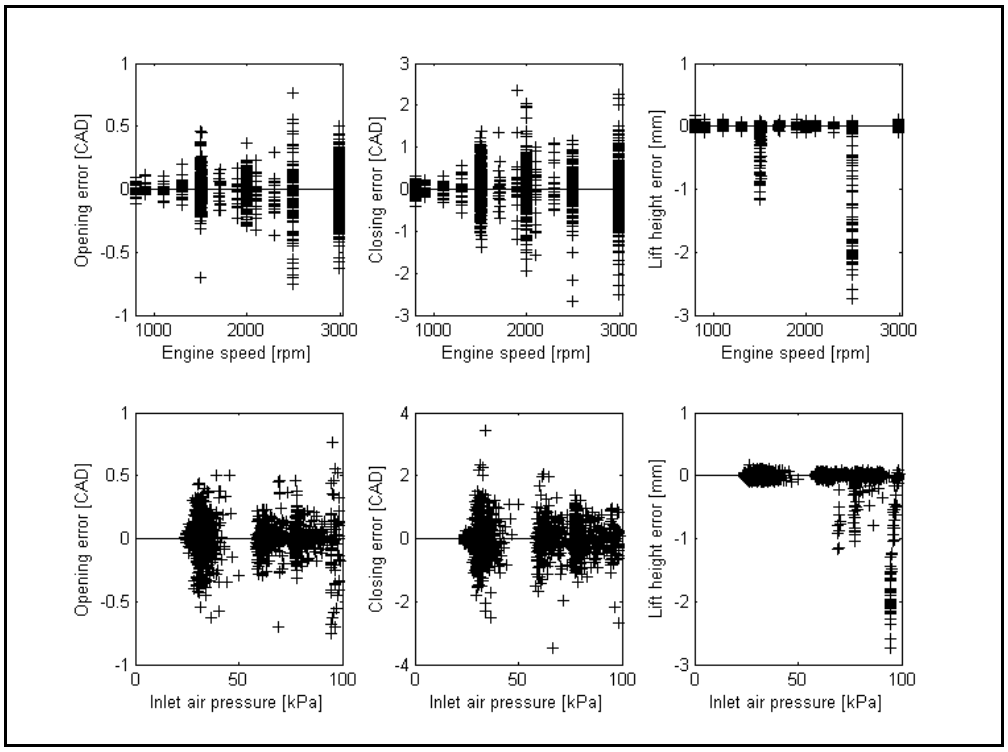

Figure 8.1. Exhaust valve control errors as function of engine speed (top) and intake pressure (bottom). As engine speed increases, EVC stability decreases and for higher engine loads the requested valve lift is not always fulfilled.

A similar analysis is performed for the intake valve, see figure 8.2.

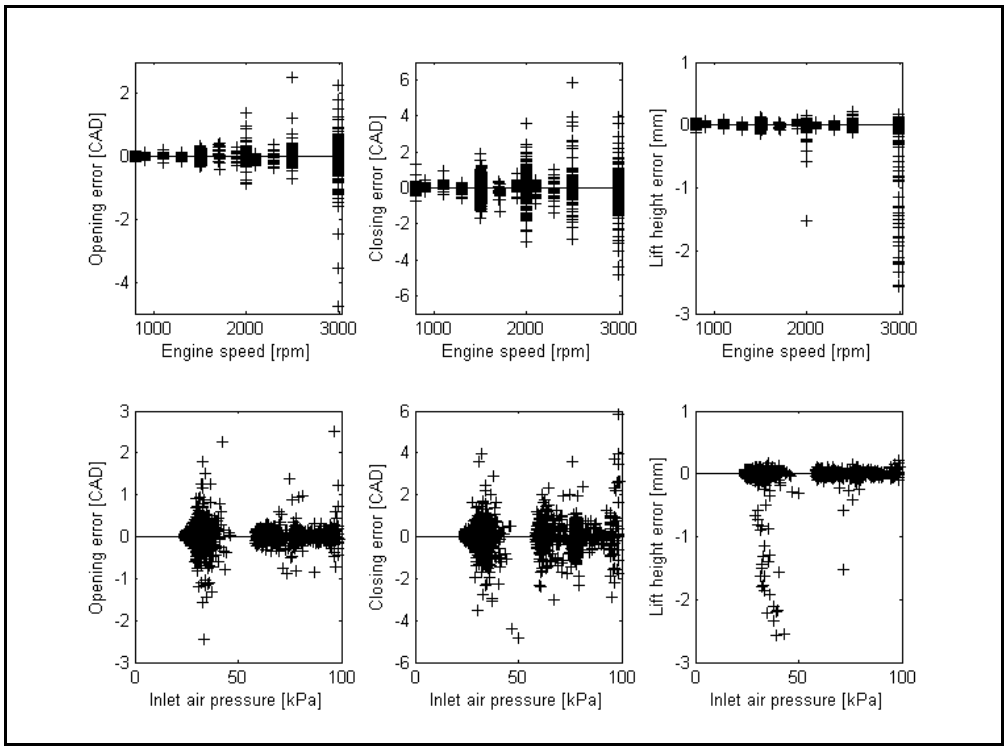

Figure 8.2. Intake valve control errors as function of engine speed (top) and intake pressure (bottom). As engine speed increases, both valve lift and IVC stability decreases.

A general tendency is that valve opening (exhaust and intake) is easy to control with good accuracy, regardless of engine speeds and loads. Intake valve lift shows no significant dependence on engine load, while the exhaust valve does. This error comes from the counteracting cylinder pressure existing during early EVO requests, making the lift height request impossible to fulfill.

The most difficult valve setting to control is the closing time. This because the closing velocity is approximately constant, making the closing time dependent on valve lift height. Since the actual lift height during a measurement sequence sometimes fluctuates +/- 1 mm from the requested value, valve closing is naturally directly affected by this. This instability becomes more severe for increasing engine speeds, but is fairly load independent.

8.2 Model accuracy

The overall model accuracy can be quantified primarily in terms of statistical measures as suggested in chapter 7.2. These numbers indicate that the model shows high prediction accuracy for a large number of operating points and also for a wide range of parameter changes. Another way to assess the model performance is to inspect the cylinder pressure traces visually. In figure 8.3, four different operating points are displayed. It can be seen that the model captures large parameter variations as well as different engine speeds and loads.

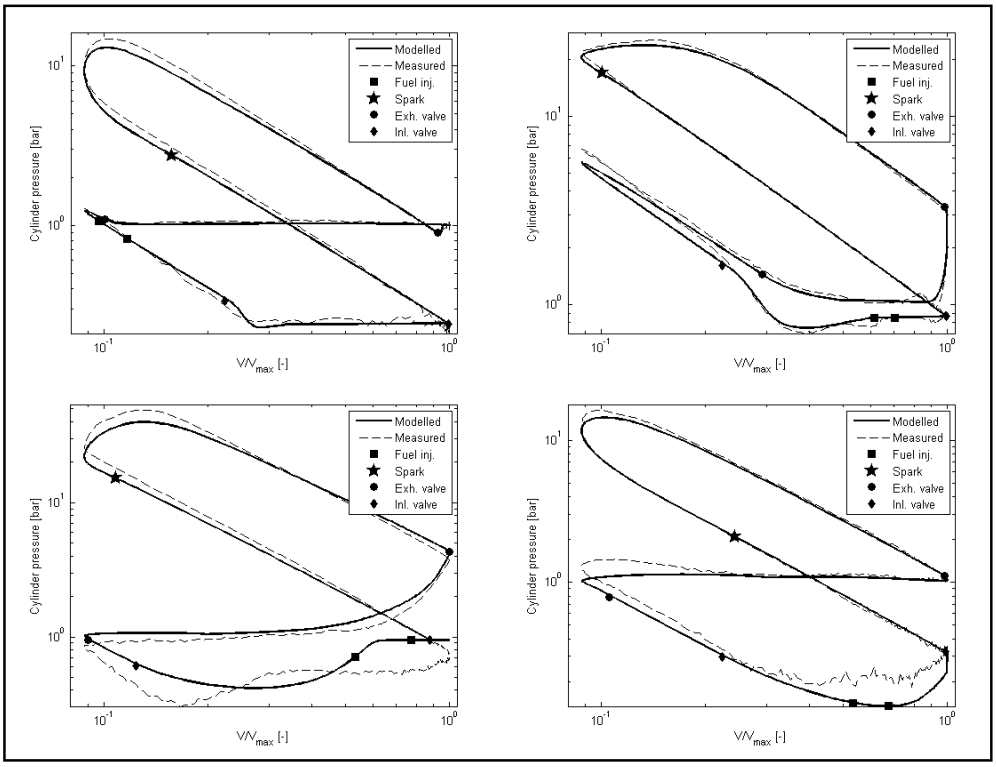

Figure 8.3. For different cylinder pressure traces spanning the entire parameter variation interval; top left – 800 rpm, intake and exhaust valve lift 4 mm, top right – 1500 rpm, intake and exhaust valve lift 6 mm, bottom left – 2500 rpm, intake and exhaust valve lift 8 mm, bottom right – 3000 rpm, intake and exhaust valve lift 7 mm.

It is also interesting to study the influence from individual parameters on the relative XMEP estimation error. This is an indicator on how well different parameters are captured in the model. Figure 8.4 exemplifies this by showing the absolute IMEP estimation error as function of measured IMEP, residual gas estimation and engine speed.

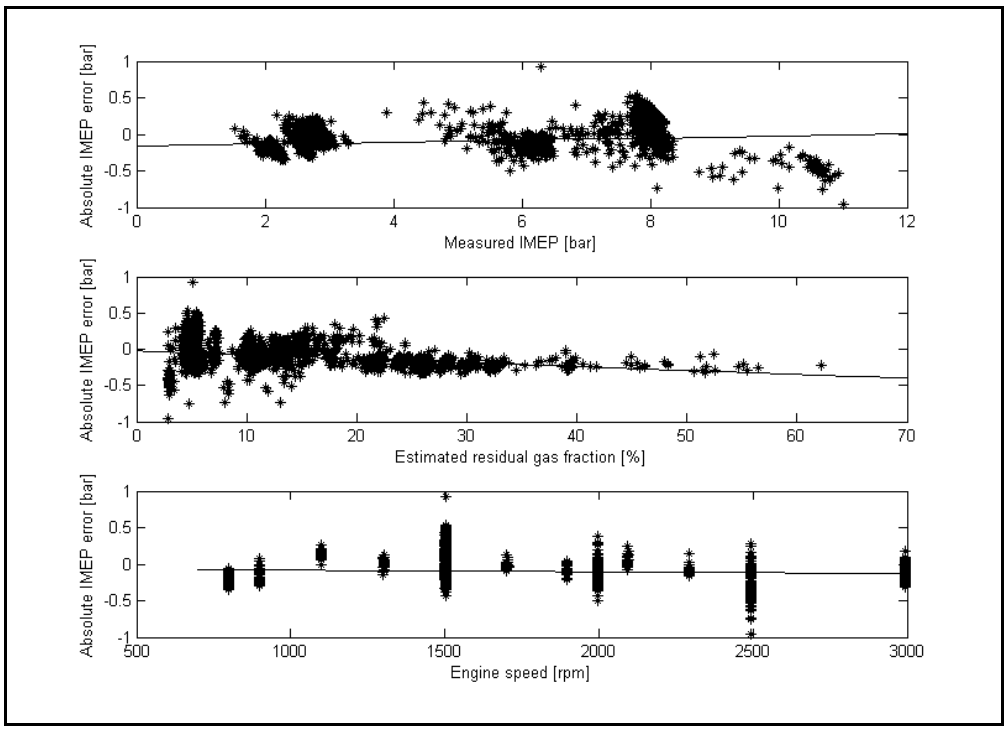

Figure 8.4. Absolute IMEP estimation error including trend lines as function of measured IMEP, estimated residual gas fraction and engine speed.

It can be seen that the model has some difficulties capturing the combustion characteristics at lower loads. This is partly because small absolute errors appear as large relative errors, but there also appears to be some inaccuracy involved in estimating the specific heat ratio. The start of compression phase after IVC correlates nicely with measured data, which should be an indication of a relatively correct residual gas estimation and initial intake port temperature. The exact cause for this error has therefore not been determined and figure 8.5 shows an example of a cylinder pressure trace where the modeled specific heat ratio during the compression stroke diverges from the measured one.

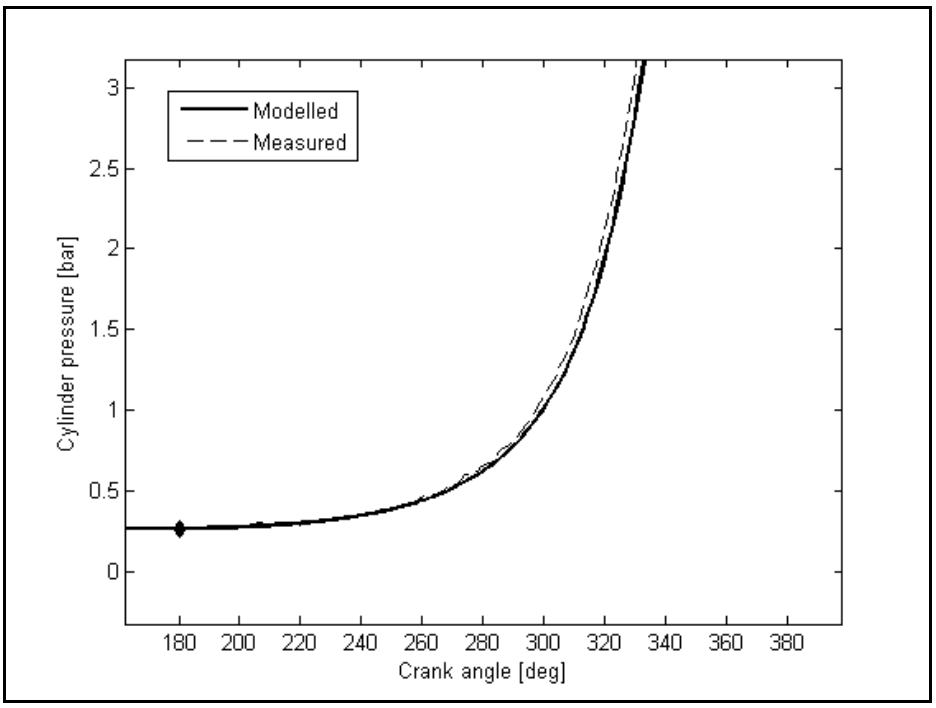

Figure 8.5. Operating point where the pressure buildup after IVC (diamond) is underpredicted when compared to measured data.

The same overall error analysis is carried out for the PMEP estimation, figure 8.6.

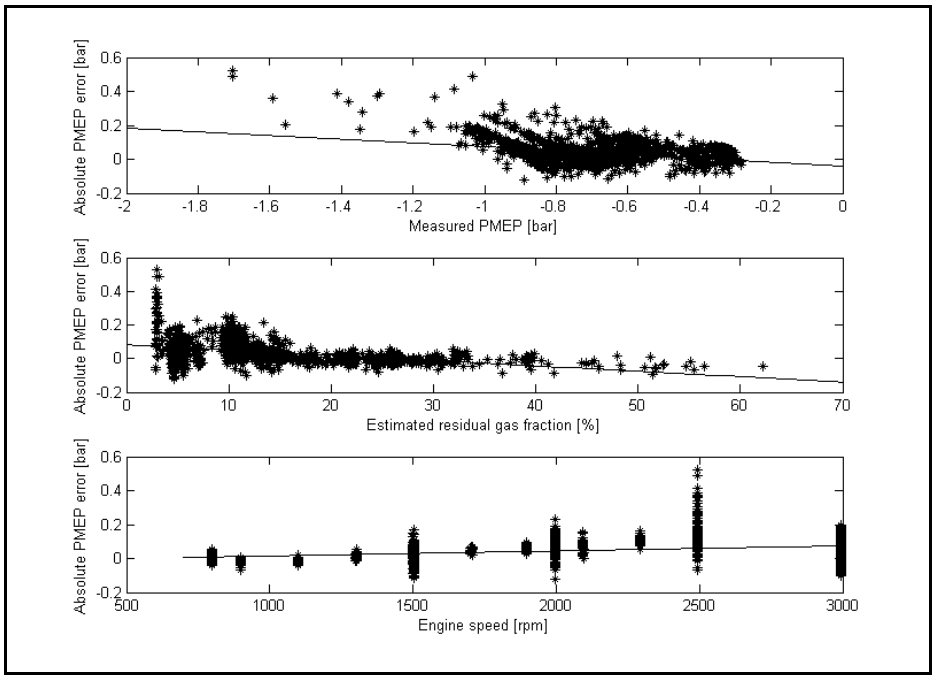

Figure 8.6. Absolute PMEP estimation error including trend lines as function of measured IMEP, estimated residual gas fraction and engine speed.

It is evident that increasing engine speeds are not completely captured in the model. The operating points with higher loads also deviate considerably, this could be due to more unsteady valve behaviour but the exact cause is difficult to determine.

8.3 Problems and uncertainties

In both the control system development and the modelling part of this work, many problems have risen along the way. Some of them have simply been ignored due to lack of time or insufficient measurement resources, while others have been implemented but need to be analyzed with respect to reliability and repeatability. Three key features are listed below.

8.3.1 Valve stability and residual gas resistance

One potential use of the flexible valvetrain is, as previously stated, the possibility to run HCCI combustion. In practice, this can be done by shortening both intake and exhaust valve duration to around 120 degrees and then phase the valves to operate the engine with large NVO. This means that a lot of the exhaust gases are maintained in the combustion chamber and a significant recompression occurs. The high residual gas fraction can then cause the engine to enter a CAI or HCCI mode.

One practical issue is the mode switch between regular Otto combustion and HCCI combustion. In the transition phase, large cyclic variations occur since the trapped residual gas fraction varies unsteadily. These cyclic variations consequently mean that the counteracting cylinder pressure at requested valve opening will vary from cycle to cycle. This pressure variation causes unsteady valve behavior and because of this it is difficult to make the engine operate steadily in HCCI mode.

8.3.2 Cylinder pressure mean value trace

The data logging of the cylinder pressure trace is of course another topic for robustness analysis. Because it is not currently possible to stream data with crank angle resolution, a mean value adaption has been implemented. There are two main limitations with this implementation; firstly the measurement time must be long enough so that a high enough number of combustions can occur in the available time window. This is of course most critical at lower engine speeds. Secondly, the combustion variability cannot be too large, since this will increase the risk of an unreliable mean value.

To test this implementation, the combustion model is used on a random data set where both valves nominally have 180 degrees duration and 6 mm lift height. For 60 cycles (i.e. 60 combustions) the valve lifts are then randomly varied between 4 and 8 mm and the valve closing times are varied ± 5 degrees from the nominal value. This can be compared to a typical practical operation point where CoV is around 15%. The generated cylinder pressure traces are then formed as mean values both according to the implementation in *Raptor* and the more conventional element-wise mean value for all 60 cycles. The result is seen in figure 8.7 where the *Raptor* IMEP value is compared to the element-wise IMEP value. The absolute IMEP error between the two methods has a standard deviation of approximately 0.04 bar. This number needs to be related to the standard deviation presented in chapter 7.2, which was 0.17 bar. Hence, this number could potentially drop slightly if a continuous cylinder pressure measurement would have been possible.

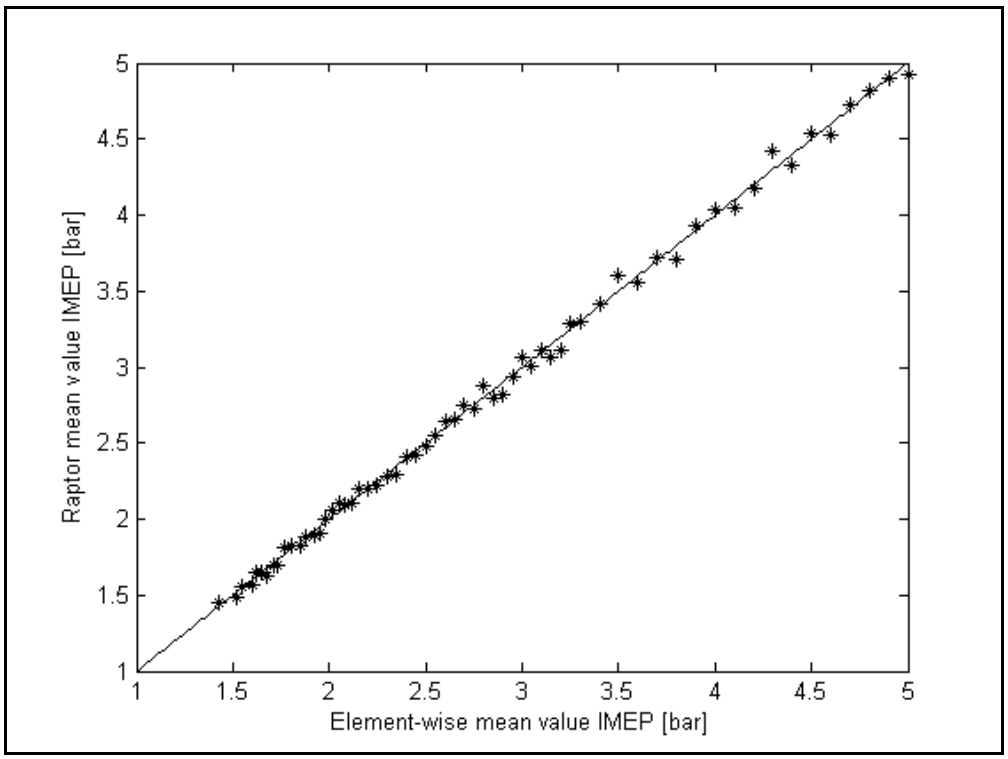

Figure 8.7. Comparison between the two cylinder pressure mean value formations. For comparison, the ideal line is also plotted. Engine is operating at 1200 rpm.

It can be seen that in most cases, the current implementation provides a satisfactory cylinder pressure trace. Based on empirical results and visual inspection, the reliability limit for this validity can be said to be a CoV of around 15%.

8.3.3 Standing wave oscillations

In any normal passenger car or other vehicle, the intake system is usually tuned for a certain power band, meaning that a certain engine speed range is optimal with respect to power output. This power band can be altered by adjusting manifold geometry, intake runner length and other physical parameters. The same design logic applies for the exhaust manifold, although it is of slightly less importance here. From the data set generated during this work, no real standing wave oscillations have been observed. This could be because of the valve lift instability described earlier. By constantly changing the length of the intake system (because of the fluctuating valve lift) it is possible that the resonance wave gets subjected to a small phase translation and the mean value adaption then reduces the amplitude even further.

8.4 Future work

The modifications to the control system and the combustion model done in this work have improved the overall system and model behaviour considerably, but there is still some more work to do.

8.4.1 Control performance

Even though the closed loop control for valve timings and lift heights work satisfactory, it is far from finished. Integrators based on error control have proven to work quite well, but the integrators themselves can be modified to be much more versatile. At the moment, they only work with digital step signals, meaning that no ramps or other types of smooth activations/deactivations are used. This works well as long as the original algorithms are accurate enough, but as e.g. engine speed increases, the integrators must work harder to meet the desired timing requests. This could be an indication that e.g. the air charging algorithms does not fully capture the dynamic behaviour of the valvetrain across the entire operating range.

8.4.2 Engine and test bed hardware

Certain limitations in the engine and cell environment hardware setup have become apparent during this work. Firstly, the electric engine brake becomes unstable when running above approximately 3500 rpm. This means that the valves have not been put to test at high engine speeds typical for a conventional SI engine.

Secondly, the cell control system can sometimes be a bit unsteady and it is especially difficult to handle when it comes to error debugging. This can be fixed by letting *Raptor* take more and more control of the test bed actuators. One example of this is the actuator air supply pressure, which at the moment is manually controlled from a pressure regulator. This could relatively easily be integrated into *Raptor* combined with a simple controller e.g. to operate at the lowest possible supply pressure in order to reduce power consumption.

Thirdly, the measurement system could also be expanded additionally. It might be possible to let *Raptor* trigger a measurement in the *IndiCom* system for instance, enabling high resolution sampling of cylinder pressure and valve lift heights.

8.4.3 Detailed valve lift profiles

For the combustion model, the simplified valve lift profile can of course be made increasingly complex. In [9], five different polynomial segments are suggested to connect the entire valve lift profile. Currently, the slightly uncertain valve position readings combined with the individual differences between actuators makes the actual appearance of the valve lift curve rather difficult to visualize. With a more accurate valve lift profile, it would be possible to additionally improve the flow model and increase accuracy in both air mass flow and residual gas estimations.

8.4.4 Flow rig measurements

In order to fully capture the gas exchange behaviour, the actual flow across the valves should be appropriately measured. The discharge coefficient should be implemented as a function of valve lift height, which should improve simulation results additionally.

8.4.5 Improved optimization routine

With respect to computational efficiency, a lot of potential in the optimization routine is still unused. At the moment, all valve timings are evaluated against each other and the only points that are discarded are the ones that would be rejected by the safety system. A more efficient approach would be to initialize the routine with a starting guess, and then start evaluating timing variations in the vicinity of this point. When negative slopes in the level curve are detected, it is possible to move to another area in the map or stop the routine and consider an optimal area to be found.

Unfortunately though, the optimization routine turned out to be slightly unsatisfactory because of the combustion parameters, and perhaps this is where the largest amount of work should be done.

8.4.6 Vibe parameter estimation

The need for recalibration of the Vibe parameters makes it difficult to use the model as fully predictive with respect to locating the optimal setting region. The black-box approach used to fit the Vibe parameters to measured data contains little physical modeling and has turned out to be unexpectedly sensitive to parameter changes.

It is difficult to find the actual reason for this modelling error, but one thing that is clear is that the two data sets where recorded with three months apart. Perhaps it is possible that the fuel somehow has undergone degenerative changes during this time, causing the entire burn rate profile to change appearance enough to make a difference. Another possible improvement of the parameter estimation accuracy would be to expand the engine's operating map. Looking at figure 3.4, the gaps in the evaluated operating map should preferably be eliminated. An increased number of points in these areas should provide a better overall foundation for the regression model.

To get to the root of this problem, more research is needed. Perhaps it is possible to find a more physical approach to modelling the actual Vibe parameters or it might be possible to find another way of modelling the burn rate.

9. Conclusions

The primary objective for the first part of this thesis work was to stabilize the valve control system and expand the measurement system to enable gathering of large amounts of data. Based on empirical and analytical evaluations, the conclusion is that the valvetrain system behaves better than before, but some issues are yet to be resolved. Stable operating conditions are difficult to maintain as engine speed and load increases, and the different operating characteristics between individual actuators also make it somewhat difficult to obtain completely repeatable operating conditions. The entire measurement system including the introduction of the automatic script works satisfactory when it comes to generating large quantities of data. For higher precision requirements, it might be necessary to use even higher sampling rates, but for most applications the current data logging strategy is sufficient.

This instability, even if it is only seen in the measured valve lifts and don't exist in real life, causes a difficult situation for the safety algorithm. Since the algorithm is based on current valve lift, fluctuations in this parameter will cause consequent fluctuations in timing of IVO and EVC if the operator uses valve settings beyond the critical safety limit. Because of these lift height fluctuations, the lift height is buffered for 10 cycles before it is passed on to the safety system. This procedure reduces variations in valve timings caused by fluctuating lift heights, but of course also introduces a system delay and thereby increases the response time slightly. This problem can only be more thoroughly analyzed and sorted out with a more reliable valve position measurement. In practice, if the operator wishes to run more aggressive strategies with e.g. more overlap, the safety system has to be switched off since it is currently too conservative as suggested in chapter 4.1.

The primary part of the thesis was to modify the in-house developed cylinder pressure model used to generate predictive cylinder pressure traces based on measured input signals. The main focus on the modelling part was directed towards the gas exchange process, and with the introduction of a differential equation model during both intake and exhaust stroke, overall model accuracy has significantly improved. The model spans across all possible parameter variations without any systematic errors and the statistical analysis shows that all error margins are within a narrow band.

The intention with this improved model accuracy was to use it as a method of finding the optimal valve settings with respect to overall engine efficiency. This turned out to work well in some cases, while other operating conditions displayed lower prediction accuracy. The reason for this was found to be the regression model used to adjust the combustion burn rate as a polynomial function of several input parameters. With a recalibrated polynomial, the model accuracy seen in the initial analysis was once again achieved. The obvious conclusion drawn from this would then be that more effort needs to be put in to understanding (and from that modelling) the actual combustion process from the point where the spark is initiated. If it is possible to find a better modelling approach here, locating an optimal settings region for the valve parameters should be manageable.

For practical applications of this valvetrain installation, one parameter that increases in importance is the power consumption. The idea proposed by Cargine for handling this problem is to supply only a small amount of air inside the actuator and then use the thermal expansion to push the valve downward. The control algorithm proposed in equations 4.7 to 4.10 use the ideal gas law as a basis to estimate the air mass needed to deliver a certain valve lift. This model does not take dynamic effects such as in-cylinder pressure drop (after valve opening the resisting pressure from combustion will decrease over time) into account. Exactly how much this

approach deviates from Cargine's suggestion is unverified, but since the calculations provide the requested valve behaviour, the possible errors leading to higher air consumption is more likely due to the actual hardware installation. This has not been the main topic for this thesis and is not further analyzed here.

Regarding the estimated air power consumed by the valvetrain operation, this must be investigated in more detail before mass production is an option. It could be possible to optimize power consumption by reducing the number of valves and lowering the lift height as much as possible, but this requires an immense calibration effort. Nevertheless, the potential of valve control freedom is uncontroverted and with hardware improvements as well as control algorithm tuning the system should not be completely discarded at this stage.

One final interesting observation was done towards the latter stages of the project. When testing the model sensitivity towards parameter changes, it appeared that the intake valve lift height had only a minor influence on trapped air charge, especially at low intake manifold pressures. To investigate if this behaviour was physically realistic, a comparison with a generic *GT Power* model was carried out. *GT Power* is a one-dimensional thermodynamic simulation code used for evaluation and tuning of different engine design aspects.

By feeding this simulation model with the same square-like intake valve lift profiles that can be seen in the single cylinder test bed and varying it from 1 to 5 mm while maintaining constant volumetric efficiency, the inlet pressure varies as shown in figure 9.1.

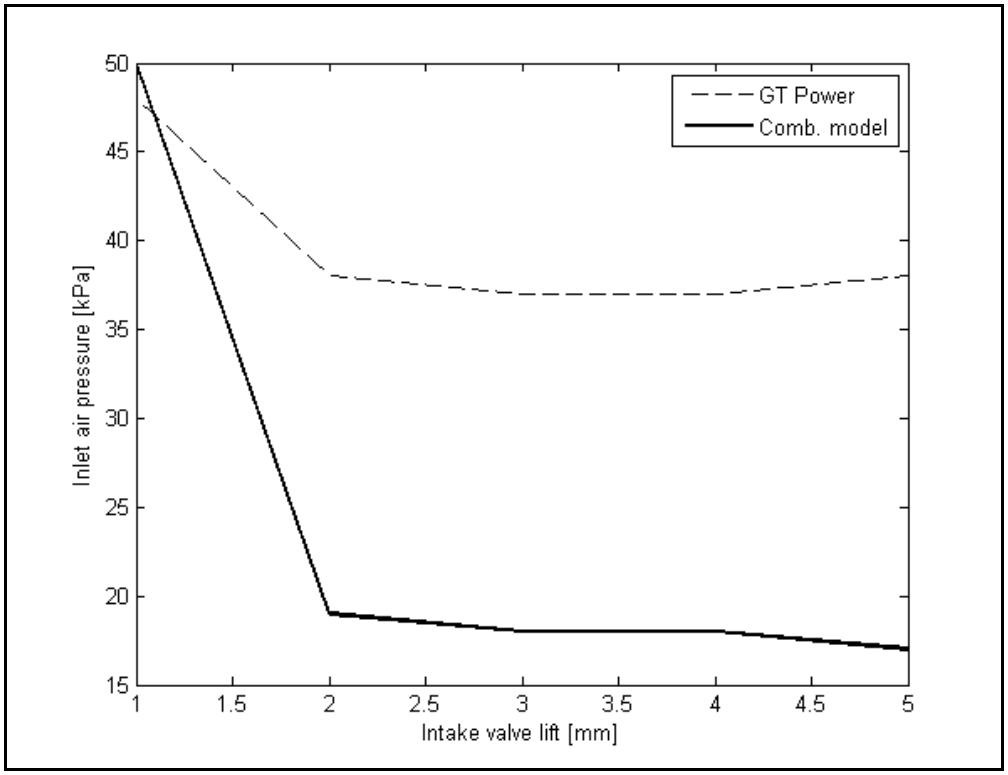

Figure 9.1. The influence of intake valve lift on air mass flow. Intake valve in both cases opens at TDC and closes at BDC, engine speed in both cases is 2000 rpm and volumetric efficiency is kept constant.

The absolute values are different because the engines and specific operating points are different, but the tendency in both cases is that only very low lift heights matter. The large difference from 1 to 2 mm seen in the combustion model could be due to numerical sensitivity and the fact that the engine has not been run with these low lift heights. Concerning practical usage of the valves, it is therefore recommendable to keep intake valve lift as low as possible to reduce power consumption.

10. References

[1] Ø. Gundersen. *Free Valve Technology*. M.Sc. thesis, Royal Institute of Technology, 2009

[2] J. Ma, H. Schock, U. Carlson, A. Höglund and M. Hedman. *Analysis and Modeling of an Electronically Controlled Pneumatic Hydraulic Valve for an Automotive Engine*. SAE 2006-01-0042, 2006

[3] B. Johansson. *Förbränningsmotorer*. Course literature, Lund University, 2006

[4] R. Backman. *RaComb - Raptor Combustion Model*. Technical Report, AVL SPEAB, 2010

[5] M. Klein. *A Specific Heat Ratio Model and Compression Ratio Estimation*. Lic. thesis, Linköping University, 2004

[6] J.B. Heywood. *Internal Combustion Engine Fundamentals*. McGraw-Hill International Editions, 1988

[7] H.K. Khalil. *Nonlinear systems*. Prentice Hall, 3rd edition, 2002

[8] L. Nielsen and L. Eriksson. *Course Material Vehicular Systems*. Course Literature, Linköping University, 2004

[9] G.P. Blair. *Design and Simulation of Four-stroke Engines*. Society of Automotive Engineers, Inc., 1999

[10] F. Lindström. *Empirical Combustion Modeling in SI Engines*. Lic. thesis, Royal Institute of Technology, 2005.

[11] J. Karlsson and F. Königsson, *Analytical Cylinder Pressure Model for Rapid Simulations*. Technical report, Royal Institute of Technology, 2009

[12] F. Lindström, H-E Ångström, G. Kalghatgi and C. Elmqvist-Möller. *An Empirical SI Combustion Model Using Laminar Burning Velocity Correlations*. SAE 2005-01-2106, 2005

11. Definitions, acronyms and abbreviations

Below follows a list (sorted alphabetically) of the most important abbreviations and variable names used in the report along with a short explanation.

A_{AP}	Surface area of actuator piston
A_{nom}	Valve curtain area, equivalent to geometric (nominal) flow area
B	Cylinder bore
BDC	Bottom Dead Center
BMEP	Brake Mean Effective Pressure
C_D	Valve discharge coefficient
CA50	Crank angle when 50% of the fuel is burned
CAD	Crank Angle Degrees
CAI	Controlled Auto Ignition
CFD	Computational Fluid Dynamics
CI	Compression Ignition, e.g. Diesel engine
CoV_{IMEP}	Coefficient of Variation based on IMEP
DOHC	Double Over-Head Camshaft
ECM	Engine Control Module
EGR	Exhaust Gas Recirculation
EPVA	Electronically controlled Pneumatic/hydraulic Valve Actuation system
EVC	Exhaust Valve Closing time relative to gas exchange TDC
EVO	Exhaust Valve Opening time relative to BDC
FMEP	Friction Mean Effective Pressure
GUI	Graphical User Interface
HCCI	Homogeneous Charge Compression Ignition
ICE	Internal Combustion Engine
IMEP	Indicated Mean Effective Pressure
IVC	Intake Valve Closing time relative to BDC
IVO	Intake Valve Opening time relative to gas exchange TDC
L	Piston stroke
M_{trq}	Engine torque
MBT	Maximum Brake Torque timing relative to combustion TDC
N	Engine speed
NMEP	Net Mean Effective Pressure
NVO	Negative Valve Overlap
OL	Valve overlap, when intake and exhaust valves are open simultaneously
P_a	Air power consumption
PMEP	Pumping Mean Effective Pressure
PVO	Positive Valve Overlap
Q	Heat released during combustion
R	Specific gas constant
SI	Spark Ignition, e.g. Otto engine
SOC	Start Of Combustion, here defined as crank angle for spark actuation
SOI	Start Of Injection relative to combustion TDC
T	Instantaneous cylinder temperature
T_{IVC}	Intake port temperature
T_{amb}	Ambient air temperature
$T_{coolant}$	Engine water temperature
T_{exh}	Exhaust manifold temperature
T_{inl}	Intake manifold temperature

TDC	Top Dead Center
TDC_{firing}	Combustion Top Dead Center
U	Internal energy
V_d	Displaced cylinder volume
VVT	Variable Valve Timing
W	Produced piston work
$XMEP$	Arbitrary mean effective pressure
Z_{st}	Stoichiometric air/fuel ratio, normally 14.5 kg/kg
a	Crank radius or Vibe parameter
c_v	Specific heat at constant volume
d_{EV}	Exhaust valve diameter
d_{IV}	Intake valve diameter
h_p	Piston height from piston pin center
k	Valve spring constant
l	Connecting rod length
l_{EV}	Exhaust valve lift
l_{IV}	Intake valve lift
m	Vibe shape factor
m_{fuel}	Injected fuel mass
p	Instantaneous cylinder pressure
p_a	Actuator supply pressure
p_{airMEP}	Mean Effective Pressure air consumption
p_{atm}	Ambient pressure
p_{exh}	Exhaust manifold pressure
p_{fuel}	Fuel pressure
p_{inl}	Intake manifold pressure
q_{HV}	Fuel lower heating value
r_c	Geometric compression ratio
$r_{c,real}$	Compression ratio based on IVC timing
x_0	Actuator dead volume height
x_b	Fuel mass fraction burned
x_{off}	Piston pin offset
x_{pc}	Spring precompression length
x_{rg}	Residual gas mass fraction
x_{tc}	Top clearance at TDC
$\Delta\theta$	Vibe combustion duration
α	Valve mounting angle
φ_{SOI}	Crank angle for Start Of Injection
φ_{spk}	Crank angle for spark timing
γ	Specific heat ratio
η_p	Pumping efficiency – air compressor
η_{tot}	Overall engine efficiency
η_{vol}	Volumetric efficiency
λ	Normalized air/fuel ratio
θ	Instantaneous crank angle
θ_0	Crank angle for Start Of Combustion
θ_{EVC}	Crank angle for EVC timing
θ_{EVO}	Crank angle for EVO timing
θ_{IVC}	Crank angle for IVC timing
θ_{IVO}	Crank angle for IVO timing
$\rho_{a,i}$	Intake air density

Appendix A - Degree project specification

This project is an integrated part of the M.Sc. program at the *Royal Institute of Technology, faculty of Internal Combustion Engines*. The project is commissioned by *AVL SPEAB*.

Background

As emission legislations and performance requirements continuously pushes the engine development forward, it is necessary to find possible areas of improvement in any subsystem related to the vehicle. If the SI engine is to be considered a possible alternative for the future, numerous enhancements are necessary. One key feature where improvements are possible is the valvetrain system, where most production vehicles today use strictly mechanical (i.e. via cam shafts) actuation. The main reason for this is its simplicity, reliability and inherent synchronization with the crank shaft. However, since the SI engine operates over a wide speed and load range a compromise in the valvetrain design is unavoidable. This can be solved by using a different actuating principle, for instance an electro-pneumatic system.

A system of this sort has been developed by *Cargine Engineering AB* and *AVL* has used this hardware to create a control system for the Free Valve Technology. The system is currently implemented on a single cylinder research engine with an LNF cylinder head (4 valves). The control system is based on a platform developed in *dSpace* and *Simulink* and from this user interface all controllable inputs can be adjusted.

Purpose

The main challenge with this valvetrain system installed is the increased number of degrees of freedom. With full variability of valve lifts and durations for each valve separately, combined with adjustability of spark timing, lambda value, fuel injection parameters, etc., mapping with respect to all possible operating points is an immensely time consuming task. Instead, modeling of the engine behavior is a necessary and helpful aid in order to shorten development and calibration time of the engine control unit.

The ambition with this project therefore is to further investigate the potential of Free Valve Technology and the end result should consist of possible setpoint recommendations with respect to optimized engine operation. The determination of these setpoints should be based on a *Simulink* model which takes all above stated input parameters into account. The recommendations will then in turn serve as a basis for further investigation of different combustion modes and alternative gas exchange processes, hopefully resulting in a valvetrain system which some day can be installed in a vehicle and render improved performance compared to conventional engines.

Assignment

The end result should be a set of recommendations for valve setpoints depending on whether it is desirable to want minimized emission levels or maximized power output. Therefore, a number of process steps need to be completed. When necessary, the existing control system and/or test bed hardware should be replaced or modified in order to be able to complete the tasks below.

1. Adjust the existing control system as follows:
    a. Implement correct adaptations for valve opening/closing and duration
    b. Improve the current safety system – make it less conservative (i.e. smaller safety margins are possible) and make sure that the safety system more precisely tracks the piston motion, particularly for varying engine speeds
    c. Use an existing model for the cylinder pressure trace to predict the exhaust back pressure at EVO (and from that determine the appropriate control signal), thus eliminating the one cycle lag existing today
    d. Implement a higher sampling frequency for the valve lift signal to improve measurement accuracy
    e. Assure that the engine and control system behaves in a stable manner at higher loads, where it's currently a bit unreliable
2. If possible, suggest an improved method for measuring the valve positions.
3. For end result verification, tune a handful of operating points manually with respect to valve strategy, spark timing, SOI, etc., as well as combustion mode.
4. Implement an already existing script for automatic generation of predefined operating points, thus making the entire measurement process more efficient. This means that the cell technician only needs to specify changes in parameter values and define appropriate time intervals between logged measurements and the cell control system will take care of the rest.
5. In order to be able to use this automatic script, the entire test bed system needs to be analyzed with respect to time delays. This means establishing response times for emission measurements, stabilization time for reaching steady state operation, etc. This analysis is necessary in order to be able to specify the autorun scheme correctly.
6. Use the knowledge obtained and conduct measurements necessary for the upcoming model development. This means, loop through all variable input parameters, i.e. valve lift and duration for each valve respectively, spark timing, injection timing (start and duration), lambda value, etc. This must of course be done for a number of engine speeds and loads to cover as much of the engine operating map as possible.
7. Continue developing an existing engine model, where the essential part is to include the variability of the free valves. The model should then serve as a foundation for locating optimal stationary operating points, either with respect to emissions or performance depending on situation and application. The main parameter for this analysis is specific fuel consumption or equivalently IMEP + PMEP = NMEP, which in turn is connected to e.g. the volumetric efficiency. This will depend strongly on the valve settings as well as the other input parameters.
8. For a few suitable operating points, try to evaluate different combustion modes and determine which is best suited to meet the performance requests. Compare regular 4-stroke combustion to for example HCCI and Atkinson cycles. Determine in which regions of the operating map these various modes deliver the best performance when full advantage of the free valves can be utilized. For example, if NO_x levels are an issue, lean combustion (i.e. HCCI) might be of interest. From an emission perspective it might also be interesting to try and use the free valves to control internal EGR, thereby further reducing NO_x emissions.

Appendix B – Test bed operating instructions and file list

The fundamental functionality of the single cylinder test bed in Södertälje has been described in other documents, which are available for anyone who is operating the engine. The functionality that has been included during this work requires some additional explanations.

The GUI currently used for operating the engine is divided into three parts, figure 3.1. The top left corner contains all controllable variables managed via *Raptor*. This allows the user to choose whether to run with e.g. lambda control or MBT feedback on or off. All four valves are operated manually and individually, since no functionality for automatic setpoints is implemented at the moment. The top middle area in the GUI window contains the automatic script control. The operator can choose to load a text file containing all the variables that he or she wishes to log with 10 ms resolution. When this is done, any predefined test sequence can be loaded from an *Excel* sheet and the script will execute automatically. The third region in the GUI contains sensor and signal information for surveillance purposes. Apart from the common pressure and temperature sensor readings, all control signals and integrator adjustments are presented here. This is particularly useful for debugging purposes in order to keep track on how the closed loop control performs. If an integrator signal saturates for example, this could be an indication of an underlying error.

File summary on DVD disc:

Folder ‘EngineModel’:

- 'Backup' - contains old model versions at different evolution steps
- 'CalcValveTimingOffset.m' - script for a rough estimate of actual pressure buildup in the region of valve closing
- 'ChangeLogStats.xls' - summary of model accuracy improvements throughout the model versions
- 'CombustionModel.m' - the cylinder pressure model
- 'combustionparameters.c' - used to analyze cylinder pressure trace
- 'CompareCombustionModels.m' - loop script that goes through wanted operating points and delivers a result overview
- 'ControlErrorPresent.m' - plotting the closed loop performance of the valves
- 'DataAnalysis.m' - script for reading measured mat-files and converting them to structs
- 'EstimateBlowdown.m' - script for rough estimate of blowdown duration after valve opening
- 'MeasurementNumbering.txt' - list of the 1790 operating points
- 'OptimumCombustion.m' - the optimization routine
- 'OptimumNumbering.txt' - list of the 357 operating points from the validation
- 'OptimumResult.m' - visualize results from the optimization routine
- 'PresentResult.m' - visualize results after running CompareCombustionModels.m
- 's1rotate.m' - function for sorting the measured cylinder pressure trace vector correctly
- 'ShowOnePres.m' - script for presenting one chosen operating point
- 'Tune_m_data.m' - script for finding a Vibe parameter regression model
- 'ValveLiftProfile.m' - script for visualizing the schematic valve lift curves used in CombustionModel.m
- 'VolEff.m' - script for evaluating different volumetric efficiency models

All .mat-files are different data sets that have been stored.

Folder ‘Free Valve Technology’:

- 'Cal' - contains initiation scripts with variable declarations
- 'ControlDeskGUI' - contains layouts and templates for the auto-script
- 'Doc' - contains naming guidelines and other overview documents
- 'Joakim' - contains short simulation scripts and some old model versions
- 'Lib' - contains plant models, etc.
- 'Tools' - contains useful scripts like cdconv.m or raplot.m for format conversion/visualization of data, etc.

The different dbc-files in the 'Raptor' folder contains information about the CAN messages in the cell. To change message composition, follow these steps:

1. Turn on the entire test bed (including Horiba, smoke meter, etc.) so that all rigg variables are visible in LabMeas

2. Click 'Test' --> 'Make DBC-file', file will be created in the C: root (name EnCylinder.dbc)

3. Load the file into Raptor by doing the following:
    a. Open Raptor.mdl
    b. Click 'Inputs' - 'Inputs' - 'RapidPro_Setup'
    c. Click the CAN controller setup with Group ID RTICAN4
    d. Click 'Replace data file' and load the new DBC-file
    e. Move up one level and select 'TimeBased_Inputs_10ms' --> 'CAN' --> ‘EnCyl_Dyno_Communication’
    f. Select one message block at a time and load the new message to update the message composition

4. Rebuild the model and flash it in ControlDesk

The folder ‘SingleCylMeas’ contains all data files, i.e. test sequences, *Excel* result files and *Matlab* files that have been used for the tests.

Appendix C – Equation summary of pre-existing cycle model

C.1 Geometric model

It is natural to let the engine geometry provide the basis for the geometric model. The cylinder volume at any given crank angle can be written

$$V(\theta) = V_c + \frac{\pi B^2}{4}\left[\sqrt{(l+a)^2 - x_{off}^2} - s(\theta)\right] \tag{C.1}$$

where V_c is the clearance volume defined by

$$V_c = \frac{\frac{\pi B^2}{4} L}{r_c - 1} \tag{C.2}$$

For estimations of heat transfer, the convective surface area of the cylinder must be calculated. If both cylinder head and piston crown are assumed to be flat, this surface area can be written

$$A = \frac{\pi B^2}{2} + \pi B\left[\sqrt{(l+a)^2 - x_{off}^2} - s\right] \tag{C.3}$$

This thermodynamic equation can, via the ideal gas law and known relationships for the specific heats, be rewritten as a pressure differential according to

$$dp = \frac{dQ_{ch} - \frac{\gamma}{\gamma - 1} p dV - dQ_{ht}}{\frac{1}{\gamma - 1} V + dQ_{cr}} \tag{C.4}$$

under the assumption that there is no mass flow across the valves, i.e. during the closed part of the cycle. The corresponding temperature differential is given by

$$dT = \frac{T_{IVC}}{p_{IVC} V_{IVC}}\left(p dV + V dp\right) \tag{C.5}$$

where subscript *IVC* denotes the thermodynamic state at the time when the intake valve closes. The next step is then to model the individual terms in these equations and a brief summary of these models is given here below.

C.2 Modelling crevice losses

A small, but not insignificant portion of the injected fuel will be transported to the gap above the top piston ring where it will fail to ignite in the vicinity of the cold combustion chamber wall. The heat flux into these crevice regions will depend on whether the peak pressure has been reached or not. The heat lost to the crevice regions can be written

$$dQ_{cr} = \left[\frac{1}{\gamma - 1} T + T' + \frac{1}{b} \ln\left(\frac{\gamma' - 1}{\gamma - 1} \right) \right] \frac{V_{cr}}{T_{wall}} dp \tag{C.6}$$

where T' is the gas temperature before p_{max} and the cylinder wall temperature after p_{max}, γ' is γ at gas temperature before p_{max} and γ at cylinder wall temperature after p_{max} and V_{cr} is the crevice volume. The constant b is determined via a linear specific heat ratio model around temperatures of 500 K (roughly corresponding to the cylinder wall temperature) and the model $\gamma = \gamma + b(T\text{-}500)$ gives $b = -1.43 \cdot 10^{-5}$. A reasonable value for the crevice volume is 10^{-6} m^3, corresponding to around 1.5% of the total cylinder volume.

C.3 Modelling cylinder wall temperature

The cylinder wall temperature determines the temperature gradient between the hot combustion chamber and the relatively cold surroundings. This will give rise to a heat flux which, to a certain extent, influences the cylinder pressure curve. The cylinder wall temperature is modelled as suggested in [5], where the available fuel energy is scaled with a factor 0.005 and replaces the mean effective pressure as

$$T_{wall} = 4.6(0.005 Q_{fuel}) + \frac{N}{60}(0.945 - 0.078 T_{coolant}) + T_{coolant} \tag{C.7}$$

In this equation, Q_{fuel} is the lower heating value of the fuel, N is the engine speed and $T_{coolant}$ is the engine water temperature.

C.4 Modelling heat transfer losses

As a consequence of the temperature gradient described above, heat transfer plays an important role in combustion engine modelling. Heat losses are difficult to validate accurately but a traditional model is based on Newton's law of cooling which, in crank angle domain, can be written

$$dQ_{ht} = h_c A (T - T_{wall}) \frac{60}{2\pi N} \tag{C.8}$$

The heat transfer coefficient h_c is determined according to a proposal by Hohenberg as

$$h_c = C_1 V^{-0.06} p^{0.8} T^{-0.4} (S_p + C_2)^{0.8} \tag{C.9}$$

where S_p is the piston mean velocity, C_1 is 0.013 and C_2 is 1.4 during combustion and 0 otherwise.

C.5 Modelling combustion efficiency

The global combustion reaction for an arbitrary air/fuel mixture can be written

$$\begin{aligned} &\mathrm{C_xH_yO_z} + \lambda\left(x + \frac{y}{4} - \frac{z}{2}\right)(\mathrm{O_2} + 3.773\mathrm{N_2}) \rightarrow \\ &\rightarrow x\mathrm{CO_2} + \frac{y}{2}\mathrm{H_2O} + (\lambda - 1)\left(x + \frac{y}{4} - \frac{z}{2}\right)\mathrm{O_2} + 3.773\lambda\left(x + \frac{y}{4} - \frac{z}{2}\right)\mathrm{N_2} \end{aligned} \tag{C.10}$$

For different molecular fuel compositions, this chemical reaction can be analyzed with respect to reactant and product components. The concluding result is that combustion efficiency is very close to 1 for stoichiometric and lean mixtures. For fuel rich mixtures, however, completeness of combustion diminishes rapidly.

C.6 Modelling specific heat ratio and dissociation

The single most important parameter to model accurately is the specific heat ratio, which is defined as

$$\gamma = \frac{c_p}{c_v} = \frac{c_v + R}{c_v} \tag{C.11}$$

where lower-case letters for c_p and c_v indicate mass specific units and R is the gas constant calculated from

$$R = \frac{\tilde{R}}{M} \tag{C.12}$$

where M is the molar mass of the gas mixture and $\tilde{R}$ = 8314.3 J/(kmol·K) is the universal gas constant. In practice, the specific heat ratio, will vary significantly with varying pressure, temperature, mixture composition, fuel type, etc. The complexity of these relations is difficult to capture even with a very advanced model, and a good compromise between computational efficiency and model accuracy is to use chemical equilibrium calculations. The implementation of this model has been done prior to this work and the principal idea is briefly explained below.

The global combustion reaction C.10 can be broken down into its elementary reactions, each with its own equilibrium constant. This constant varies exponentially with temperature and, as a consequence, all chemical reactions are strongly temperature dependent. From the elementary reactions it is then possible to determine the molar fraction of each individual species, i.e. N, O, H, etc. and this enables an accurate calculation of the specific heat.

Since the ICE operates across a relatively large temperature span, it is impossible to avoid dissociation at some point. This means that if temperature increases enough, the mixture molecules will start disintegrating to eventually form new species. Since the dissociation process requires a more complex solution algorithm, it is only accounted for when the modelled in-cylinder temperature exceeds 1700 K. Below this temperature, little or no difference can be seen in the calculation of specific heats.

Because of this well defined temperature limit, it is also suitable to use two different calculation models depending on the situation in each time step. As long as the temperature is below 1700 K, an assumption known as frozen composition is used. For higher temperatures, this assumption is not valid as the enthalpy of the mixture will change considerably. Instead, a slightly more complicated integration process must be used. The final result becomes an equation for calculating the molar specific heat at constant pressure according to

$$C_{p,u} = \frac{1}{m_{RP}} \sum_i n_i C_{p,i} M_i \tag{C.13}$$

$$C_{p,b} = \frac{1}{m_{RP}} \sum_i n_{b,i} C_{p,i} M_i, \ \mathrm{T} \le 1700 \ \mathrm{K} \tag{C.14}$$

$$C_{p,b} = \sum_i \left(\chi_i C_{p,i} + H_i \frac{\partial \chi_i}{\partial T} \right), \ \mathrm{T} > 1700 \ \mathrm{K} \tag{C.15}$$

where subscripts *u* and *b* denote unburned and burned mixture respectively. The molar specific enthalpy H_i is associated with the dissociation term, n_i represents the number of moles of species *i* per mole O_2 in the mixture and m_{RP} is the mass of mixture per mole O_2 in the mixture. The partial derivative in the bottom equation is approximated by performing the equilibrium calculation twice with a mutual offset of 1 K.

Once the specific heats are known, the specific heat ratio can be calculated from equation C.11.

Appendix D – Discarded data points

Based on the predefined tolerances needed to be able to trust the mean value formation in the cylinder pressure logging, a number of operating points from the original data set of 1790 points are removed. The excluded operating points are (file name and operating point number are identical):

33, 75, 76, 80, 81, 82, 83, 384, 813, 814, 1054, 1067, 1068, 1069, 1148, 1190, 1192, 1228, 1229, 1230, 1483, 1484, 1485, 1486, 1487, 1488, 1489, 1490, 1491, 1492, 1493, 1494